

STATUS OF THESIS

Title of thesis

COMPUTER AIDED SYSTEM FOR BREAST CANCER  
DIAGNOSIS USING CURVELET TRANSFORM

I, MOHAMED MESELHY MOHAMED ELTOUKHY

hereby allow my thesis to be placed at the Information Resource Center (IRC) of  
Universiti Teknologi PETRONAS (UTP) with the following conditions:

1. The thesis becomes the property of UTP.
2. The IRC of UTP may make copies of the thesis for academic purposes only.
3. This thesis is classified as:

Confidential

Non-confidential

If this thesis is confidential, please state the reason:

---

---

The content of the thesis will remain confidential for \_\_\_\_\_ years.

Remarks on disclosure:

---

---

Endorsed by

\_\_\_\_\_  
Signature of Author

\_\_\_\_\_  
Signature of Supervisor

Dr. Ibrahima Faye

Permanent address:

Egypt, Elmenofiya

Ashmoon, Shanaway.

Date: \_\_\_\_\_

Date: \_\_\_\_\_

UNIVERSITI TEKNOLOGI PETRONAS  
COMPUTER AIDED SYSTEM FOR BREAST CANCER DIAGNOSIS  
USING CURVELET TRANSFORM

by

MOHAMED MESELHY MOHAMED ELTOUKHY

The undersigned certify that they have read, and recommend to the Postgraduate Studies Programme for acceptance this thesis for the fulfillment of the requirements for the degree stated.

Signature: \_\_\_\_\_

Main Supervisor Dr. Ibrahima Faye

Signature: \_\_\_\_\_

Co-Supervisor Dr. Brahim Belhouari Samir

Signature: \_\_\_\_\_

Head of Department: Dr. Nor Hisham Bin Hamid

Date: \_\_\_\_\_

COMPUTER AIDED SYSTEM FOR BREAST CANCER DIAGNOSIS  
USING CURVELET TRANSFORM

by

MOHAMED MESELHY MOHAMED ELTOUKHY

A Thesis

Submitted to the Postgraduate Studies Programme

as a Requirement for the Degree of

DOCTOR OF PHILOSOPHY

ELECTRICAL AND ELECTRONIC ENGINEERING

UNIVERSITI TEKNOLOGI PETRONAS

BANDAR SERI ISKANDAR

PERAK

FEBRUARY 2011

## DECLARATION OF THESIS

Title of thesis

COMPUTER AIDED SYSTEM FOR BREAST CANCER  
DIAGNOSIS USING CURVELET TRANSFORM

I, MOHAMED MESELHY MOHAMED ELTOUKHY

hereby declare that the thesis is based on my original work except for quotations and citations which have been duly acknowledged. I also declare that it has not been previously or concurrently submitted for any other degree at UTP or other institutions.

Witnessed by

\_\_\_\_\_  
Signature of Author

\_\_\_\_\_  
Signature of Supervisor

Permanent address:

Dr. Ibrahima Faye

Egypt, Elmenofiya

Ashmoon, Shanaway.

Date: \_\_\_\_\_

Date: \_\_\_\_\_

## ACKNOWLEDGEMENT

I wish to thank God the Almighty, without his consent, it would be impossible to achieve what had been done in this work. I would also like to thank my supervisors Dr. Ibrahima Faye and Dr. Brahim Belhaouari Samir for their help and supervision in conducting this research. I greatly appreciate their care, dedication and constructive criticism. I have truly benefited and enjoyed working with them.

I would like to thank the management and authorities of Universiti Teknologi PETRONAS for the generous financial support, providing different administrative and facilities throughout Electrical and Electronic Engineering department.

I would like to express my sincere appreciation to my friends especially Dr. Ahmed Maher for their support during the progress of this work.

I also would like to extend my appreciation to my wife for her understanding and for my kids Hagar and Abdullah for their patience.

## DEDICATION

*To my mother and brothers,  
To my late father and my late uncle Salamah.*

## ABSTRACT

Breast cancer is a leading cause of death among women worldwide. Early detection is the key for improving breast cancer prognosis. Digital mammography remains one of the most suitable tools for early detection of breast cancer. Hence, there are strong needs for the development of computer aided diagnosis (CAD) systems which have the capability to help radiologists in decision making. The main goal is to increase the diagnostic accuracy rate.

In this thesis we developed a computer aided system for the diagnosis and detection of breast cancer using curvelet transform. Curvelet is a multiscale transform which possess directionality and anisotropy, and it breaks some inherent limitations of wavelet in representing edges in images. We started this study by developing a diagnosis system. Five feature extraction methods were developed with curvelet and wavelet coefficients to differentiate between different breast cancer classes. The results with curvelet and wavelet were compared. The experimental results show a high performance of the proposed methods and classification accuracy rate achieved 97.30%.

The thesis then provides an automatic system for breast cancer detection. An automatic thresholding algorithm was used to separate the area composed of the breast and the pectoral muscle from the background of the image. Subsequently, a region growing algorithm was used to locate the pectoral muscle and suppress it from the breast. Then, the work concentrates on the segmentation of region of interest (ROI). Two methods are suggested to accomplish the segmentation stage: an adaptive thresholding method and a pattern matching method. Once the ROI has been identified, an automatic cropping is performed to extract it from the original mammogram. Subsequently, the suggested feature extraction methods were applied to the segmented ROIs. Finally, the K-Nearest Neighbor (KNN) and Support Vector Machine (SVM) classifiers were used to determine whether the region is abnormal or normal. At this level, the study focuses on two abnormality types (mammographic

masses and architectural distortion). Experimental results show that the introduced methods have very high detection accuracies.

The effectiveness of the proposed methods has been tested with Mammographic Image Analysis Society (MIAS) dataset. Throughout the thesis all proposed methods and algorithms have been applied with both curvelet and wavelet for comparison and statistical tests were also performed. The overall results show that curvelet transform performs better than wavelet and the difference is statistically significant.



## ABSTRAK

Kanser payudara adalah penyebab utama kematian di kalangan wanita di seluruh dunia. Pengesanan awal dan rawatan dianggap sebagai pendekatan yang unik untuk mengurangkan angka kematian yang berpunca dari kanser payudara. Digital mamografi menjadi salah satu cara yang paling sesuai untuk pengesanan awal kanser payudara. Oleh sebab itu, terdapat satu keperluan dalam perkembangan sistem bantuan-komputer diagnosis (CAD) yang mempunyai keupayaan untuk membantu ahli radiologi dalam membuat keputusan. Tujuan utamanya adalah untuk meningkatkan ketepatan dalam proses diagnosis.

Dalam tesis ini, kami merangka sebuah sistem berpandukan komputer untuk diagnosis dan pengesanan kanser payudara dengan menggunakan curvelet transformasi. Curvelet adalah transformasi yang boleh digunakan dalam skala yang pelbagai dan mempunyai arah yang tersendiri dan isotropi yang berbeza, dan berhenti dalam beberapa had-had wavelet yang wujud dalam menggambarkan pinggiran gambar. Kami telah memulakan penyelidikan ini dengan membina sistem diagnosis. Pertama, kaedah pemilihan dua ciri, yang mana sebelum ini digunakan dengan pekali wavelet, digunakan dengan pekali curvelet. Kemudian, hasil daripada curvelet dan wavelet tersebut dibandingkan. Setelah itu, tiga kaedah untuk pemilihan ciri-ciri disaran dan diterapkan dengan curvelet dan wavelet masing-masing untuk membezakan antara kelas kanser payudara yang berbeza. Hasil daripada eksperimen menunjukkan prestasi yang tinggi dari kaedah yang dicadangkan iaitu tahap ketepatan klasifikasinya mencapai 97.30%.

Tesis ini juga menyediakan sebuah sistem automatik untuk pengesanan kanser payudara. Pertama, sebuah penahapan algoritma secara automatik digunakan untuk memisahkan kawasan yang terdiri daripada payudara dan otot dada dari latar belakang gambar. Selanjutnya, kawasan algoritma yang berkembang digunakan untuk mencari otot dada dan berhenti sehingga kawasan payudara. Kemudian, prosedur ditumpukan di pembezaan kawasan yang dikehendaki (ROI). Dua kaedah

yang disarankan untuk mencapai pembezaan ini: sebuah penahapan yang bersesuaian dan kaedah pepadanan corak. Setelah ROI dikenalpasti, pemotongan gambar secara automatik dilakukan untuk mengekstraknya dari mammogram asli. Selanjutnya, cara memilih yang disyorkan, diterapkan terhadap ROI yang dipilih. Akhirnya, *K-Nearest Neighbor* (KNN) dan *Support Vector Machine* (SVM) pengklasifikasi digunakan untuk menentukan sama ada kawasan ini adalah normal atau tidak. Pada peringkat ini, kajian ini menumpukan pada dua jenis kelainan (Massa mammographi dan pemusnahan binaan). Keputusan ujian menunjukkan bahawa kaedah yang diperkenalkan mempunyai ketepatan pengesanan yang sangat tinggi.

Keberkesanan kaedah yang dicadangkan telah diuji dengan *Mammographic Image Analysis Society* (MIAS) dalam sebilangan data. Sepanjang tesis ini, semua kaedah dan algoritma yang dicadangkan, dilaksanakan dengan curvelet dan wavelet untuk perbandingan dan ujian statistik turut dilakukan. Keseluruhan keputusan kajian menunjukkan bahawa curvelet transformasi menunjukkan hasil yang lebih baik daripada wavelet dan perbezaannya sangat bermakna secara statistiknya.

## COPYRIGHT

In compliance with the terms of the Copyright Act 1987 and the IP Policy of the university, the copyright of this thesis has been reassigned by the author to the legal entity of the university,

Institute of Technology PETRONAS Sdn Bhd.

Due acknowledgement shall always be made of the use of any material contained in, or derived from, this thesis.

© Mohamed Meselhy Mohamed Eltoukhy, 2011

Institute of Technology PETRONAS Sdn Bhd

All rights reserved.

## TABLE OF CONTENTS

STATUS OF THESIS.....	i
DECLARATION OF THESIS.....	iv
ACKNOWLEDGEMENT .....	v
DEDICATION .....	vi
COPYRIGHT .....	XI
LIST OF TABLES.....	xvii
LIST OF FIGURES .....	xix
LIST OF ABBREVIATIONS .....	xxii
CHAPTER 1 INTRODUCTION.....	1
1.1 Overview .....	1
1.1.1 Microcalcifications.....	1
1.1.2 Masses .....	2
1.1.3 Architectural Distortion.....	2
1.1.4 Bilateral Asymmetry .....	2
1.2 Mammography .....	3
1.3 Double Reading .....	5
1.4 Computer Aided Diagnosis System .....	5
1.5 Clinical Computer-Aided Diagnosis Evaluation .....	6
1.6 Problem Statement .....	10
1.7 Objectives of the Study .....	11
1.8 Scope of the Work.....	11
1.9 Thesis Organization .....	12
CHAPTER 2 LITERATURE REVIEW .....	14
2.1 Overview .....	14
2.2 Image Enhancement for Diagnosis of Breast Cancer .....	14

2.3 Segmentation of Breast Region in Mammogram .....	15
2.4 Feature Extraction.....	16
2.4.1 Intensity Histogram Features .....	16
2.4.2 Morphological Features .....	17
2.4.3 Textural Features .....	17
2.5 Classifiers Used For Breast Cancer Diagnosis.....	18
2.5.1 Artificial Neural Networks (ANNs) .....	18
2.5.2 K-Nearest Neighbor Classifier .....	19
2.5.3 Binary Decision Tree.....	19
2.5.4 Support Vector Machine (SVM) .....	19
2.6 Mammographic Mass Detection and Classification .....	19
2.6.1 Mammographic Mass Segmentation .....	20
2.6.1.1 Thresholding Techniques .....	20
2.6.1.2 Region Based Techniques .....	22
A. Region Growing .....	22
B. Region Clustering .....	23
2.6.1.3 Edge Detection Techniques .....	24
2.6.1.4 Model Based Method .....	25
2.6.2 Feature Extraction and Classification of Mammographic Mass .....	28
2.7 Microcalcification Detection and Classification .....	37
2.7.1 Enhancement Techniques of Microcalcification.....	37
2.7.2 Segmentation of Microcalcification in Digital Mammogram.....	39
2.7.2.1 Thresholding Based Methods .....	40
2.7.2.2 Region Growing Based Methods.....	40
2.7.2.3 Morphological Operators Based Methods.....	41
2.7.2.4 Wavelet Based Segmentation .....	41
2.7.3 Feature Extraction and Classification of Microcalcifications .....	42
2.7.3.1 Microcalcification Detection Based on its Features .....	42
2.7.3.2 Microcalcification Detection Based On Statistical Texture Features.....	43

2.7.3.3 Microcalcification Detection Based on Multiscale Texture	
Features: Wavelet Based Method .....	44
2.8 Detection of Architectural Distortion.....	47
2.9 Analysis of Bilateral Asymmetry.....	51
2.10 Summary.....	54
CHAPTER 3 THEORETICAL BACKGROUND .....	57
3.1 Overview .....	57
3.2 Wavelet Transform.....	57
3.2.1 Multiresolution and One Dimensional Wavelet Representation .....	58
3.2.2 Two-Dimensional Wavelet Representation.....	61
3.3 Curvelet Transform .....	62
3.4 Classifiers Used in the Work .....	65
3.4.1 KNN Classifier .....	65
3.4.2 SVM classifier .....	66
3.5 Summary.....	68
CHAPTER 4 COMPUTER AIDED DIAGNOSIS SYSTEM DEVELOPMENT.....	69
4.1 Overview .....	69
4.2 Part I: Computer Aided Diagnosis System.....	70
4.2.1 Mammogram Cropping .....	71
4.2.2 Feature Extraction Techniques .....	72
4.2.2.1 Feature Extraction Based on Extracting a Percentage of the Biggest Coefficients.....	72
4.2.2.2 Feature Extraction Based on Extracting the Biggest 100 Coefficients.....	74
4.2.2.3 Feature Extraction Utilizing Standard Deviation of Means	76
4.2.2.4 Feature Extraction Based on Ranking Features Method ....	79
4.2.2.5 Curvelet Based Texture Feature Extraction Method .....	80
4.3 Part II: Automatic ROI Detection .....	82
4.3.1 Stage One: Breast Region Localization .....	85
4.3.2 Stage Two: ROI Segmentation .....	86

4.3.2.1 ROI Segmentation Using an Adaptive Threshold Method	.86
4.3.2.2 ROI Segmentation Using Pattern Matching Method	.....87
4.3.2.3 False Positive Reduction	.....88
4.4 Summary	.....88
CHAPTER 5 RESULTS AND DISCUSSION	.....90
5.1 Overview	.....90
5.2 Dataset	.....90
5.3 Part I: Computer Aided Diagnosis System	.....92
5.3.1 Results of Computer Aided Diagnosis System by Extracting a Percentage of the Biggest Coefficients	.....92
5.3.2 Results of Computer Aided Diagnosis System by Extracting the 100 Biggest Coefficients	.....98
5.3.3 Results of Computer Aided Diagnosis System by Extracting Features Using Standard Deviation of Means	.....107
5.3.4 Results of Computer Aided Diagnosis System by Extracting Features Based on Feature Ranking Method	.....115
5.3.5 Results of Computer Aided Diagnosis System Using Curvelet Based Texture Feature Extraction Technique	.....121
5.4 Part II: Automatic ROI Detection	.....124
5.4.1 Stage One: Breast Region Segmentation	.....124
5.4.1.1 Step 1: Black Background Removal	.....124
5.4.1.2 Step 2: Image Binarization	.....125
5.4.1.3 Step 3: Label Removal	.....126
5.4.1.4 Step 4: Breast Orientation	.....126
5.4.1.5 Step 5: Pectoral Muscle Suppression	.....127
5.4.2 Stage Two: Region of Interest (ROI) Segmentation	.....128
5.4.2.1 An Adaptive Threshold Method to Identify the Suspicious Region	.....129
5.4.2.2 The Results Obtained by Developing a Pattern Matching Method to Identify the Suspicious Region	.....138

5.5 Summary.....	140
CHAPTER 6 CONCLUSIONS AND FUTURE WORK.....	141
6.1 Conclusions of the Proposed Systems.....	141
6.1.1 Part I: Developing Computer Aided Diagnosis System.....	141
6.1.2 Part II: Automatic ROI Detection.....	144
6.2 Contributions of the Work.....	145
6.3 Recommendations for Future Work.....	146
REFERENCES.....	147
PUBLICATIONS DERIVED FROM THIS STUDY .....	163



## LIST OF TABLES

Table 1.1 United States clinical trials of screening mammography with computer aided diagnosis. ....	7
Table 2.1 Advantages and disadvantages of different segmentation methods. ....	27
Table 2.2 Summary of the performance of selected methods for the detection and classification of masses. ....	33
Table 2.3 Summary of the performance of selected methods for the detection and classification of microcalcifications. ....	46
Table 2.4 Summary of the performance of selected methods for the detection and classification of Architectural distortion. ....	50
Table 2.5 Summary of the performance of selected methods for the detection and classification of bilateral asymmetry. ....	54
Table 4.1 The seven texture features extracted from each wedge in curvelet decomposition. ....	81
Table 4.2 The obtained number of features before and after feature extraction method applied. ....	82
Table 5.1 The distribution of (MIAS) dataset into different classes. ....	91
Table 5.2 The classification accuracy rates between abnormal and normal classes by extracting different percentages from each decomposition level of curvelet and wavelet. ....	93
Table 5.3 The classification accuracy rate between different abnormality types by extracting different percentages from each decomposition level of curvelet and wavelet. ....	95
Table 5.4 The classification accuracy rates between benign and malignant types by extracting different percentages from each decomposition level of curvelet and wavelet. ....	97
Table 5.5 The classification accuracy rates obtained over the 2x5-folds to classify the normal and abnormal classes by extracting the biggest 100 coefficients for each decomposition level. ....	99
Table 5.6 The classification accuracy rates obtained over the 2x5-folds to differentiate between abnormality types by extracting the biggest 100 coefficients from each decomposition level. ....	101

Table 5.7 The classification accuracy rates obtained over the 2x5-folds to classify the benign and the malignant classes by extracting the biggest 100 coefficients from each decomposition level. ....	104
Table 5.8 The results of <i>t</i> -test at significance level $\alpha = 5\%$ to compare curvelet and wavelet decompositions. ....	106
Table 5.9 The obtained coefficients from wavelet and curvelet before and after applying threshold .....	108
Table 5.10 The classification accuracy rates obtained over the 2x5-folds to differentiate between the normal and abnormal classes using standard deviation of means feature extraction method.....	109
Table 5.11 The classification accuracy rates obtained over the 2x5-folds to differentiate between abnormality types using standard deviation of means feature extraction method.....	111
Table 5.12 The classification accuracy rates obtained over the 2x5-folds to differentiate between benign and malignant classes using standard deviation of means feature extraction method.....	113
Table 5.13 The results of <i>t</i> -test at significance level $\alpha=5\%$ between the standard deviation of means and the biggest 100 coefficients feature extraction methods. ....	115
Table 5.14 The results of <i>t</i> -test at significance level $\alpha=5\%$ , between the feature ranking method and the biggest 100 coefficients method.....	120
Table 5.15 The results of <i>t</i> -test at significance level $\alpha=5\%$ between the feature ranking method and the standard deviation of means method. ....	120
Table 5.16 The obtained features before and after feature extraction method applied .....	121
Table 5.17 The classification accuracy rates obtained over the 2x5-folds to classify between normal and abnormal classes using texture features method. ....	123
Table 5.18 The classification accuracy rates obtained over the 2x5-folds to classify between benign and malignant classes using texture features method. ....	123

## LIST OF FIGURES

Figure 1.1	The standard mammographic views displayed back-to-back (A) Medio-Lateral Oblique (MLO) views. (B) Cranio Caudal (CC) views.....	4
Figure 1.2	Flow chart of the main steps of CAD and CADx system. ....	9
Figure 3.1	A wavelet decomposition of a signal.....	60
Figure 3.2	A wavelet decomposition of an image.....	61
Figure 3.3	Three levels multiresolution decomposition wavelet. ....	61
Figure 3.4	Curvelet basic digital tiling in two dimensions. The shaded region represents one such typical wedge. ....	63
Figure 4.1	The proposed computer aided diagnosis system. ....	70
Figure 4.2	(a) Original image (1024 x 1024), (b) Cropped image (128 x 128). ....	71
Figure 4.3	Samples of used ROIs of mammograms.....	72
Figure 4.4	The proposed system for mammogram diagnosis by extracting a ratio of the biggest coefficients from each decomposition level.....	73
Figure 4.5	The proposed system for mammogram diagnosis by extracting the biggest 100 coefficients from each decomposition level.....	75
Figure 4.6	The proposed feature extraction technique. (a) Show the overlapping between the different classes' features. (b) The overlapped features are removed. ....	77
Figure 4.7	An example illustrates the proposed feature extraction method using standard deviation of means. ....	77
Figure 4.8	The proposed feature extraction method using the standard deviation of means to develop a computer aided system for mammogram diagnosis. ....	78
Figure 4.9	The proposed method for mammogram classification using feature ranking method. ....	80
Figure 4.10	The proposed fully automatic detection and diagnosis of breast cancer in mammograms.....	84
Figure 4.11	(a) The template region, (b) The dynamic window through the image, (c) The correlation matrix values of the corresponding window. ....	87
Figure 5.1	The average classification accuracy rates for normal and abnormal classes obtained using curvelet and wavelet decompositions with different percentage ratios of coefficients.....	94

Figure 5.2 The classification accuracy rates for abnormal classes obtained using curvelet and wavelet decompositions with different percentage ratios of coefficients. ....	96
Figure 5.3 The classification accuracy rates for abnormal classes obtained using curvelet and wavelet decompositions with different percentage ratios of coefficients. ....	96
Figure 5.4 The average of the results of 2x5 folds obtained for classifying the normal and abnormal classes by extracting the biggest 100 coefficients. ....	100
Figure 5.5 The average of the results of 2x5 folds obtained for classification of abnormal classes by extracting the biggest 100 coefficients.....	103
Figure 5.6 The average of the results of 2x5 folds obtained for classification of benign and malignant classes by extracting the biggest 100 coefficients. ....	105
Figure 5.7 The average of the classification rates of 2x5 folds obtained for classification of normal and abnormal classes using standard deviation of means feature extraction method.....	110
Figure 5.8 The average of the classification rates of 2x5 folds obtained for classification of abnormal classes using standard deviations of means feature extraction method. ....	112
Figure 5.9 The average of the classification rates of 2x5 folds obtained for classification of benign and malignant classes using standard deviations of means feature extraction method. ....	114
Figure 5.10 The classification accuracy rates for normal and abnormal classes corresponding to the number of features with different thresholds using wavelet coefficients. ....	116
Figure 5.11 The classification accuracy rates for benign and malignant classes corresponding to the number of features with different thresholds using wavelet coefficients. ....	117
Figure 5.12 The classification accuracy rates for normal and abnormal classes corresponding to the number of features with different thresholds using curvelet coefficients. ....	118
Figure 5.13 The classification accuracy rates for benign and malignant classes corresponding to the number of features with different thresholds using curvelet coefficients. ....	118
Figure 5.14 Classification accuracy rates obtained through 2x5-folds cross validation. ....	119
Figure 5.15 The average classification accuracy rate for two mammogram classification problems using texture feature method.....	122
Figure 5.16 The black background removal. (a) Original mammogram image, (b) The captured region of the original mammogram. ....	125

Figure 5.17 The binarized image to define the label of the image and the breast region.....	125
Figure 5.18 The label removal step. (a) The binarized image after removing the label. (b) The obtained area from the original mammogram image. ....	126
Figure 5.19 The orientation of the breast. (a) Left mammogram (b) Right mammogram. ....	127
Figure 5.20 Region growing result of two different mammogram images. ....	128
Figure 5.21 Thresholding the mammogram breast region to extract the suspicious regions in mammographic mass. (a) The original breast region image. (b) The thresholded image (c) The suspicious regions appear after suppression of the small regions. ....	130
Figure 5.22 Thresholding the mammogram breast region to extract the suspicious regions in architectural distortion. (a) The original breast region image. (b) The thresholded image (c) The suspicious regions appear after suppression of the small regions. ....	131
Figure 5.23 Set of suspicious mammographic mass regions segmented automatically.....	132
Figure 5.24 Set of suspicious mammographic architectural distortion regions segmented automatically. ....	133
Figure 5.25 The classification accuracy rate when extracting features by the standard deviation of means method to differentiate between mass and normal tissue. ....	135
Figure 5.26 The classification accuracy rate when extracting features by feature ranking method to differentiate between mass and normal tissue. ....	135
Figure 5.27 The classification accuracy rate when extracting features by the standard deviation of means method to differentiate between architectural distortion and normal tissue. ....	137
Figure 5.28 The classification accuracy rate of 2x5 folds cross validation when extracting features by feature ranking method to differentiate between architectural distortion and normal tissue. ....	137
Figure 5.29 The classification accuracy rate of 2x5 folds cross validation using the automatically detected ROIs by pattern matching method.....	139

## LIST OF ABBREVIATIONS

ACM	Active Contour Model
ANFIS	Adaptive Neuro-Fuzzy Inference System
ANN	Artificial Neural Network
CAD	Computer Aided Diagnosis
CC	Cranio-Caudal View
CT	Computed Tomography
DDSM	Digital Database for Screening Mammography
DWCE	Density Weighted Contrast Enhancement
DWT	Discrete Wavelet Transformation
FCM	Fuzzy C-Mean
FDA	Food and Drug Administration
FFDM	Full Field Digital Mammography
FN	False Negative
FP	False Positives
FROC	Free Response Operating Characteristics
GLCM	Gray Level Co-occurrence Matrix
GLDS	Gray Level Difference Statistics
GVF	Gradient Vector Flow Field
KNN	K-Nearest Neighbor
LDA	Linear Discriminant Analysis
MIAS	Mammographic Image Analysis Society
MLO	Medio-Lateral Oblique view
MRI	Magnetic Resonance Imaging
NCL	Normalized Chord Length
NRL	Normalized Radial Length
PCA	Principal Components Analysis
PCNN	Pulse Coupled Neural Network

PPV	Positive Predictive Value
RGI	Radial Gradient Index
RLS	Run Length Statistics
ROC	Receiver Operating Characteristic curve
ROI	Regions Of Interest
SBS	Sequential Backward Search
SFS	Sequential Forward Search
SGLD	Spatial Gray Level Dependence
SNR	Signal-to-Noise Ratio
SVM	Support Vector Machine
TN	True Negative
TP	True Positive
W. Average	Weighted Average
WHO	World Health Organization





## CHAPTER 1

### INTRODUCTION

#### **1.1 Overview**

Cancer is a leading cause of death worldwide; it is accounted for 7.6 million deaths (around 13% of all deaths) in 2008. More than 70% of all cancer deaths occurred in low and middle income countries. Deaths from cancer worldwide are projected to continue to rise to over 11 million in 2030 [1]. Breast cancer is the first one of the major concerns deaths among women. According to published statistics of World Health Organization (WHO) there were 460,000 deaths from this disease in 2008 [1]. Breast cancer is the leading cause of cancer in Malaysia. At least one in every 19 women in Malaysia is at risk of having breast cancer in her lifetime [2]. Early detection and treatment are considered the most promising approaches to reduce breast cancer mortality, since the causes of the disease are still unknown [3]. When breast cancer is detected and treated early, the chances for recovery are high. The current methods for early detection of breast cancer are clinical breast exams and mammography. Mammography is able to show changes in the breast up to two years before a patient or physician could feel them [4]. Mammographic abnormalities that can indicate breast cancer can be characterized into four classes: microcalcifications, masses, architectural distortion and bilateral asymmetry. These mammographic abnormalities are described as follows.

##### **1.1.1 Microcalcifications**

Microcalcifications are deposits of calcium in breast tissue. Microcalcifications detected on a mammogram are an important indicator for malignant breast disease but they also present in many benign changes. Benign microcalcifications are usually larger and coarser with round and smooth contours. Malignant microcalcifications tend to be numerous, clustered, small, varying in size and shape, angular, irregularly

shaped and branching in orientation [5]. Microcalcifications are generally very small and they may be missed in the dense breast tissue.

### **1.1.2 Masses**

A mass is defined as a space-occupying lesion seen in at least two different projections [6]. Masses are described by their shape (round, oval, lobular, irregular) and margin characteristics (circumscribed, microlobular, obscured, indistinct, spiculated). Mass areas usually appear brighter than healthy tissues. However, the patterns of mass lesion are hard to be defined by simple features such as intensities or gradients because of huge variations among individuals. Round and oval shaped masses with smooth and circumscribed margins usually indicate benign changes. On the other hand, a malignant mass usually has a spiculated, rough and blurry boundary. However, there exist typical cases of macrolobulated or spiculated benign masses, as well as microlobulated or well-circumscribed malignant masses [5].

### **1.1.3 Architectural Distortion**

Architectural distortion is defined as distortion of the normal architecture with no definite mass visible, including spiculations radiating from a point and focal retraction or distortion at the edge of the parenchyma. Architectural distortion of breast tissue can indicate malignant changes especially when integrated with visible lesions such as mass, asymmetry or calcifications. Architectural distortion can be classified as benign when including scar and soft-tissue damage due to trauma [7].

### **1.1.4 Bilateral Asymmetry**

Asymmetry of breast parenchyma between the two sides is a useful sign for detecting primary breast cancer. Bilateral asymmetries of concern are those that are changing or enlarging or new, those that are palpable and those that are associated with other findings, such as microcalcifications or architectural distortion. If a

palpable thickening or mass corresponds to an asymmetric density, the density is regarded with a greater degree of suspicion for malignancy.

## **1.2 Mammography**

Mammography is an x-ray imaging used to create images of the breast. It is now the main tool for early detection of breast cancer [8]. The Food and Drug Administration (FDA) reports that mammography can find 85% to 90% of breast cancers in women over 50 years and can discover a lump up to two years before it can be felt [4]. Once a lump is discovered, mammography can be a key in evaluating the lump to determine if it is cancerous. If a breast abnormality is found or confirmed with mammography, additional breast imaging tests such as ultrasound or a breast biopsy may be performed. A biopsy involves taking a sample of breast tissue and examining it under a microscope to determine whether it contains cancerous cells. A surgical biopsy is not without risk; it causes additional anxiety and distorts the breast tissue, which makes it difficult to interpret on subsequent mammograms [9]. Therefore, it is important to detect the disease carefully to minimize the number of biopsies. Mammography is usually used to help the radiologist or surgeon guide the needle to the correct area in the breast during biopsy.

There are two types of mammography exams, screening and diagnostic. Screening mammography is an x-ray examination of the breasts in a woman who is asymptomatic (has no complaints or symptoms of breast cancer). The goal of screening mammography is to detect cancer when it is still too small to be felt by a woman or her physician. Early detection of small breast cancers by screening mammography greatly improves a woman's chances for successful treatment [10]. Screening mammography is recommended every one to two years for women once they reach 40 years of age and every year once they reach 50 years of age. In some cases, physicians may recommend beginning screening mammography before age 40 i.e. if the woman has a strong family history of breast cancer.

Diagnostic mammography is an x-ray examination of the breast in a woman who either has a breast complaint, for example, a breast lump or nipple discharge is

found during self-exam or has had an abnormality found during screening mammography. Diagnostic mammography is more time-consuming than screening mammography and is used to determine exact size and location of breast abnormalities and their surrounding tissue and lymph nodes. Typically, several additional views of the breast are imaged and interpreted during diagnostic mammography. Thus, diagnostic mammography is more expensive than screening mammography.

The mammogram image can be taken using different angles and positions of the patient relative to the machine. To ensure the detection of cancerous cells, radiologists require more than one mammographic image of a patient's breast. For the same reason, it is also important that different angles are used to achieve different views of a patient's breast. There are two views most commonly performed in mammography. The first is the Cranio-Caudal (CC) view of the breast, in which the X-rays pass through the breast in direction from the head toward the feet. The second is the Medio-Lateral Oblique (MLO) view, which is taken diagonally across the body in a direction from the shoulder towards the opposite hip. CC and MLO are used in combination; it has become the international standard views in mammographic screening [11]. The diagram in Figure 1.1 shows the respective views CC and MLO. The MLO view in general is regarded as the most important view because it is most likely to visualize all the breast tissue including the pectoral muscle and other tissue adjacent to the chest wall.

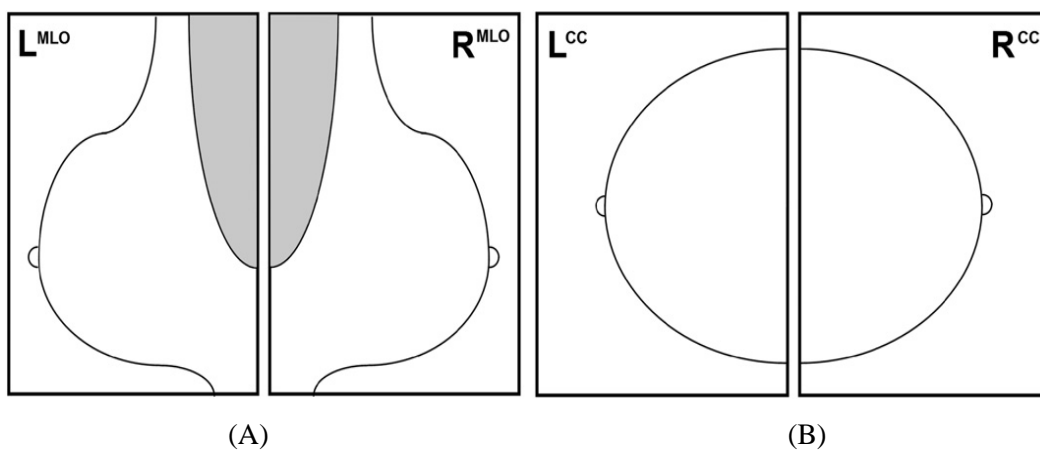


Figure 1.1 The standard mammographic views displayed back-to-back (A) Medio-Lateral Oblique (MLO) views. (B) Cranio Caudal (CC) views [12].

### **1.3 Double Reading**

Mammographic assessment is a difficult and complex task. It involves image interpretation and a clinical decision threshold regarding the need for tissue biopsy or follow-up. Double reading has been advocated as a method to improve detection of overlooked findings by a single reader. It has been suggested for reducing false positive rates in single reading of mammograms. Double reading requires the same mammogram to be analyzed by two different radiologists. Although double reading has been shown to increase the sensitivity of mammogram results by as much as 15%, it is a very time consuming and costly procedure [13]. Computer Aided Diagnosis (CAD) is an active area of study because it may provide the benefits of double reading in an efficient and cost-effective way [14]. The CAD system would replace one of the radiologists, saving considerable time and money.

### **1.4 Computer Aided Diagnosis System**

Computer-Aided Diagnosis (CAD) systems have been developed to aid radiologists in detecting mammographic lesions that may indicate the presence of breast cancer. These systems act only as a second reader and the final decision is made by the radiologist. CAD systems analyze digitized or digital mammography images using software programs to find features that are associated with breast cancer [15]. Computer aided methods in the field of digital mammography are divided into two main categories: computer aided detection (CADe) methods that are capable of pinpointing regions of interest (ROI) in mammograms for further analysis from an expert radiologist and computer aided diagnosis (CADx) methods which are capable of making a decision whether the examined ROI consists of abnormal or healthy tissue and distinguishing between malignant and benign ROIs.

It should be noted that here CAD refers to the whole field and comprises both CADe and CADx. Computer aided diagnosis (CADx) systems for aiding in the decision between follow-up and biopsy are still in development. With the explosive improvements in computer technology, further developments of the current CAD systems are expected. It is important to restate that one of the aims of computerized classification is to reduce the number of women undergoing biopsy for benign

disease, i.e. to increase the positive predictive value (PPV); ratio of the number of breast cancers found to the total number of biopsies without reducing the sensitivity of breast cancer detection.

It is important to realize that mammographic image analysis is an extremely challenging task for a number of reasons. First, since the efficacy of CAD/CADx systems can have very serious implications, there is a need for near perfection. Second, the large variability in the appearance of abnormalities makes it very difficult image analysis task. Finally, abnormalities are often occluded or hidden in dense breast tissue, which makes detection difficult. However, CAD systems for detecting masses or microcalcifications in mammograms have already been used and proven to be a potentially powerful tool [16]. The development of methods for finding a ROI in general of any kind of abnormalities is still limited and challenging [17].

### **1.5 Clinical Computer-Aided Diagnosis Evaluation**

Two methods have been used to test CAD in clinical trials. One method is sequential, i.e. presents the radiologist with an image without CAD information, requires interpretation, and then presents the same image with CAD markings and allows the radiologist to modify his assessment. Changes in sensitivity, specificity, recall rate, biopsy rate, and cancer detection are calculated. The second method uses historical control periods without CAD followed by the time period after CAD introduction. Both experimental methods are subject to potential bias. In the sequential method, radiologists may decrease their vigilance in interpretation of the examination without CAD, knowing that CAD has high sensitivity. This would tend to decrease sensitivity without CAD. Conversely, radiologists may compete versus CAD and be more sensitive than usual care. Table 1.1 summarizes United States clinical trials of CAD [15].

Table 1.1 United States clinical trials of screening mammography with computer aided diagnosis.

Study	Total Numbers Screened	CAD Sensitivity %	% Change
Freer and Ulissey, [18]	12,860	82	+ 19.5
Gur <i>et al</i> , [19]	115,571	Not recorded	+ 1.7
Helvie <i>et al</i> , [20]	2389	91	+ 9.1
Birdwell <i>et al</i> , [21]	8682	79	+ 7.4
Cupples <i>et al</i> , [22]	27,274	Not recorded	+ 16
Morton <i>et al</i> , [23]	21,349	76	+ 7.6
Dean and Ilvento, [24]	5631	89	+ 13.3
Ko <i>et al</i> , [25]	5016	79	+ 4.7

Radiologists are attracted by the effectiveness of clinical applications of CAD systems. CAD systems still need to be improved to meet the requirements of clinics and screening programs [26]. Research on CAD systems and related techniques has attracted great attention. There are several papers published [27] – [31] and there are now a number of commercially available CAD systems on the market in the United States, of which the market leader is currently the R2 ImageChecker. It has transformed the practice of mammography by helping radiologists read analog and digital mammograms. ImageChecker CAD identifies regions of interest (ROI) on mammography images and brings them to the attention of the radiologist in order to decrease false negative (FN) readings. ImageChecker CAD [32] was the first FDA approved mammography computer aided detection system. To date, two other systems also have the FDA approval, the iCAD system [33] and Kodak’s system [34]. However, there is still a long way to go before CAD systems become widely used in clinics and screening centers. The most important need is to demonstrate clearly that the accuracy of interpretation of screening mammograms with CAD systems is better than the accuracy without CAD. Several researches have shown that CAD represents a useful tool for the detection of breast cancer. Thus, improving

the performance of CAD systems remains a key issue for future research and development. Nevertheless, now that CAD systems can successfully identify almost all malignant microcalcifications and most malignant masses, the capability of the systems to detect the more subtle signs of malignancy, such as architectural distortion and asymmetry should be addressed [35].

A significant drawback to mammography is its poor positive predictive value. Less than a third of mammographic suspicious breast lesions that are biopsied are found to be cancer [36]. Thus, it would be exceedingly valuable to produce CAD systems that could aid in the decision to recommend biopsy or short-term follow-up mammography. Avoiding benign biopsies would spare many women stress, anxiety, discomfort and expense. Moreover, there is the possibility of increasing the sensitivity of mammography through CADx since it is estimated that about half of missed cancers are missed due to misinterpretation or fatigue of human observers [37]. Reducing the number of false positives (FPs) while maintaining a high rate of cancer detection remains a challenging problem.

The flowchart in Figure 1.2 shows the main steps involved in the detection CADe and diagnosis CADx of mammographic abnormalities. Most CAD algorithms consist of two stages. In stage one; the aim is to detect suspicious lesions at a high sensitivity. In stage two; the aim is to reduce the number of false positives without decreasing the sensitivity drastically. The steps that are involved in designing algorithms for both stages are shown in Figure 1.2.

The performance criteria of a radiologist or a diagnostic system are generally appraised by two indices: sensitivity and specificity [38]. The sensitivity of a recognized test is the fraction of positively diagnosed cases over the total of afflicted cases, which can be expressed by:

$$sensitivity = \frac{true\ positives\ (TPs)}{true\ positives\ (TPs) + false\ negatives\ (FNs)}$$

A test with a high value of sensitivity must have a minimal number of false negatives and is therefore useful in order to characterize the disease.



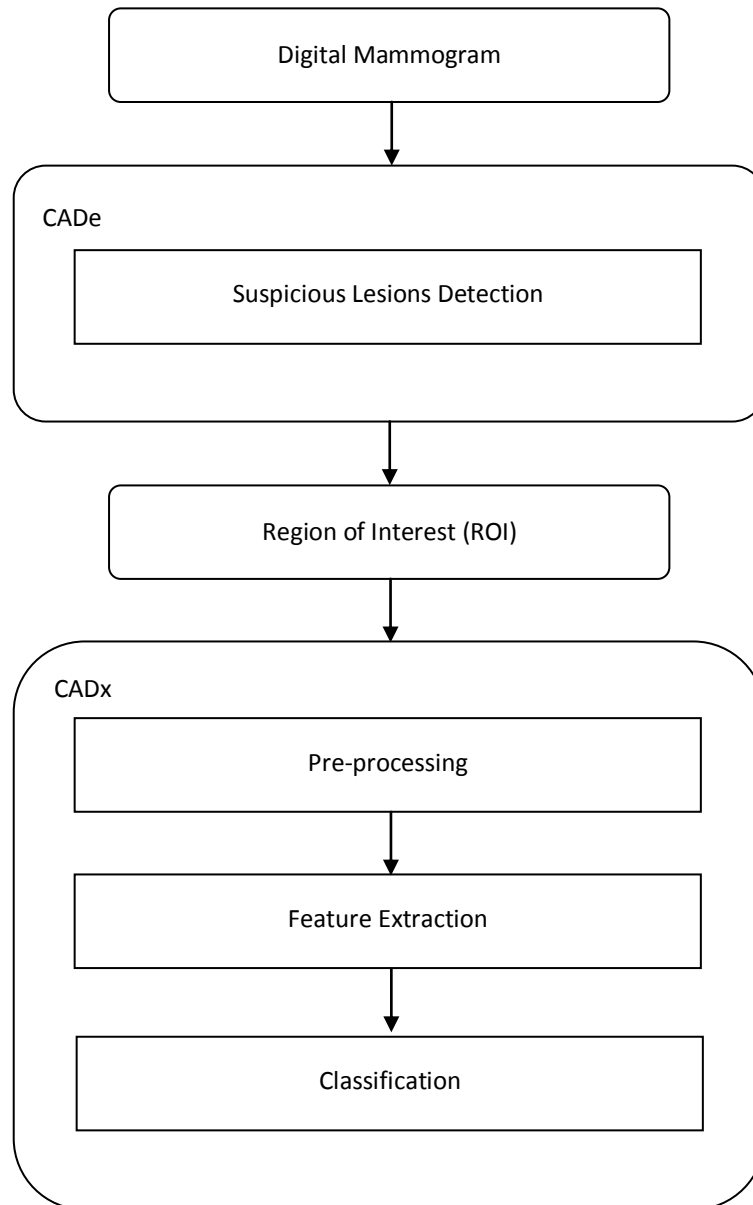


Figure 1.2 Flow chart of the main steps of CAD and CADx system.

The specificity of a test is the fraction of healthy cases over the total of un-afflicted cases, which can be expressed by:

$$specificity = \frac{true\ negatives\ (TNs)}{true\ negatives\ (TNs) + false\ positives\ (FPs)}$$

A test with a high value of specificity must have a minimal number of false positives and is therefore useful to exclude the disease.

Using sensitivity and specificity, the results obtained with the analysis are described in terms of the Receiver Operating Characteristic (ROC) curve which is defined as the probability of correct detection with the probability of false alert to varying decision threshold [17].

## **1.6 Problem Statement**

Computer-aided detection (CAD) systems have been developed to aid radiologists in detecting mammographic lesions that may indicate the presence of breast cancer. These systems act only as a second reader and the final decision is made by the radiologist. Computer-aided diagnosis (CADx) systems for aiding in the decision between follow-up and biopsy are still in development. The low accuracy of CAD/CADx produces high proportion of biopsies needed to be performed on benign lesions. Avoiding benign biopsies would spare women anxiety, discomfort, and expense. The mammographic image analysis is an extremely challenging task for a number of reasons: Since the efficacy of CAD/CADx systems can have serious implications, so there is a need for near perfection. The large variability of appearance of abnormalities makes it a very difficult image analysis task. Finally, abnormalities are often occluded or hidden in dense breast tissue, which makes the detection difficult [38]. The task of discriminating between the normal and abnormal, benign and malignant lesions and the shape of abnormality usually starts with a region of interest (ROI) detection. The lesion that shall be classified, ROI may have been extracted manually by a radiologist or automatically by a computer aided detection system. It is usually a rectangular sub-image cut from a mammogram. Most CADx systems have four stages process: lesion segmentation, feature extraction and finally classification.

Although by now some progress has been achieved, there are still remaining challenges and directions for future research, such as:

- 1) Developing better enhancement and segmentation algorithms.
- 2) Designing better feature extraction algorithms.
- 3) Developing high accuracy classifiers to reduce both FPs and FNs.

- 4) Integrating other imaging modalities with X-ray mammography. The current CAD systems for breast cancer uses mainly X-ray mammography. A combination of other image acquisition methods such as Ultrasound, magnetic resonance imaging (MRI) and computed tomography (CT) with X-ray mammography may lead to a novel effective CAD system for breast cancer control.

### **1.7 Objectives of the Study**

The overall objective of the study is to increase diagnostic accuracy and efficiency of the CAD system for breast cancer in digital mammogram. To fulfill this overall objective, the following specific objectives were taken into consideration:

- 1) Investigate the application of curvelet as a multiresolution representation to the mammogram images. This work focuses on using multiresolution representation advantages to study its effect in classifying between mammogram images.
- 2) Develop methods of feature extraction from multiresolution representation; curvelet and wavelet.
- 3) Develop an algorithm for breast region localization and ROI detection or segmentation in order to identify the abnormality type in such region.
- 4) Analysis the obtained results and compare between two types of multiresolution representations; curvelet and wavelet.
- 5) Validate the proposed methods and compare to a previous work of the computer aided diagnosis systems.
- 6) Study the architectural distortion and bilateral asymmetry types that has not been very much investigated.

### **1.8 Scope of the Work**

The scope of this work is to implement the curvelet as a multiresolution representation method. The work concentrates on feature extraction step. A set of feature extraction methods from multiresolution representation are suggested,

compared and a statistical analysis is accomplished. In this step, the work uses ROIs segmented manually using the given abnormality centres. In another part of the work, ROIs will be detected automatically. A new mammogram image segmentation algorithm that effectively and efficiently divides mammogram images into distinct components, breast region, background, labels and pectoral muscle is presented. The region growing and threshold methods are used to accomplish the task. Finally, an automatic system for masses and architectural distortion detection that identifies and extracts the suspicious areas in mammogram images using two different methods; adaptive thresholding method and pattern matching method.

## **1.9 Thesis Organization**

This thesis has been organized into the following six chapters:

Chapter 1 introduces the breast cancer, mammography and computer aided diagnosis challenges, objectives and contributions of the work.

Chapter 2 is a literature review on computer aided diagnosis of different breast cancer types. A brief description of some feature extraction methods from digital mammograms is also included.

Chapter 3 presents an overview of multiresolution representation analysis; the preliminaries of both wavelet and curvelet are discussed.

Chapter 4 presents the methodology of the proposed system. The chapter is divided into two parts. The first part uses the manually segmented ROIs in order to analyze and classify these ROIs to different breast cancer types. The work in this part is presented through five methods for feature extraction from multiresolution decomposition. The second part presents the proposed algorithm for mammogram image segmentation that effectively and efficiently divides mammogram images into distinct regions. It is divided into two main stages. The first stage presents the breast region localization. The second stage uses two methods to automatically segment the ROIs of masses and architecture distortion. These methods are the adaptive thresholding method and the pattern matching method.

Chapter 5 presents the results and the classification accuracy rates obtained from applying each feature extraction method suggested in part one of the work. The chapter gives a comparison between curvelet and wavelet, then compares between different feature extraction methods. Finally, the results of breast region localization and automatic ROI segmentation are presented.

Chapter 6 gives the conclusions of the work and recommendations for the future work.

## CHAPTER 2

### LITERATURE REVIEW

#### **2.1 Overview**

The success of few commercial computer aided systems for breast cancer detection and diagnosis opened the way to the development of new algorithms. This chapter provides a review of the state of the art of the computer aided detection and diagnosis of different types of breast cancer. Firstly, an overview of computer aided diagnosis components is given as it follows. In the Sections 2.2, 2.3, 2.4 and 2.5 are respectively presented the techniques of image enhancement, image segmentation, feature extraction and classification. It is then followed by the previous works done for mass detection in digital mammograms in Section 2.6. The work done for detection of microcalcifications is discussed in Section 2.7. The new developments for detection of architectural distortion and bilateral asymmetry are presented in Section 2.8 and Section 2.9, respectively. The different challenges are then summarized in Section 2.10.

#### **2.2 Image Enhancement for Diagnosis of Breast Cancer**

Image enhancement techniques have been proposed to improve the quality and readability of mammograms. It is also used to detect abnormalities because mammographic images generally have poor contrast and visibility of details. The goal of image enhancement is to improve the image quality so that the processed image is better than the original image for a specific application or a set of objectives. Abnormality signs in mammograms may be small and have low contrast with respect to the surrounding breast tissues. The nature of these abnormalities leads to difficulty to identify their features to be detected. Contrast enhancement techniques can improve the ability of radiologists to perceive subtle diagnostic

features, leading to earlier and more accurate diagnosis of breast cancer. The enhancement of mammographic images could improve the detection accuracy rate of breast cancer. Since many methods for the enhancement of mammograms may cause an amplification of noise or distortion of the anatomical features present in the image, radiologists would prefer to have the enhanced image with maintaining the familiar appearance of the original mammogram, which may limit the scope of enhancement techniques. However, with the introduction of direct digital imaging systems to mammography with increased contrast, dynamic range, and signal-to-noise ratio (SNR) there may no longer remain a need to enhance mammogram images.

### **2.3 Segmentation of Breast Region in Mammogram**

The identification of abnormalities in the breast tissue and the feature extraction process is affected if the region processed is not well focused. Therefore, it is important to split the mammogram into its interesting regions to achieve optimal breast measurements. In the CAD environment, one of the roles of image processing would be to detect region of interest (ROI) from the given mammogram image. Once the ROI has been detected; the subsequent tasks would be the characterization of ROIs and their classification into one of the categories such as normal, mass, microcalcification or architectural distortion, etc. The segmentation of the breast from the background is a fundamental step in mammogram image analysis. Segmentation is the process that divides an image into its constituent parts. It is an important step before the description and classification of an image. The aim of breast profile segmentation is to separate the breast from other objects in the mammogram with a minimum loss of breast tissue. In general two independent steps are performed. The first one aims to segment the background and annotations from the whole breast area. The second involves separating the pectoral muscle from the rest of the breast area.

A mammogram mainly contains two regions: the exposed breast region and the unexposed non-breast region [39]. It is necessary to identify first the breast region for the reduction of the subsequent processing and then to remove the non-exposed

breast region. Methods for the analysis of breast region should incorporate prior segmentation and removal of the pectoral muscle from mammograms Mediolateral Oblique (MLO) views, as well as the detection of the breast boundary and removal of artifacts.

## **2.4 Feature Extraction**

The feature extraction is the step that characterizes the features of a specific region. The features that are important are selected for the classification step. The features can be calculated from the ROI characteristics such as the size, shape, density, and smoothness of borders, etc. [40]. The feature space is very large and complex due to the wide diversity of the normal tissues and the variety of the abnormalities. Some of the features are not significant when observed alone, but in combination with other features can be significant for classification. Using excessive features may degrade the performance of the algorithm and increase the complexity of the classifier. The redundant features should be removed to improve the performance of the classifier. The feature extraction is a key step in breast cancer detection since the performance of CAD depends more on the optimization of the feature extraction than the classification step. Feature extraction is the process of selecting an optimum subset of features from the enormous potential features available in a given problem domain. The general guidelines to select significant features mainly include four considerations: discrimination, reliability, independence, and optimality [40]. The feature space can be divided into three sub-spaces according to what features are selected, intensity features, morphological (shape or geometric) features, and texture features.

### **2.4.1 Intensity Histogram Features**

Intensity histogram analysis has been extensively researched in feature extraction algorithm. Intensity histogram features like mean, variance, standard deviations, entropy etc, are the simplest among the three types of features.



### 2.4.2 Morphological Features

The morphological features are also called the shape or geometric features. These kinds of features are based on the shapes of ROIs. Morphological features are directly inspired by characteristics that a radiologist looks for. A set of these features are directly calculated from the boundaries and areas of ROIs such as (margin speculation, margin sharpness, area measure and circularity measure). Another set are the statistics based on the distribution of the normalized radial length (NRL) such as boundary roughness, mean, entropy and zero-crossing count. The radial length of a point on the tumor boundary is the Euclidean distance from this point to the mass centroid, whose co-ordinates are the average of the co-ordinates of all the points on the mass boundary. The NRL distribution is a set of data, each of which is normalized by dividing the maximum radial length. The last set of features is based on the distribution of the normalized chord length (NCL) such as mean, variance, skewness and kurtosis. The definition of the NCL is similar to the NRL. The difference between them is the definition of the length. The chord length is defined as the Euclidean distance of a pair of points on the tumor boundary.

### 2.4.3 Textural Features

The third group of features is based on the texture of the ROI. The spatial gray level dependence (SGLD) matrices called SGLD-based features are used to measure the texture-context information. It is a 2-D histogram. An element of the SGLD matrix  $P(i, j, d, \theta)$  is defined as the joint probability that the gray levels  $i$  and  $j$  occur separated by a distance  $d$  and along direction  $\theta$  of the image. In order to simplify the computational complexity of the algorithm, the  $\theta$  is often given as  $0^\circ$ ,  $45^\circ$ ,  $90^\circ$ , and  $135^\circ$ , and the distance  $d$  is often defined as the Manhattan or city block distance.  $I(x, y)$  is the intensity value of the pixel at the position  $(x, y)$ . The element  $P(i, j, d, \theta)$  of the SGLD matrix can be expressed as follows [41]:

$$P(i, j, d, 0) = \# \left\{ \left( (x_1, y_1), (x_2, y_2) \right), \left. \begin{array}{l} |x_2 - x_1| = d, y_2 - y_1 = 0, \\ I(x_1, y_1) = i, I(x_2, y_2) = j \end{array} \right\}$$

$$P(i, j, d, 45) = \# \left\{ \begin{array}{l} ((x_1, y_1), (x_2, y_2)), (x_2 - x_1 = d, y_2 - y_1 = -d) \\ \text{or} \\ (x_2 - x_1 = -d, y_2 - y_1 = d), I(x_1, y_1) = i, I(x_2, y_2) = j \end{array} \right\},$$

$$P(i, j, d, 90) = \# \left\{ \begin{array}{l} ((x_1, y_1), (x_2, y_2)), x_2 - x_1 = 0, |y_2 - y_1| = d \\ I(x_1, y_1) = i, I(x_2, y_2) = j \end{array} \right\},$$

$$P(i, j, d, 135) = \# \left\{ \begin{array}{l} ((x_1, y_1), (x_2, y_2)), (x_2 - x_1 = d, y_2 - y_1 = d) \\ \text{or} \\ (x_2 - x_1 = -d, y_2 - y_1 = -d), I(x_1, y_1) = i, I(x_2, y_2) = j \end{array} \right\},$$

## 2.5 Classifiers Used For Breast Cancer Diagnosis

Classifiers play an important role in the implementation of computer aided diagnosis of mammography. The features or a subset of these features are employed to classify a mammogram into its different categories such as normal or abnormal, and benign or malignant. A brief introduction of four kinds of classifiers is given here.

### 2.5.1 Artificial Neural Networks (ANNs)

An artificial neural network (ANN) is a parallel, distributed information processing structure consisting of processing elements directionally interconnected. The key characteristics of the ANNs are the distributed representation, local operations and nonlinear processing. These attributes make ANNs suitable for applications where only a few decisions are required from a massive amount of data, and also for the applications where a complex nonlinear relation needs to be learned. Thus, when the expert knowledge is not explicitly defined or cannot be represented in terms of statistically independent rules, ANNs may provide a better solution than expert systems. ANNs can efficiently learn nonlinear mappings through examples contained in a training set, and conduct complex decision making. Finally, ANNs can be effectively updated to learn new features.

### **2.5.2 K-Nearest Neighbor Classifier**

K-Nearest Neighbor (KNN) classifier distinguishes unknown patterns based on the similarity to known samples. The KNN algorithm computes the distances from an unknown pattern to every sample and selects the K-nearest samples as the base for classification. The unknown pattern is assigned to the class containing the most samples among the K-nearest samples.

### **2.5.3 Binary Decision Tree**

Binary decision tree is an ordered list of binary threshold operations on the features organized as a tree. Each node will move down to its two descendents by thresholding values of the features. This procedure will continue until it arrives at a terminal node which assigns a classification. The control parameters at each node are selected by simply determining the feature and threshold that separates well the current data into two classes. The process recursively partitions the remaining training samples and generates a tree. Comparing with neural networks, the decision tree approach is much simpler with low computational overhead.

### **2.5.4 Support Vector Machine (SVM)**

The SVM approach is based on intuitive geometric principles. Given a collection of vectors in  $R^d$ , labeled +1 or -1, a SVM finds the hyperplane with the maximum separation margins, meaning that it maximizes the distance between the hyperplane and the nearest labeled vectors. Since most problems in  $R^d$  are not linearly separable, SVM uses the soft margin technique to maximize the margin in the feature space. To simplify the computations, the feature space is taken to be non-linear projection of the input data to higher dimensional space by kernel function.

## **2.6 Mammographic Mass Detection and Classification**

A mass is defined as a space occupying lesion seen in at least two different projections defined with wide range of features that can indicate benign or malignant

changes. Masses with round, smooth and circumscribed margins usually indicate benign changes while masses with spiculated, rough and blurry margins usually indicate a malignant mass. Several techniques have been developed for the detection and classification of breast masses in mammograms. Algorithms for breast mass detection in digital mammography usually consist of several steps: segmentation, feature extraction and classification. In the segmentation step, regions of interest (ROI) that contain abnormalities are segmented from the normal breast tissue. In the second stage of the algorithm, each ROI is characterized with the set of features, followed by a feature extraction step to identify the best set of features. Consequently, in the classification step, each suspicious ROI is classified whether it is benign mass or malignant mass.

### **2.6.1 Mammographic Mass Segmentation**

The aim of the segmentation is to extract ROIs containing all masses and locate the suspicious mass candidates from the background parenchyma, i.e. to partition the mammogram into several non-overlapping regions, then extract regions of interests (ROIs), and locate the suspicious mass candidates from ROIs. Segmentation of the suspicious regions on a mammographic image is designed to have a high sensitivity and a large number of false positives are acceptable since they are expected to be removed in later stage of the algorithm (classification) [38]. Researchers have used several segmentation techniques and their combinations.

#### *2.6.1.1 Thresholding Techniques*

Global thresholding [42] is one of the common techniques for image segmentation. It is based on the global information such as histogram. Since the masses usually have greater intensity than the surrounding tissue, this fact can be used for finding global threshold value. In the histogram representation, the regions with an abnormality impose extra peaks while a healthy region has only a single peak [40]. After finding a threshold value, the regions with abnormalities can be segmented. Global thresholding has good results when used as a primary step of some other segmentation techniques. Local thresholding is slightly better than global

thresholding. The threshold value is defined locally for each pixel based on the intensity values of its neighbor pixels [40]. Two variables of the local thresholding should be considered: the window size and the threshold value.

Li *et al.* [43] used local adaptive thresholding in a wavelet multiresolution framework to segment mammographic image into parts belonging to same classes and an adaptive k-means clustering to refine the results. Matsubara *et al.* [44] developed an adaptive thresholding technique that uses histogram analysis to divide mammographic images into three categories based on the density of the tissue ranging from fatty to dense. ROIs containing potential masses are detected using multiple threshold values based on the category of the mammographic image. Dominguez and Nandi [45] presented a method for automatic detection of mammographic masses. An enhancement algorithm that improves image contrast based on local statistical measures of the mammograms was proposed. Then, regions were segmented via thresholding at multiple levels, and a set of features was computed from each of the segmented regions. A region-ranking system was presented to identify the region's most likely to represent abnormalities. The method achieved a sensitivity of 80% at 2.3 false positives (FPs) per image. Varela *et al* [46] developed a method using iris filter to enhance tumor mass lesion. An adaptive threshold was applied to select and segment potential lesions. Subsequently, some features based on iris filter output, gray level, texture contour related and morphological are presented to artificial neural network (ANN). The developed method yielded a sensitivity of 88% and 94% at 1.02 FPs per image for two different datasets. Li *et al.* [47] used adaptive gray-level thresholding to obtain an initial segmentation of suspicious regions followed by a multiresolution Markov random field model-based method.

Abdel-Dayem and El-Sakka [48] proposed a method based on image thresholding. The optimal threshold is determined by minimizing the fuzzy entropy of the image. The average global sensitivity and specificity for the proposed method are 98.5% and 88%, respectively. The method proposed by Kom *et al.* [49] consists of three main steps. Firstly, the original image is enhanced using an approach based on a linear transformation filter in which the local contrast of each pixel is modified. Secondly, by subtracting the enhanced image from the original image, they obtained

an image with segmented masses. The last step consists of the binarization of the obtained image using a local adaptive thresholding technique, after which a high pass and a median filter are applied to the binary image to remove noise. Their algorithm for mass detection gave a sensitivity of 95.91% and 93.87%, respectively when the preprocessing step is either applied or not.

### 2.6.1.2 *Region Based Techniques*

Region based segmentation relies on the principle of homogeneity, which means that there has to be at least one feature that remains uniform for all pixels within a region. It divides the image into homogenous and spatially connected regions. Region based methods can be split in two basic strategies: the region growing and region clustering approaches. Both are very similar. The difference is that the region clustering searches the regions directly without any prior information, while the region growing based algorithms firstly need to seed points and thresholds, and then to grow iteratively and aggregate with the pixels that have similar properties. If the region is not growing any more, then the grown region and surrounding region are obtained.

#### A. *Region Growing*

The key issue of region growing is to find a criterion that checks whether the gray level values of its neighbors are within a specified deviation from the seed. Another key issue of region growing is to find the suitable seeds. There are three parts in mammograms, a fat region, a fatty and glandular region, and a dense region. According to the intensity values and local contrast between a seed pixel and its neighbors in the three partitions, three seeds pixels are selected from the partitioned regions. An automatic seed selection was introduced in [50]. The region growing process was applied for segmentation in [51]. Huo *et al.* [52] developed a semi-automatic region growing approach, in which the growing step was automatically computed after a radiologist had manually placed the seed point. Kupinski and Giger [53] compared this initial approach to two improved versions, one based on a single feature called the radial gradient index (RGI) and one based on simple probabilistic

models to segment mass lesions, or other similar nodular structures, from surrounding background. In both methods a series of image partitions is created using gray-level information as well as prior knowledge of the shape of typical mass lesions. With the former method the partition that maximizes the RGI is selected. In the latter method, probability distributions for gray-levels inside and outside the partitions are estimated, and subsequently used to determine the probability that the image occurred for each given partition. The partition that maximizes this probability is selected as the final lesion partition (contour). They showed that the latter version improved performance compared to the other approach. Kinnard *et al.* [54] proposed a similar approach. The segmentation method utilized a maximum likelihood steep change analysis technique that is capable of delineating ill-defined borders of the masses, where the cost function depends on the contours of the image. Subsequently, the boundary of the mass was located by using those points where a significant change in the cost function was found.

Other researchers concentrated their efforts on improving the region growing algorithm by identifying the optimal set of initial seeds (mass detection). Zhang *et al.* [55] proposed a method to segment the breast masses in digitized mammograms; it operates on the whole mammograms instead of manually selected regions. Pixels with local maximum gray levels are flagged as seed points, from which many candidate objects are grown using modified region growing technique. False positive reduction technique using decision tree is applied to discard the normal tissue regions. The resulting sensitivity was 90% at 1.3 FPs per image. Another way to locate the initial starting points of the algorithm is to find the local maxima in the mammograms, which can be done using mathematical morphological operations, as suggested by Hejazi and Ho [56].

### *B. Region Clustering*

Region clustering searches the region directly without initial seed pixel [40]. Pappas [57] used a generalization of K-means clustering algorithm to separate the pixels into clusters based on their intensity and their relative location. Li *et al.* [43] used an adaptive k-means clustering to refine the result attained from the localized adaptive

thresholding. Cao *et al.* [58] presented a mass constrained clustering approach based on deterministic annealing approach for segmentation of breast mass on digital mammograms. They segment the suspicious mass within the ROI, which has been selected according to the information provided by the image database. Hassanien [37] applied the fuzzy c-mean (FCM) algorithm to the preprocessed mammogram image to initialize the segmentation step. The authors reported that the proposed algorithm is successful and has high detection accuracy. Sahiner *et al.* [59] used K-means clustering algorithm followed by object selection to detect initial mass shape within the ROI. The ROI is extracted based on the location of the biopsied mass identified by a qualified radiologist. Initial mass shape detection is followed by an active contour segmentation method to refine the boundaries of the segmented mass.

### 2.6.1.3 Edge Detection Techniques

Edge detection algorithms are based on the gray level discontinuities in the image. Basis for edge detection are gradients or derivatives that measure the rate of change in the gray level. Rangayyan [8] described standard operators for edge detection such as Prewitt operator, Sobel operator, Roberts operator and Laplacian of Gaussian operator. Petrick [60] used Laplacian of Gaussian filter in conjunction with density weighted contrast enhancement (DWCE). DWCE method enhances the structures within the mammographic image to make the edge detection algorithm able to detect the boundaries of the objects. Hong and Brady [61] proposed topographic representation of the mammogram in order to detect salient regions. By thresholding at different topographic levels they were able to find different types of regions, like the pectoral muscle, breast density, or masses. Yin *et al.* [62] investigated the use of an intelligent mesh for finding the masses. The mesh is represented by a set of nodes and springs connecting them. The nodes are adapted to the edges of the image, and suspicious regions are those with a high density of nodes. Fauci *et al.* [63] looked for the contours of the mass using an iterative algorithm. At each local maxima a threshold was selected which was used to draw an iso-intensity contour. The threshold value was based on user interaction and histogram information. Subsequently, the area of the selected region was refined by adjusting the threshold. Yuan *et al.* [64] utilizes a geometric active contour model



that minimizes an energy function based on the homogeneities inside and outside of the evolving contour. Prior to the application of the active contour model, a radial gradient index (RGI) based segmentation method is applied to yield an initial contour closer to the lesion boundary location in a computationally efficient manner. Based on the initial segmentation, an automatic background estimation method is applied to identify the effective circumference of the lesion, and a dynamic stopping criterion is implemented to terminate the contour evolution when it reaches the lesion boundary. Zou *et al.* [65] proposed a method that uses gradient vector flow field (GVF) which is a parametric deformable contour model. After the enhancement of mammographic images with adaptive histogram equalization, the GVF field component with the larger entropy is used to generate the ROI. Ferreira *et al.* [66] used active contour model (ACM) based on self-organizing network to segment the ROI. This model explores the principle of isomorphism and self-organization to create flexible contours that characterizes the shapes in the image. Yuan *et al.* [67] employed a dual stages method to extract masses from the surrounding tissues. Radial gradient index (RGI) based segmentation is used to yield an initial contour close to the lesion boundary location and a region based active contour model is utilized to evolve the contour further to the lesion boundary.

#### 2.6.1.4 Model Based Method

A model based segmentation method can be defined as the method that includes a training stage to learn about the specific objects to be detected. Subsequently, the system has to be able to detect and classify new images depending on the presence or absence of similar objects. The training step covers examples with and without the object present. For example, if the object is a mass, from the mammograms containing masses, the system learns the probable location and the variation in shape and size of the mass. From normal mammograms that does not contain mass, the systems can learn features that represent and describe the normality.

One of the most commonly used model based segmentation methods is pattern matching. Pattern matching is one of the most common approaches for medical image segmentation. This method uses the prior information of mammograms, and

segments possible masses from the background using the prototypes. The prototypes of possible masses are created based on the characteristics or physical features of the targeted masses [68], or based on the two-dimensional search function [69]. In pattern matching, the training is usually based on images containing the object to detect. When the priori information about the size of the masses is not available, a range of sizes for the templates is used. The matching criterion is measured by the least square technique [69] or by a cross correlation coefficient of the template [70]. The sub-regions that match the templates will produce high correlation coefficients whereas the sub-regions that do not match will produce low correlation coefficients. The main drawback of this method is the difficulty to account for the large variation in the shapes of masses. A different similarity measure that can be used to determine if a query ROI contains a true mass is mutual information, as used by Tourassi *et al.* [68]. Oliver *et al.* [71] proposed to use a probabilistic template matching scheme to detect masses. The shape and deformations of a deformable template were learnt from real mass examples. Subsequently, a Bayesian scheme was used to adapt the learnt deformable template to the real contours of the mammogram. Freixenet *et al.* [72] used the Eigen analysis for describing variation in mass shape and size, and then, they used two dimensional principal components analysis (PCA) approach to facilitate false positives reduction. On the other hand, Hantaka *et al.* [73] proposed a template matching algorithm that can solve the problem by using the similarity. The similarity was calculated for all ROIs with a partial loss to improve the performance of template matching.

Zwiggelaar *et al.* [74] introduced a technique to detect abnormal patterns of linear structures by detecting the radiating pattern of linear structures and the central mass expected to occur with spiculated lesions. PCA was applied to a training set of mammograms including normal tissue patterns and spiculated lesions. The results of PCA were used to construct a basis set of oriented texture patterns, which was used to analyze radiating structures. Szekely *et al.* [75] used a decision tree to classify a sliding window to contain mass or normal tissue. In similar work, Liu *et al.* [76] decomposed the image using multiresolution wavelet decomposition and at each resolution level, extracted a set of features, including an edge orientation histogram. Subsequently, each pixel was classified by using a binary decision tree.

Sakellaropoulos *et al.* [77] used wavelet analysis and feature extraction to classify the pixels of the dense region as mass or normal tissue.

Finally, there is a large set of approaches based on ANN classifiers. These usually formulated the problem of segmentation as a classification of ROI as suspicious or not. The features for training are intensity or texture related information based on a set of known ROI containing masses and a set of random samples from normal tissue [78]. Christoyianni *et al.* [16] used a radial-based function neural network to classify features derived from the histograms of each ROI. Hassanien *et al.* [79] and Ali and Hassanien [80] tested a pulse coupled neural network (PCNN), which has the ability to extract edges, image segments, and texture information from images. Mousa *et al.* [81] proposed a system based on wavelets analysis. They used an adaptive neuro-fuzzy inference system (ANFIS) for building the classifier to distinguish normal from abnormal. Table 2.1 presents the advantages and disadvantages of different segmentation methods.

Table 2.1 Advantages and disadvantages of different segmentation methods.

Segmentation methods	Advantage	Disadvantage
Global thresholding	Easy to implement and widely used.	Not appropriate for identifying ROIs, FPs and FNs may be high.
Local thresholding	Can improve the results of global thresholding, better than global thresholding.	Cannot accurately separate the pixels into suitable regions. Often used as an initialization of other algorithms.
Region growing	Grow iteratively and aggregate with the pixels that have similar properties.	Search for a set of seed pixel first. Depends on finding proper seeds and may be noise sensitive.

Table 2.1 Advantages and disadvantages of different segmentation methods  
(Continued).

Segmentation methods	Advantage	Disadvantage
Region clustering	Searching a region directly without any prior information.	Region clustering needs to know the number of clusters.
Edge detection	Good in detecting the contour of suspected region.	Need for prior information of the object.
Template matching	Easy to implement; if the prototypes are appropriate, it can afford good results.	Depends on the prior information of the masses, and may result large number of false positives.
Multi-scale technique	Easy to discriminate different frequencies and scales, Preserve the resolution of ROI; does not need any prior information	Needs proper selection of mother wavelet.

### 2.6.2 Feature Extraction and Classification of Mammographic Mass

In this level, the features that are characterizing a specific region are calculated then the features that are important are selected to be presented to the classifier. Chan *et al.* [82] presented a region-based algorithm in which eight texture features were calculated from spatial gray-level dependence (SGLD) matrices and stepwise linear discrimination was used to determine the importance of each feature in distinguishing masses from normal tissue. In the experiment, one half of a dataset of 168 ROIs containing biopsy-proven masses and 504 ROIs containing normal breast tissue was used for training; the other half was used for testing. They reported that

the area under the ROC curve was 0.84 for the training set and 0.82 for the testing set. In the work of Sahiner *et al.* [83] four gray-level difference statistics (GLDS) texture features and three SGLD texture features were used for mass detection. A convolution neural network was employed as the classifier to distinguish between the mass and normal breast tissue. The dataset consists of 168 ROIs containing biopsy-proven masses and 504 ROIs containing normal breast tissue, was extracted from 168 mammograms. They reported that the area under the ROC curve was 0.87.

Karssemeijer and te-Brake [84] developed a method for the detection of spiculated mass in mammograms, based on a statistical analysis of a map of the texture orientation in the mammographic images. The method for texture orientation analysis employs a multiscale technique and the orientation map is analyzed through the use of operators sensitive to stellate patterns (spiculated mass and architectural distortion). A sensitivity of 90% with one false positive per image was obtained in the detection of malignant stellate lesions and architectural distortion, using 31 normal cases and 19 cases with stellate lesions from the mammographic image analysis society (MIAS) database. In a related work, te-Brake and Karssemeijer [85] extend their work on the detection of stellate patterns for the identification of masses. The mass detection algorithm identifies patterns of radial gradient vectors, rather than radial spiculations. A sensitivity of 75% was attained with one false positive per image, with a test database of 132 mammogram images containing malignant tumors.

Rangayyan *et al.* [86] introduced two new shape factors, spiculation index and fractional concavity, then they applied them for the classification of manually segmented mammographic masses. The combined use of the spiculation index, fractional concavity and compactness yielded a benign versus malignant classification accuracy of 81.5%. Sahiner *et al.* [87], [88] mapped ribbons around breast masses in mammograms into rectangular arrays and then computed Haralick's measures of texture [89]. The boundaries of 249 mammographic masses were automatically extracted. Haralick's texture measures individually provided classification accuracies of up to 66%, whereas the Fourier descriptor based shape factor defined by Shen *et al.* [90] gave an accuracy of 82% (the highest among 13 shape features, 13 texture features, and five run-length statistics). The full set of the

shape factors provided an average accuracy of 85%, the texture feature set provided the same accuracy, and the combination of shape and texture feature sets provided an improved accuracy of 89%. These results indicate the importance of including features from a variety of perspectives and image characteristics in pattern classification. Mudigonda *et al.* [91] computed Haralick's texture measures using adaptive ribbons of pixels extracted around mammographic masses, and used the features to distinguish malignant tumors from benign masses using linear discriminant analysis (LDA). The method was tested on a database of 39 mammographic images, including 16 circumscribed benign, four circumscribed malignant, 12 spiculated benign, and seven spiculated malignant masses. The authors reported a classification accuracy of 74.4%. Mudigonda *et al.* [92] also proposed a method for the detection of masses in mammographic images based on the analysis of iso-intensity contour groups, and subsequent inspection of texture flow-field information to eliminate false positives. The test dataset consisted of 56 images from the MIAS dataset including 30 benign lesions, 13 malignant cases, and 13 normal. The authors reported a sensitivity of 81% at 2.2 false positives per image.

Li *et al.* [93] proposed a method for mass detection that employs a directional wavelet transform for multiscale representation of mammographic images, followed by segmentation of masses at different scales and elimination of false positive segments using shape analysis. A sensitivity of 91% with 3.2 false positives per image was obtained in the training phase of the proposed algorithm. The trained algorithm identified six of 10 subtle masses in a subsequent testing phase.

Liu *et al.* [76] proposed a multiresolution based method to detect spiculated lesions. The image was decomposed into a multiresolution representation and four features were extracted for every pixel at each resolution level. In their experiments, the authors selected 19 mammograms containing spiculated lesions from the MIAS dataset. The authors reported 84.2% true positive detection at less than 1 false positive per image, and 100% true positive detection at 2.2 false positives per image.

Zheng and Chan [94] devised an algorithm for the detection of masses that combines localized fractal analysis for pre-selection of suspicious regions, a multiresolution Markov random field segmentation algorithm and shape based

classification of segmented regions for reducing the number of false positives. The algorithm was evaluated using all 322 images in the MIAS dataset and a sensitivity of 97.3% with 3.9 false positives per image was obtained.

Campanini *et al.* [95] presented an SVM-based featureless approach for mass detection in digital mammograms. Instead of extracting features from ROIs, the authors used a multiresolution overcomplete wavelet representation to codify the image with redundancy of information. Two SVM classifiers were used in this approach. The first SVM classifier was used to find the mass candidates and the second SVM classifier was used to reduce the number of false positives. Experiments were conducted with 512 images containing 312 malignant tumors and 200 normal images from the DDSM database. The authors reported that the algorithm achieved nearly 80% true positive detection with a false positive rate of 1.1 marks per image for mammograms containing malignant tumors.

Ferreira and Borges [96] proposed a system to classify mammogram images by transforming the images into wavelet bases, then use a set of the biggest coefficients from first level of decomposition as the feature vector toward separating microcalcification clusters, spiculated mass, circumscribed mass and normal tissue of images. The classification rates achieved were 91.7% with 100, 200 and 300 coefficients, but decreased to 66.7% with 500 coefficients. Mousa *et al.* [81] proposed a system based on wavelet analysis. They used an ANFIS for building the classifier to distinguish normal from abnormal and to determine whether the type of abnormality is mass or microcalcification. The maximum classification rate obtained was 93.7%. Rashed *et al.* [97] studied the multiresolution analysis of digital mammogram using wavelet transform to extract a fractional amount of the biggest coefficients. They used daubechies-4,-8,-16 wavelet functions with four levels of decomposition. Euclidean distance was used to classify between microcalcification clusters, spiculated mass, circumscribed mass, ill-defined mass and normal tissue.

A CAD system for mass detection in full field digital mammography (FFDM) images was developed by Wei *et al.* [98]. First, raw FFDM images were enhanced using multiscale methods. Then, a two-stage segmentation method, which combined gradient field information and gray-level information, was used to detect suspicious

masses on FFDM images. In the third step, morphological and SGLD texture features were extracted for each suspicious mass. Stepwise linear discriminant analysis (LDA) with simplex optimization was employed to select the most useful features. The trained LDA classifier with the most useful feature set was employed to differentiate masses from normal tissues. In their experiment, a mass dataset containing 110 cases with 220 images and a no-mass set containing 90 cases with 180 images were used. The authors reported case-based sensitivity of 70%, 80% and 90% at 0.72, 1.08 and 1.82 false positive per image with the mass dataset and at 0.85, 1.31 and 2.14 false positives per image with the no-mass dataset, respectively. Bellotti *et al.* [99] proposed a completely automated CAD system for mass detection. The system included the following three steps. First, an edge-based segmentation algorithm was implemented to select the suspicious regions. Then, eight gray-tone independent texture features of the ROIs were derived from the GLCM. Finally, a supervised two-layered feed-forward neural network which was trained with the gradient-descent learning rule was employed to classify masses from normal tissues. In their experiment, a database of 3369 mammographic images which included 2307 negative cases and 1062 positive cases with at least one confirmed mass that had been diagnosed by expert radiologists was used. The authors reported that the area under the ROC curve was  $0.783 \pm 0.008$  for the ROI based classification. For mammographic images diagnosed by expert radiologists, 4.23 false positives per image were found at 80% sensitivity of mass detection.

An automated mass detection method was presented by Timp *et al.* [100] to detect temporal changes in mammographic masses between two consecutive screening rounds. Two kinds of temporal features, difference features and similarity features were designed to realize the interval change analysis. SVM was employed as a classifier to detect the temporal changes in mammographic masses. The classification performance was evaluated with and without the use of temporal features. In their experiment, the database consisted of 465 temporal mammogram pairs containing 238 benign and 227 malignant cases. The authors reported that the area under the ROC curve was 0.74 without temporal features and 0.77 with the use of temporal features. Varela *et al* [46] developed a method using iris filter to enhance tumor mass lesion then an adaptive threshold was applied to select and



segment potential lesions. Subsequently, some features based on iris filter output, gray level, texture contour related and morphological are presented to ANN. The developed method yielded a sensitivity of 88% and 94% at 1.02 FPs per image for two different dataset. Dominguez and Nandi [101] presented a method for automatic detection of mammographic masses. An enhancement algorithm that improves image contrast based on local statistical measures of the mammograms was proposed. Then, regions were segmented via thresholding at multiple levels, and a set of features was computed from each of the segmented regions. A region ranking system was presented to identify the regions representing most likely abnormalities. The method achieved a sensitivity of 80% at 2.3 false positives per image.

Moayed *et al.* [102], [103] presented a study of contourlet based mammography mass classification using SVM. In their study, a set of statistical properties of contourlet coefficients from 4 decomposition levels, co-occurrence matrix features and geometrical features is used as feature vector for the region of interest (ROI). Genetic algorithm was used for feature extraction based on neural network pattern classification. They concluded that the contourlet features offer an improvement of the classification process. Table 2.2 presents a summary of the statistical performance of selected methods for the detection, feature extraction and classification of masses. Although several methods have demonstrated good sensitivity, the accompanying false-positive rates are considered to be high. There is a need to increase the sensitivity of detection of masses to higher values at low false-positive rates of less than one per image. It is also desirable to indicate the degree of suspicion or probability of malignancy for each region identified.

Table 2.2 Summary of the performance of selected methods for the detection and classification of masses.

Authors	Size of dataset	Results
Chan <i>et al.</i> [82]	168 ROIs containing masses and 504 ROIs containing normal.	The area under the ROC curve was 0.84 for the training set and 0.82 for the testing set.

Table 2.2 Summary of the performance of selected methods for the detection and classification of masses (Continued).

Authors	Size of dataset	Results
Sahiner <i>et al.</i> [83]	dataset including 85 benign and 83 malignant masses, 45 of the malignant masses have spiculated margins. Six of the benign masses were spiculated.	The area under ROC curve 0.87, which corresponded to a true positive fraction of 90%.
Karssemeijer and te-Brake [84]	31 normal mammograms, 19 mammograms with stellate lesions	Sensitivity of 90% with one false positive per image
te-Brake and Karssemeijer [85]	132 mammograms containing malignant tumors.	Sensitivity of 75% with one false positive per image.
Rangayyan <i>et al.</i> [86]	54 mammographic masses (28 benign and 26 malignant).	Benign vs. malignant classification accuracy of 82%. Area under curve is 0.79.
Sahiner <i>et al.</i> [87]	249 automatically segmented mammographic masses.	Benign vs. malignant classification accuracy of 89%.
Mudigonda <i>et al.</i> [91]	39 mammographic images (16 circumscribed benign, four circumscribed malignant, 12 spiculated benign and seven spiculated malignant masses).	Classification rate of 74.4%, area under curve 0.67.
Mudigonda <i>et al.</i> [92]	56 mammographic images (30 benign lesions, 13 malignant cases, and 13 normal).	Sensitivity of 81% at 2.2 false positives per image.

Table 2.2 Summary of the performance of selected methods for the detection and classification of masses (Continued).

Authors	Size of dataset	Results
Li <i>et al.</i> [93]	Training dataset includes 36 normal and 24 masses, testing dataset includes 24 normal and 10 masses	Sensitivity of 91% with 3.21 false positives per image
Liu <i>et al.</i> [76]	19 mammograms exhibiting spiculated lesions, 19 normal mammograms	Sensitivity of 100% and 84.2% with 2.2 and less than one false positives per image, respectively.
Zheng and Chan [94]	322 images in the MIAS database	Sensitivity of 97.3% with 3.9 false positives per image
Campanini <i>et al.</i> [95]	512 images containing 312 malignant tumors and 200 normal images.	Sensitivity 80% with a false positive rate of 1.1 per image.
Ferreira and Borges [96]	23 circumscribed mass of MIAS.	Classification rate 91.7% with 100, 200 and 300 coefficients. But 66.7 with 500 coefficients.
Wei <i>et al.</i> [98]	masses dataset containing 110 cases with 220 images and a no-masses set containing 90 cases with 180 images were used.	Sensitivity of 70%, 80%, and 90% at 0.72, 1.08, and 1.82 false positive per image with the mass dataset, and at 0.85, 1.31, and 2.14 false positives per image with the no-mass dataset, respectively.

Table 2.2 Summary of the performance of selected methods for the detection and classification of masses (Continued).

Authors	Size of dataset	Results
Mousa <i>et al.</i> [81]	24 for training (14 benign, 10 malignant) and 16 for testing (10 benign, 6 malignant).	Classification rate of 93.7%, 81.2% and 68.7% with levels 2-3, 2-4 and 3-4, respectively.
Rashed <i>et al.</i> [97]	19 spiculated masses and 23 circumscribed masses from MIAS.	Classification rate of 81.7% and 71.5% for both types.
Bellotti <i>et al.</i> [99]	dataset of 3369 images included 2307 negative cases and 1062 positive cases.	The area under the ROC curve was $0.783 \pm 0.008$ , 4.23 false positives per image were found at 80% sensitivity of mass detection.
Timp <i>et al.</i> [100]	Dataset consisted of 465 temporal mammogram pairs containing 238 benign and 227 malignant cases.	The area under the ROC curve was 0.74 without temporal features and 0.77 with the using it.
Varela <i>et al.</i> [46]	Data set consists of 198 masses and 196 normal divided into training set containing 120 images with 60 mass and the rest are used for testing.	Sensitivity of 88% and 94% at 1.02 FPs per image for two testing and training dataset.
Dominguez and Nandi [101]	A set of 57 mass regions from MIAS dataset.	Sensitivity of 80% at 2.3 false-positives per image.
Moayedi <i>et al.</i> [103]	60 normal and 30 abnormal masses	Sensitivity of 95.8%.

## **2.7 Microcalcification Detection and Classification**

The presence of microcalcification clusters is an important sign for the detection of early breast carcinoma. Detection of microcalcifications is very important for the early breast cancer detection. Detection of microcalcifications is a very challenging task for radiologists as well as for computer-aided detection systems.

Computer aided systems try to make the diagnosis process easier and almost automatic. In mammography applications, one of the most important tasks for CAD is to detect the presence of microcalcifications, especially clustered ones, because they can be the early sign of possible cancer. Since microcalcifications are small and randomly scattered in breast tissue it is possible for a radiologist to overlook them. In that case, CAD systems should give good results by producing less false negative (FN) results. The general microcalcification detection process consists of: image enhancement, image segmentation (ROI detection), feature extraction and classification step using the selected features.

### **2.7.1 Enhancement Techniques of Microcalcification**

Image enhancement techniques have been proposed to improve the quality and readability of mammograms or to detect abnormalities because mammographic images generally have poor contrast and visibility of details. The goal of image enhancement is to improve the quality of the original image for a specific application. Most of the conventional techniques enhance not only the microcalcifications but also the background and noise [3].

Region-based approach enhances the contrast of the mammographic features of ROIs with various sizes and shapes according to the change of their surroundings [104]. The extent and shape of the grown region adapt to local variation of the gray levels. Contrast is computed with respect to its background. The definition of extent of regions is critical for region-based process. Region-based method can enhance more anatomical detail without significantly introducing artifacts, and has demonstrated that it can identify calcifications more effectively in the image of

dense breasts where the contrast between calcifications and breast tissue is quite low.

Since mammograms have some degree of fuzziness such as indistinct borders, ill-defined shapes, and different densities, the original images are transformed into a fuzzified image according to the maximum fuzzy entropy principle and then the geometrical statistics is used to measure the nonuniformity of the regions. An enhancement technique using fuzzy set theory and geometrical statistics to increase the contrast of microcalcifications was studied [105]. Cheng and Xu [106] presented an adaptive fuzzy logic contrast enhancement method for mammographic images. The method was based on the maximum fuzzy entropy principle. It transformed the image to a fuzzy domain and then a local measure of contrast called fuzzy entropy in the fuzzy domain was computed. The contrast was enhanced using both global and local information. Finally, the enhanced image was obtained using defuzzification, by which the enhanced mammogram was transformed back to the spatial domain from the fuzzy domain.

Multiscale analysis methods were also used to enhance the microcalcifications. Wavelets are mainly used because of their dilation and translation properties, suitable for non stationary signals [107]. The idea of wavelet enhancement is the microcalcifications occurred in high frequencies. So the low frequencies are suppressed. Consequently, a threshold value is applied to the highest frequencies and finally the image is reconstructed. Laine *et al.* [108] introduced the wavelet as an efficient tool for mammogram enhancement. They applied several wavelet type filter bank decomposition such as dyadic wavelet transform. Balakumaran *et al.* [109] decomposed the mammogram image up to 10 levels by applying dyadic wavelet transform. The original grayscale mammogram image was decomposed to 10 levels by applying daubechies-4 (db4) wavelet transform. Finally the lowest approximation image is set to zeroes and the detail coefficients are enhanced by a threshold. Tang *et al.* [26] presented a method for direct contrast enhancement, in which a multiscale local contrast measure was defined in the wavelet domain. The enhancement method was applied in the wavelet domain by manipulating the contrast values computed using the high-frequency and low-frequency information.

Papadopoulou *et al.* [110] compared five image enhancement algorithms: The contrast-limited adaptive histogram equalization (CLAHE), the local range modification (LRM), the redundant discrete wavelet transform (RDWT), linear stretching and shrinkage algorithms. The first two were derived from conventional image analysis methodologies, CLAHE and LRM algorithms. The rest were sustained on 2-D RDWT, (a) wavelet linear stretching (WLST) in which, the processed image results by a selective reconstruction using the 2<sup>nd</sup> and the 3<sup>rd</sup> level in a four levels decomposition scheme, (b) wavelet shrinking (WSRK) which is based on the elimination of the 1<sup>st</sup> and 4<sup>th</sup> decomposition levels, (c) wavelet background (WBGK) approximation in which, the preprocessed mammogram result from the 2<sup>nd</sup> and 3<sup>rd</sup> levels along with a background level approximation which extracted from the 4<sup>th</sup> decomposition level. The reported results show that sometimes the contrast without enhancement is better than its values with an enhancement method.

Rangayyan *et al.* [3] commented that many methods for the enhancement of mammograms may cause an amplification of noise or distortion of the anatomical features present in the image. Radiologists would prefer to have the enhanced image maintaining the familiar appearance of the original mammogram, which may limit the scope of enhancement techniques. However, with the introduction of direct digital imaging systems to mammography with increased contrast, dynamic range, and signal-to-noise ratio (SNR) the need of mammogram image enhancement may no longer remain.

### **2.7.2 Segmentation of Microcalcification in Digital Mammogram**

There are two different goals in segmentation of microcalcifications [27]. One is to obtain the locations of suspicious areas to assist radiologists for detection. The other is to classify the abnormalities of the breast into benign or malignant. Researchers have used several segmentation techniques as follows.

### 2.7.2.1 Thresholding Based Methods

It is used by setting threshold values for sub-images. It requires selection of a window size and threshold parameters. Davies *et al.* [111], [112] used a local thresholding technique to segment clustered microcalcifications. The local threshold is selected from the valley when the local histogram is bimodal. The segmented objects are analyzed using size, shape and gradient measures to extract clusters of microcalcifications. This method segments microcalcifications only based on the intensities of an image. It may not be correct and may affect the further processes. Mascio *et al.* [113] introduced a method for microcalcification segmentation in high-resolution digital mammograms. A threshold technique is applied to segment the microcalcifications. This method is limited to detect round shape microcalcifications. However, microcalcifications often occurs as variable shapes. Dengler *et al.* [114] introduced an algorithm of microcalcification segmentation. First, a high-pass filtering is performed by subtracting the low-pass Gaussian filtered image from the original image. Then, the difference between a detected spot and its neighbor spots is computed by the Gaussian operation with different weights. If the difference is less than a threshold, this spot is not considered to be a microcalcification. Li *et al.* [47] developed a technique for the detection of tumors in digital mammography. Initial segmentation scheme based on the knowledge that suspicious areas are greatly brighter than their surrounding tissues. The threshold for this separation is selected from the peak of the average contrast histogram.

### 2.7.2.2 Region Growing Based Methods

Region growing is a well-known method of segmentation. It is performed to group of pixels having similar properties with a seed point into a region. Shen *et al.* [90] proposed a technique based on region growing that requires the radiologist to manually select a seed pixel for each microcalcification particle. Paquerault *et al.* [115] also manually selected seed points, followed by an analysis of the radial gradient map. Qian *et al.* [116] applied a region grouping approach for microcalcification detection based on cluster analysis. The algorithm searches for individual regions and then stores them in a chain-form data structure to manipulate



them with great flexibility. The search of individual regions is straightforward. A pixel by pixel scan is performed from left upper corner to right lower.

### 2.7.2.3 *Morphological Operators Based Methods*

Some mathematical morphological operations such as erosion, top-hat transformation and complicated morphological filters and multi-structure elements can also be used for mammogram segmentation. Zhao *et al.* [117] developed a method to extract suspicious calcification regions based on morphological adaptive threshold and morphological skeleton information. Nishikawa *et al.* [118] combined morphological erosion operators with a difference image technique to segment calcification particles. Betal *et al.* [119] as well as Fu *et al.* [120] used the top-hat operator, which is defined as a subtraction of a morphologically opened image from the original image, followed by edge detection and flood filling for microcalcification segmentation.

### 2.7.2.4 *Wavelet Based Segmentation*

Because of their small size and their high degree of localization, microcalcifications represent high-spatial frequencies in the image. The wavelet transform is an attractive option for the detection of high-spatial-frequency components of an image because it can spatially localize high-frequency components. Hence, it was used by many authors for the segmentation of microcalcifications. The general idea of these approaches is to decompose a ROI into its subbands using the wavelet transformation and to weight the coefficients of the subbands so that microcalcifications are enhanced and background tissues, as well as noise are suppressed once the inverse wavelet transform is applied to the data. The common scheme for wavelet transform on the detection of microcalcification is to reconstruct the image from transform coefficients modified at each level by local and global nonlinear operators. Using the multiresolution capability, the wavelet transform could separate small objects (microcalcifications) from large objects (background structures). Salvado *et al.* [121] proposed a method for the microcalcification

detection that uses wavelet analysis and contrast enhancement. The proposed method has the following step, histogram analysis, 2 Dimensions-Discrete Wavelet Transformation (2D-DWT) analysis, noise removal and low-frequency band elimination, image enhancement and finally image reconstruction. The DWT uses Daubechies-6 orthogonal wavelet with 10 levels of decomposition. Yu *et al.* [122] used a wavelet filter for the detection of microcalcifications and a Markov random field model to obtain textural features from the neighborhood of every detected calcification. The Markov-random-field-based textural features, along with three auxiliary textural features (the mean pixel value, the gray-level variance, and a measure of edge density), were used to reduce the false positives. Soltanian-Zadeh *et al.* [36] compared four groups of features according to their discriminant power in separating microcalcifications into the benign and malignant categories. The microcalcifications were segmented using an automated method, and several features were extracted. Each feature belongs to one of the following four categories: multi-wavelet-based features, wavelet-based features, Haralick's texture features [89], and shape features. Within each group, a feature extraction procedure based on genetic algorithms was employed to identify the most suitable features to be used as input to a KNN classifier.

### **2.7.3 Feature Extraction and Classification of Microcalcifications**

The different approaches for microcalcifications detection are based on the feature extraction method. The following feature sets are used:

- Individual microcalcification features;
- Statistical texture features;
- Multiscale texture features.

#### *2.7.3.1 Microcalcification Detection Based on its Features*

Many researchers used features extracted from mammogram to directly describe individual microcalcification. Veldkamp and Karssemeijer [123] used a set of microcalcification features such as, perimeter, area, compactness, elongation,

eccentricity, thickness, mean intensity level of the background, mean intensity of the detected microcalcifications and contrast. These features form a feature vector and their distributions are used as cluster features. The method was tested on a set of 245 digitized mammograms having 341 clusters with a KNN classifier. The results showed the importance of the selected features. Zhang *et al.* [124] used a two stages scheme to reduce the false positive. Microcalcification features were divided into two categories, spatial features and morphology features. The first set of features includes; average gray level of the foreground, average gray level of the background, standard deviation of the gray level of the foreground, standard deviation of gray level of the background. The second set of features includes; compactness, moment, and Fourier descriptor. Features to describe clusters are also used including spatial features, morphology features and the cluster description features. In the first stage, they used a set of microcalcification features as the inputs of a back-propagation neural network to reduce the false detection. In the second stage, two more cluster features (cluster region size and cluster shape rate) are used as the inputs of the neural network to reduce the false detection rate. Fu *et al.* [120] extracted spatial domain features including both shape related features and window based features, with spectral domain features and texture features. The sequential forward search (SFS) and the sequential backward search (SBS) are used to select the most significant features.

### 2.7.3.2 *Microcalcification Detection Based On Statistical Texture Features*

Texture is a commonly used feature in the analysis and interpolation of images. It is characterized by a set of statistical properties of pixel intensities. Texture features calculated using a variety of statistical, structural and spectral techniques including co-occurrence matrices, fractal dimensions and multiresolution techniques such as wavelet. The most popular class of texture features are those derived from gray-level co-occurrence matrices, which represent second-order statistics of the gray levels in a ROI as described by Haralick *et al.* [89]. Soltanian *et al.* [36] compared four groups of features according to their discriminating power to classify microcalcifications into benign or malignant categories. Each feature belonged to one of the following four categories: shape feature, texture feature, wavelet features

and multiwavelet features. Consequently genetic algorithms based global search is used to select the most suitable features to be introduced to KNN classifier. The classification performance of each group of features was then determined using ROC analysis. The area under the ROC curve obtained ranged from 0.84 to 0.89, and it was observed that the multiwavelet features yielded the best performance, followed by the shape features. Pal *et al.* [125] proposed a multistage detection system of microcalcifications based on selecting a set of good features from a set of 87 features. Such features computed for the suspicious region. A multilayer perceptron network using back propagation algorithm is used for classification. The system is tested on seven normal and 10 abnormal mammogram images.

### *2.7.3.3 Microcalcification Detection Based on Multiscale Texture Features: Wavelet Based Method*

Wavelet theory provides a powerful framework for multiresolution analysis of mammogram images. The discrete wavelet transform is used to map the ROIs into a series of coefficients, which constituted a multiscale representation of ROIs. A set of features can be extracted from each scale of the wavelet transform. Strickland [126] developed a two-stage method based on wavelet transforms for the detection and segmentation of microcalcifications. The detection of calcifications is performed in the wavelet domain. The detected sites are enhanced in the wavelet domain, prior to the computation of the inverse wavelet transform. The appearance of microcalcifications is enhanced by this procedure; a threshold procedure suffices to segment the calcifications. The test database consisted of 40 mammograms, and a sensitivity of 91% at three false positives per image was obtained. Yu *et al.* [127] used wavelet transform coefficients and local statistic features (median contrast and normalized gray level value). The method was applied to a database of 40 mammograms from Nijmegen database containing 105 clusters of microcalcifications. A free response operating characteristics curve (FROC) was used to evaluate the performance. A 93% true positive and 1 false negative per image was reported. An improvement was presented by Yu and Guan [128] who developed a technique for the detection of clustered microcalcifications that consists of two parts; detection of potential microcalcification pixels and delineation of

individual microcalcifications by the elimination of false positives. The first part involves the extraction of features based on wavelet decomposition and gray-level statistics, followed by a neural-network classifier. The detection of individual objects requires a vector of 31 features related to gray-level statistics and shape factors, followed by a second neural-network classifier. A database of 40 mammograms containing 105 clusters of calcifications was used to assess the performance of the proposed algorithm, a sensitivity of 90% was attained with 0.5 false positive per image.

El-Naqa *et al.* [129] used support vector machines (SVM) to detect microcalcification clusters. The algorithm was tested using 76 mammograms, containing 1120 microcalcifications. A sensitivity of 94% was reported at one false positive per image. An improvement of the method was published by Wei *et al.* [130] using a relevance vector machine. A database of 141 mammograms containing microcalcifications was used to test the algorithm. The method achieved a sensitivity of 90% at one false positive per image. The statistical performance of the method was similar to that of the method of El-Naqa *et al.* [129], but the authors reported an improvement in computational speed. Ferreira and Borges [96] proposed system to classify the mammogram images by transforming the images into wavelet bases and then using a set of coefficients from first level of decomposition as the feature vector toward separating microcalcification clusters, spiculated mass, circumscribed mass and normal classes of image. Salvado *et al.* [121] proposed a method for the microcalcification detection that uses wavelet analysis. The proposed method has the following steps; histogram analysis, wavelet transform, noise removal and low-frequency band elimination, image enhancement and finally image reconstruction. The (db6) wavelet with 10 levels of decomposition was used. Mousa *et al.* [81] proposed a system based on wavelet analysis and used the adaptive neuro-fuzzy inference system (ANFIS) for building the classifier to distinguish between mass and microcalcification. The maximum classification rate obtained was 87.5%. Rashed *et al.* [97] studied the multiresolution analysis of digital mammogram using wavelet transform. They used Euclidean distance to classify between microcalcification clusters, spiculated mass, circumscribed mass, ill-defined mass and normal mammogram.

Yu *et al.* [122] used a wavelet filter for the detection of microcalcifications, and a Markov random field model to obtain textural features from the neighborhood of every detected calcification. The Markov-random-field-based textural features, along with three auxiliary textural features (the mean pixel value, the gray-level variance, and a measure of edge density), were used to reject false positives. The method was evaluated using 20 mammograms containing 25 areas of clustered microcalcifications. A sensitivity of 92% was obtained, at 0.75 false positive per image. Rizzi *et al.* [29] presented a method that preserved microcalcifications and remove the background by thresholding mammograms through a wavelet filter according to image statistical parameters (i.e. mean gray level pixel value and standard deviation). The reconstructed image is decomposed adopting another wavelet and each decomposition level is processed using a hard threshold technique. The results obtained in each level are combined to reduce false positive detections. A sensitivity of 98% at an average rate of 1 false positive per image was reported. A summary of selected methods for the detection of microcalcification is given in Table 2.3.

Table 2.3 Summary of the performance of selected methods for the detection and classification of microcalcifications.

Authors	Size of dataset	Results
Strickland [126]	40 mammograms.	Sensitivity of 91% with three false positives per image.
Yu <i>et al.</i> [127]	40 images from Nijmegen database containing 105 clusters of microcalcification.	93% true positive and 1 false negative per image
Yu and Guan [128]	40 images, 105 clusters of microcalcifications	Detection rate of 90% with 0.5 false positive per image.
El-Naqa <i>et al.</i> [129]	76 mammograms containing 1120 microcalcifications	Sensitivity of 94% at one false positive per image

Table 2.3 Summary of the performance of selected methods for the detection and classification of microcalcifications (Continued).

Authors	Size of dataset	Results
Wei <i>et al.</i> [130]	141 microcalcification mammograms.	Sensitivity of 90% at one false positive per image.
Soltanian <i>et al.</i> [36]	103 regions containing microcalcification clusters	Area under ROC curve from 0.84 to 0.89.
Ferreira and Borges [96]	25 microcalcifications from MIAS.	Classification rate of 100% with 100, 200 and 300 coefficients. But 33.3% with 500 coefficients.
Mousa <i>et al.</i> [81]	25 microcalcifications from MIAS.	Classification rate of 37.5%, 50% and 87.5% with levels 3-4, 2-4 and 2-3, respectively
Rashed <i>et al.</i> [97]	25 microcalcifications from MIAS.	82.66 % classification accuracy rate.
Yu <i>et al.</i> [122]	20 mammograms containing 25 areas of clustered microcalcification.	Sensitivity of 92% at 0.75 false positive per image
Rizzi <i>et al.</i> [29]	Microcalcifications images of MIAS dataset.	Sensitivity of 98% at one false positive per image.

## 2.8 Detection of Architectural Distortion

Architectural distortion is one of the most commonly missed abnormalities in screening mammography [3]. Architectural distortion is defined as distortion of the normal architecture with no definite mass visible, including spiculations radiating from a point and focal retraction or distortion at the edge of the parenchyma. The nonspecific definition of distortion and its subtle nature make the development of

image processing techniques for its detection a challenge [3]. Architectural distortion accounts for 12% – 45% of breast cancers overlooked or misinterpreted in screening mammography [26]. The improvement in the detection of architectural distortion could lead to an effective improvement in the prognosis of breast cancer patients. Whereas many publications have been directed toward the detection and analysis of calcifications and masses, relatively few attempts have been published on the detection of architectural distortion in mammograms [3], [27], [40].

Matsubara *et al.* [131] used mathematical morphology to detect architectural distortion around the skin line and a concentration index to detect architectural distortion within the mammary gland. The authors reported a sensitivity of 94% with 2.3 false positives per image and 84% with 2.4 false positives per image, respectively. Ichikawa *et al.* [132] developed a method to detect architectural distortion that encompasses the detection of linear structures using the mean curvature of the image. The detection of architectural distortion based on a set of local features that includes the concentration index. A sensitivity of 68% with 3.4 false positives per image was obtained.

Guo *et al.* [133] investigated the characterization of architectural distortion using the Hausdorff dimension and SVM classifier to distinguish between ROIs exhibiting architectural distortion and those with normal mammographic patterns. A set of 40 ROIs was selected from the MIAS database (19 ROIs with architectural distortion and 21 ROIs with normal tissue patterns). A classification accuracy of 72.5% was obtained. Tourassi *et al.* [134] studied the use of fractal dimension to differentiate between normal and architectural distortion patterns in mammographic ROIs. The dataset used in the investigation contained 112 ROIs with architectural distortion patterns and 1388 ROIs exhibiting normal tissue patterns. An area under the ROC curve achieved was 0.89. Eltonsy *et al.* [135] proposed a method for the detection of masses and architectural distortion based on the identification of points surrounded by concentric layers of image activity. A test dataset of 80 images was used in the evaluation of the technique containing 13 masses, 38 masses accompanied by architectural distortion and 29 images exhibiting only architectural distortion. The authors reported an overall sensitivity of 91.3% with 9.1 false positives per image. A sensitivity of 93.1% in the detection of pure architectural



distortion was also reported at the same level of false positives per image in the overall dataset.

Ayres and Rangayyan [136] studied the characterization of architectural distortion in mammographic ROIs using phase portraits. A database of 106 ROIs extracted from the MIAS dataset was used containing 17 cases of architectural distortion, 45 normals, two ROIs with malignant calcifications and 44 masses (eight spiculated malignant, four circumscribed malignant, 11 spiculated benign and 19 circumscribed benign masses). A sensitivity of 76.5% and a specificity of 76.4% were obtained, with an area under the ROC curve of 0.77. Ayres and Rangayyan [137] extend their work based on the analysis of oriented texture through the application of Gabor filters and a linear phase portrait model. They applied the proposed method to a set of 19 cases of architectural distortion and 41 normal mammograms, and another set of 37 cases with architectural distortion. The resulting FROC curve gave the sensitivity rates of 84% at 4.5 false positives per image and 81% at 10 false positives per image for the two sets of images. Banik *et al.* [138] presented a method based upon Gabor filters, phase portrait modeling, fractal analysis and Haralick's texture features [89]. The method was used to detect initial candidates for sites of architectural distortion in prior mammograms of interval-cancer and also normal cases. A total of 4212 regions of interest (ROIs) were automatically obtained from 106 prior mammograms of 56 interval-cancer cases including 262 ROIs related to architectural distortion, and from 52 prior mammograms of 13 normal cases. The results achieved are 0.75 with the Bayesian classifier, 0.71 with Fisher linear discriminant analysis (LDA) and 0.76 with an ANN based on radial basis functions (RBF). Analysis of the performance of the methods with FROC curve indicated a sensitivity of 0.80 at 10.5 false positives per image.

The current methods to detect architectural distortions are likely fail because they are typically designed to detect a radio-opaque circular density. New methods that focus on identifying radiating lines, regardless of the presence of a central mass region have the potential to be more sensitive for the detection of architectural distortions. We believe that a multiscale and multiorientation approaches would be most ideal for the detection of architectural distortions. Another important issue to

contend with is that radiating lines may have variable widths, frequencies, and so forth knowledge of degree of variation would help in the design of more sophisticated architectural distortions detection algorithms. It is clear that there is a need for further methods for objective characterization of the subtle and diverse patterns associated with architectural distortion from the perspectives of image processing and computer vision. Accurate detection of architectural distortion could be the key to efficient detection of early breast cancer at pre-mass formation stages. A summary of selected methods for the detection of architectural distortion is given in Table 2.4.

Table 2.4 Summary of the performance of selected methods for the detection and classification of architectural distortion.

Authors	Size of dataset	Results
Matsubara <i>et al.</i> [131]	55 mammograms exhibiting architectural distortion (17 with focal retraction, 38 with architectural distortion within the fibroglandular disk).	Detection of architectural distortion around the skinline: sensitivity of 94% with 2.3 false positives per image. Detection of architectural distortion within the fibroglandular disk: sensitivity of 84% with 2.4 false positives per image.
Ichikawa <i>et al.</i> [132]	94 mammograms exhibiting architectural distortion	Sensitivity of 68% with 3.4 false positives per image.
Guo <i>et al.</i> [133]	40 ROIs (19 ROIs with architectural distortion and 21 ROIs with normal tissues).	Classification accuracy of 72.5%.
Tourassi <i>et al.</i> [134]	112 ROIs with architectural distortion and 1388 ROIs exhibiting normal tissues.	Area under ROC curve 0.89.

Table 2.4 Summary of the performance of selected methods for the detection and classification of architectural distortion (Continued).

Authors	Size of dataset	results
Eltonsy <i>et al.</i> [135]	80 images (13 masses, 38 masses accompanied by architectural distortion, and 29 images exhibiting only architectural distortion).	Overall sensitivity of 91.3% with 9.1 false positives per image. Sensitivity of 93.1% in the detection of pure architectural distortion.
Ayres and Rangayyan [136]	106 ROIs (17 of architectural distortion, 45 normal, two malignant calcifications, eight spiculated malignant, four circumscribed malignant, 11 spiculated benign and 19 circumscribed benign masses).	Sensitivity of 76.5% and specificity of 76.4%, area under ROC curve 0.77
Ayres and Rangayyan, [137]	Two sets (19 mammograms with architectural distortion and 41 normal mammograms), and another set of 37 cases with architectural distortion.	The FROC curve gave the sensitivity rates of 84% at 4.5 false positives per image and 81% at 10 false positives per image for the two sets, respectively.
Banik <i>et al.</i> [138]	4212 (ROIs) were automatically obtained from 106 prior mammograms.	FROC curve indicated a sensitivity of 0.80 at 10.5 false positives per image.

## 2.9 Analysis of Bilateral Asymmetry

One of the cues used by radiologists to detect the presence of breast cancer is bilateral asymmetry, where the left and right breasts differ from each other in overall appearance in the corresponding mammographic images. Analysis of asymmetry can provide clues about the early signs of breast cancer such as developing densities,

parenchymal distortion and small asymmetric dense regions. Unlike for the detection and analysis of calcifications and masses, there are only a few publications on the detection of bilateral asymmetry in mammograms [26].

Scutt *et al.* [139] compared measures of bilateral breast asymmetry among women in a study group that included 252 asymptomatic women who had normal mammography but developed breast cancer later. With those of 252 age-matched women in a control group whose mammograms were normal and free of cancer during the study period. The breast volume was calculated from Cranio-Caudal (CC) mammograms and the relationships between asymmetry and the presence or absence of breast cancer were studied. Asymmetry was found to be a significant predictor of breast cancer.

A few studies have been presented in the literature on digital image processing techniques addressing bilateral asymmetry, with most of them applying some type of alignment of the left and right breast images before performing asymmetry analysis [140], [141]. Lau and Bischof [140] proposed procedures to compare the corresponding anatomical regions between the left and right breast images in terms of shape, texture and density. They also proposed a directional feature to quantify oriented patterns. However, alignment procedures encounter problems such as the natural asymmetry of the breasts of a given subject, the lack of good corresponding points between the left and right breast images to perform matching and distortions inherent to mammographic imaging. They devised a method for the detection of breast tumors using a localized definition of asymmetry that encompassed measures of brightness, roughness and directionality. The method was evaluated using 10 pairs of mammograms where asymmetry was a significant factor in the radiologists' diagnosis. A sensitivity of 92% was obtained with 4.9 false positives per mammogram image.

Miller and Astley [141] proposed procedures to compare the corresponding anatomical regions between the left and right breast images in terms of shape, texture and density. They also proposed a technique for the detection of bilateral asymmetry that comprised a semi-automated texture-based procedure for the segmentation of the glandular tissue and measures of shape and registration cost

between views for detection of the occurrence of asymmetry. An accuracy of 86.7% was reported on a test dataset of 30 screening mammogram pairs. They also presented a method for the detection of bilateral asymmetry based on measures of shape, topology and distribution of brightness in the fibroglandular disk [142]. The method was tested on 104 mammogram pairs and a classification accuracy of 74% was obtained.

Ferrari *et al.* [143] developed a method for the analysis of asymmetry in mammograms using directional filtering with Gabor wavelets. In their method, which was applied to MLO views, the breast boundary is detected first and all artifacts outside the breast are removed [144]. Then, the pectoral muscle is detected and removed [145]. The fibroglandular disk is segmented [146] and the resulting image is decomposed using a bank of Gabor filters at 12 orientations and four scales. The Karhunen–Loeve transform is employed to select the principal components of the filters responses. A database of 80 images containing 20 normal cases, 14 asymmetric cases, and six architectural distortion cases was used to evaluate the algorithm. The reported classification accuracy rates were up to 74.4%.

Rangayyan *et al.* [147] extended the method of Ferrari *et al.* [143] by including morphological measures quantifying differences in fibroglandular tissue covered area in the left and right breasts, which relate to size and shape; in addition, the directional data were aligned with reference to the edge of the pectoral muscle (in MLO views). A sensitivity of 82.6% and a specificity of 86.4% were obtained in the detection of bilateral asymmetry. The presence of bilateral asymmetry has been shown to be an important predictor of breast cancer. More methods are desirable in this area to analyze asymmetry from multiple perspectives, including pattern asymmetry in the fibroglandular tissue as well as morphological and density measures related to the breast and the fibroglandular disk. Table 2.5 summarizes the performance of selected methods for bilateral asymmetry detection in digital mammogram.

Table 2.5 Summary of the performance of selected methods for the detection and classification of bilateral asymmetry.

Authors	Size of dataset	Results
Lau and Bischof [140]	Dataset of 10 pairs of mammograms.	Sensitivity of 92% was obtained with 4.9 false positives per image.
Miller and Astley [141]	Dataset of 30 screening mammogram pairs.	An accuracy of 86.7% was reported.
Miller and Astley [142]	104 mammogram pairs.	Classification accuracy of 74% was obtained.
Ferrari <i>et al.</i> [143]	A database of 80 images containing 20 normal cases, 14 asymmetric cases and six architectural distortion cases.	The reported classification accuracy rates were up to 74.4%.
Rangayyan <i>et al.</i> [147]	88 mammograms from the MIAS database.	Sensitivity of 82.6% and specificity of 86.4% were obtained.

## 2.10 Summary

In the literature, there exists a substantial record of research on the detection and classification of masses and calcifications. These two types are generally considered to be well studied. The new developments must meet or exceed the high standards of performance set by the existing algorithms. Furthermore, commercial CAD systems have achieved a satisfactory degree of effectiveness in the detection of masses and calcifications. Future work on computer aided systems for breast cancer diagnosis should focus on improving the performance of CAD systems. Feature extraction is one of the important steps in developing CAD system. A broad variety of features for the characterization of breast cancer have been developed in the past years. Hence more researches seem to be necessary to measure the robustness features that

can produce a high classification accuracy rate. Selecting the optimal feature subset for supervised learning problems requires an exhaustive search. The discriminative power of features employed in CAD systems varies. While some are highly significant for the discrimination of mammographic lesions, others are redundant or even irrelevant. Hence, automatic extraction of a subset of features from a higher dimensional feature vector is a common module in mammography CAD approaches.

A variety of classifiers have been applied in the state of the art CAD approaches to solve this problem. The KNN classifier is not only one of the most commonly employed classifiers for the discrimination of mammographic lesions, but also one of the simplest and most popular classifiers in general. ANNs and SVM have also been used as classifiers in mammography CAD systems.

Masses are more difficult to detect than microcalcifications because the features of a mass may be obscured by or be similar to those of normal breast parenchyma. Thus, mass detection remains an important topic in breast cancer detection. We note that masses can have a range of sizes. Thus, a major limitation of the proposed methods is that the analysis is not done over a continuous range of scales. Cancerous lesions are stochastic biologic phenomena that manifest in images as having various structures occurring at different sizes and over ranges of spatial scales. Masses are occupying definite regions; this region occupancy can be approached at a coarse scale of description or processing. However, the boundaries of masses require a more localized approach, although the sharpness, and hence the scales of interpretation of the lesion boundaries, can vary considerably. Moreover, the spiculations that are associated with many cancerous lesions occur with different widths, lengths, and densities, which suggest that their characterization will require analysis over scales. Since wavelets are ideal for capturing point discontinuities but not edges. We believe that this fact intuitively explains the tremendous success of wavelet transform-based methods in the detection of calcifications and why they have been less successful for the detection of masses. In addition to wavelets, other multiscale methods such as curvelet need to investigate.

Besides mass detection, other important topics are the detection of architectural distortion and the detection of bilateral asymmetry in mammograms. These two

types of abnormality still demand attention of research in CAD systems for breast cancer. A relatively small number of researchers have concentrated their attention on the problem of detecting architectural distortion and bilateral asymmetry. Currently, the detection of both architectural distortion and bilateral asymmetry in mammograms are important research topics, and efficient solutions to these two issues could improve the performance of CAD systems.



## CHAPTER 3

### THEORETICAL BACKGROUND

#### 3.1 Overview

This chapter presents the theoretical background of wavelet, curvelet and multiresolution representation. They show an effective performance in image processing applications. Multiresolution representation allows zooming in and out on the underlying texture structure. The multiresolution quality is one of the reasons that make wavelet and curvelet useful in many applications. In this chapter we introduce an overview of wavelet and curvelet. This chapter starts by introducing wavelet in one and two dimensions in Section 3.2. Section 3.3 gives an introduction and description of the mathematical background of curvelet. Then, KNN classifier and SVM are presented in Section 3.4. Finally, the chapter is summarized in Section 3.5.

#### 3.2 Wavelet Transform

Wavelet transform is one of the most popular techniques of obtaining multiresolution representations of signals. It has the advantage of localizing the information in both time and frequency domain. The wavelet is the function used as basis for represent another function [148]. It denoted as

$$\Psi_{a,b} = \frac{1}{\sqrt{|a|}} \Psi\left(\frac{x-b}{a}\right) \quad (3.1)$$

where  $b$  is location parameter and  $a$  is scaling parameter. For the function to be wavelet it should be limited. The basic idea of the wavelet transform is approximating a signal through a set of basic mathematical functions.

The wavelet transform of a function  $f(x) \in L^2(\mathbf{R})$  is

$$\mathbf{C}_f(a, b) = \frac{1}{\sqrt{|a|}} \int_{-\infty}^{\infty} f(x) \Psi\left(\frac{x-b}{a}\right) dx \quad (3.2)$$

The function  $f(x)$  is then described by its wavelet coefficients  $\mathbf{C}_f(a, b)$ , where  $a > 0, b \in \mathbf{R}$ . The discrete wavelet transform is obtained by taking  $a = 2^j, b = k2^j = ka$  for  $k, j \in \mathbf{Z}^2$ .

In the following section, we give an overview of wavelet based multiresolution representation of signals. We present the concept of one dimensional signal and then the model is extended to two dimensions.

### 3.2.1 Multiresolution and One Dimensional Wavelet Representation

The multiresolution approximation of one dimensional signal  $f(x) \in L^2(\mathbf{R})$  at a resolution  $2^j$  is defined as the orthogonal projection of a signal on subspace  $V_{2^j}$  of  $L^2(\mathbf{R})$ .  $V_{2^j}$  can be interpreted as the set of all possible approximations at the resolution  $2^j$  of functions in  $L^2(\mathbf{R})$ . The set of vector spaces  $V_{2^j}$  is said to be a multiresolution representation of  $L^2(\mathbf{R})$  if it satisfies the following properties [149]:

- 1) The approximation of a signal at resolution  $2^{j+1}$  contains all the necessary information to obtain its approximation at coarser resolution  $2^j$ :

$$V_{2^j} \subset V_{2^{j+1}}, \forall j \in \mathbf{Z} \quad (3.3)$$

- 2) The space of approximated function can be derived from one another by scaling each approximated function by the ratio of their resolution:

$$f(x) \in V_{2^j} \Leftrightarrow f(2x) \in V_{2^{j+1}}, \forall j \in \mathbf{Z} \quad (3.4)$$

- 3) The approximation  $A_{2^j} f(x)$  of a signal  $f(x)$  can be characterized by  $2^j$  samples per length unit, or equivalently, there exist a mapping  $M: V_1 \rightarrow l^2(\mathbf{Z})$  such that

signals in  $V_1$  can be represented at 1 sample per length unit. This is essentially the sampling theorem:

$$M(V_1) = (\alpha_i)_{i \in \mathbf{Z}} \quad (3.5)$$

- 4) When  $f(x)$  is translated by length proportional to  $2^j$ ,  $A_{2^j}f(x)$  is translated by the same amount and is characterized by the same sample that have been translated. As a consequence of property 2, it is sufficient to express this for resolution  $j = 0$ :

$$A_1 f_k(x) = A_1 f(x - k), \text{ where } f_k(x) = f(x - k), \forall k \in \mathbf{Z} \quad (3.6)$$

$$M(A_1 f(x)) = (\alpha_i)_{i \in \mathbf{Z}} \Leftrightarrow M(A_1 f_k(x)) = (\alpha_{i-k})_{i \in \mathbf{Z}}, \forall k \in \mathbf{Z} \quad (3.7)$$

- 5) As the resolution increases to  $+\infty$  the approximated signal converges to the original signal. On the other hand, as the resolution decreases to zero, the approximated signal converges to zero:

$$\lim_{j \rightarrow +\infty} V_{2^j} = \bigcup_{j=-\infty}^{+\infty} V_{2^j} \text{ is dense in } \mathbf{L}^2(\mathbf{R}) \quad (3.8)$$

$$\lim_{j \rightarrow -\infty} V_{2^j} = \bigcap_{j=-\infty}^{+\infty} V_{2^j} = \{0\} \quad (3.9)$$

Let  $O_{2^j}$  be the vector space that satisfies that:  $O_{2^j}$  is orthogonal to  $V_{2^j}$  and  $O_{2^j} \oplus V_{2^j} = V_{2^{j+1}}$ , i.e. the orthogonal complement of  $V_{2^j}$  in  $V_{2^{j+1}}$ . The approximation  $A_{2^{j+1}}f(x)$  at resolution  $2^{j+1}$  contains more information than the approximation  $A_{2^j}f(x)$  at resolution  $2^j$ . The details signal of  $f(x)$  at resolution  $2^j$  are denoted by  $D_{2^j}f(x)$ . The details can be defined as the difference between  $A_{2^{j+1}}f(x)$  and  $A_{2^j}f(x)$ .  $D_{2^j}f(x)$  is equivalent to the orthogonal projection of  $f(x)$  on the complement  $O_{2^j}$  of vector space  $V_{2^j}$  in  $V_{2^{j+1}}$ . According to the theory of multiresolution signal decomposition [149], there exists a unique scaling function  $\varphi(x) \in \mathbf{L}^2(\mathbf{R})$  and a unique corresponding wavelet function  $\psi(x) \in \mathbf{L}^2(\mathbf{R})$ , where

$\varphi_{2^j}(x) = 2^j \varphi(2^j x)$  and  $\psi_{2^j}(x) = 2^j \psi(2^j x)$ , such that  $\{2^{-j/2} \varphi_{2^j}(x - 2^{-j} k)\}_{k \in \mathbb{Z}}$  and  $\{2^{-j/2} \psi_{2^j}(x - 2^{-j} k)\}_{k \in \mathbb{Z}}$  are orthogonal bases of  $O_{2^j}$  and  $V_{2^j}$ , respectively. The approximation and detail signals of the original signal  $f(x)$  at resolution  $2^j$  are completely characterized by the sequence of inner products of  $f(x)$  with  $\varphi_{2^j}$  and  $\psi_{2^j}$  as follows:

$$\{A_{2^j} f(k)\}_{k \in \mathbb{Z}} = \{\langle f(o), \varphi_{2^j}(o - 2^{-j} k) \rangle\}_{k \in \mathbb{Z}} \quad (3.10)$$

$$\{D_{2^j} f(k)\}_{k \in \mathbb{Z}} = \{\langle f(o), \psi_{2^j}(o - 2^{-j} k) \rangle\}_{k \in \mathbb{Z}} \quad (3.11)$$

Let  $H$  be a low-pass filter and  $G$  be a high-pass filter, where the impulse response of the filter  $H$  is  $h(k) = \langle \varphi_{-1}(x), \varphi(x - k) \rangle$ , and the impulse response of the filter  $G$  is  $g(x) = \langle \psi_{-1}(x), \psi(x - k) \rangle$ . Define  $\tilde{H}$  with impulse response  $\tilde{h}(k) = h(-k)$  to be the mirror filter of  $H$ , and  $\tilde{G}$  with impulse response  $\tilde{g}(k) = g(-k)$  to be the mirror filter of  $G$ . The multiresolution representation of  $f(x)$  at any resolution  $2^j$  can be implemented by a pyramidal algorithm as shown in Figure 3.1:

$$A_{2^{j-1}} f(x) = \sum_{k=-\infty}^{\infty} \tilde{h}(2x - k) A_{2^j} f(k) \quad \text{where } j=0,-1,-2,\dots \quad (3.12)$$

$$D_{2^{j-1}} f(x) = \sum_{k=-\infty}^{\infty} \tilde{g}(2x - k) A_{2^j} f(k) \quad \text{where } j=0,-1,-2,\dots \quad (3.13)$$

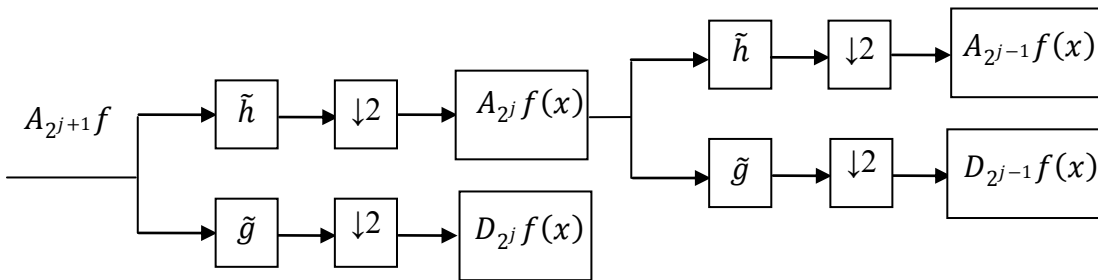


Figure 3.1 A wavelet decomposition of a signal  $A_{2^{j+1}}f$ .

### 3.2.2 Two-Dimensional Wavelet Representation

The wavelet model can be extended to two-dimensional signals by separable multiresolution approximation of  $L^2(\mathbb{R}^2)$  with scaling function  $\varphi(x, y) = \varphi(x)\varphi(y)$ . And  $\psi(x)$  is the one-dimensional wavelet function associated with  $\varphi(x)$ . There are three associated wavelet functions  $\psi^1(x, y) = \varphi(x)\psi(y)$ ,  $\psi^2(x, y) = \psi(x)\varphi(y)$  and  $\psi^3(x, y) = \psi(x)\psi(y)$ . With this formulation, the wavelet decomposition of a two dimensional signal can be computed with a separable extension of the one-dimensional decomposition algorithm as shown in Figure 3.2.

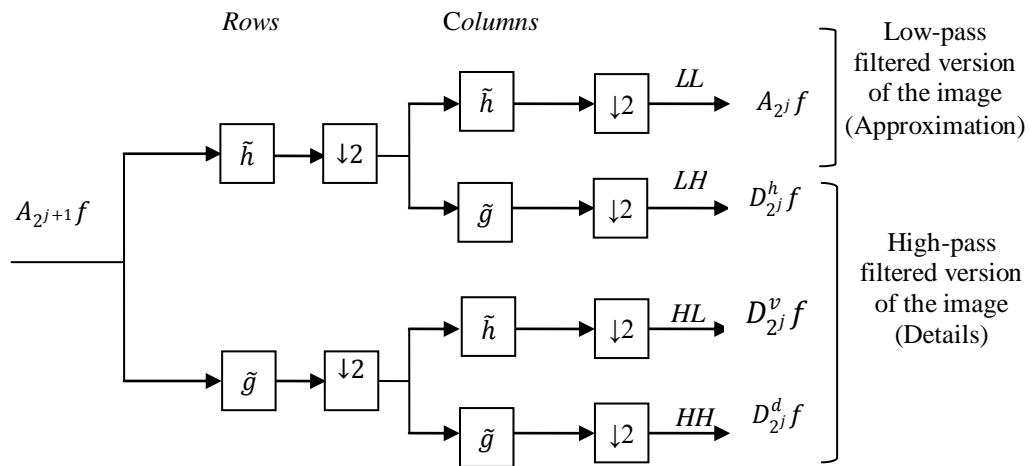


Figure 3.2 A wavelet decomposition of an image.

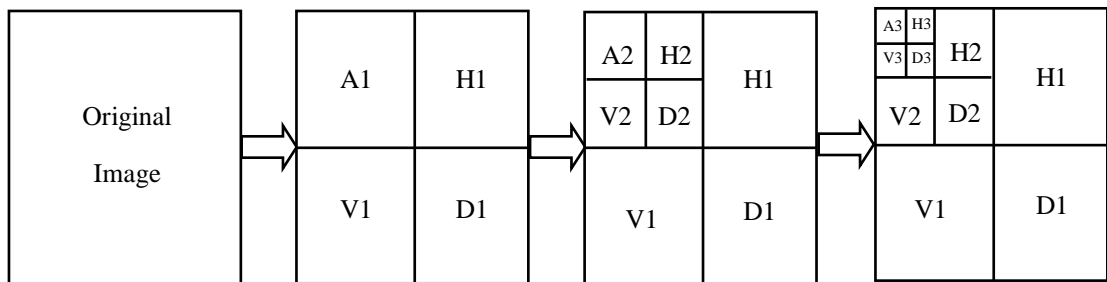


Figure 3.3 Three levels multiresolution decomposition wavelet.

Figure 3.3, illustrates the decomposition of the image  $A_{2^{j+1}}f$  into  $A_{2^j}f$ ,  $D_{2^j}^h f$ ,  $D_{2^j}^v f$ , and  $D_{2^j}^d f$  in the frequency domain. The images  $A_{2^j}f$ ,  $D_{2^j}^h f$ ,  $D_{2^j}^v f$  and  $D_{2^j}^d f$  corresponding to the lowest frequencies, the vertical high frequencies

(horizontal edges), the horizontal high frequencies (vertical edges) and the high frequencies in both directions (diagonal), respectively. i.e., the image  $A_{2^{j+1}}f = A_{2^j}f + D_{2^j}^h f + D_{2^j}^v f + D_{2^j}^d f$ . This set of images is called an orthogonal wavelet representation in two dimensions [149]. The image  $A_{2^j}f$  is the coarse approximation at the resolution  $2^j$ , and the images  $D_{2^j}^h f, D_{2^j}^v f$  and  $D_{2^j}^d f$  give the detail signals for different orientations and resolutions. If the original image has  $N$  pixels, then each of the images  $D_{2^j}^h f, D_{2^j}^v f$  and  $D_{2^j}^d f$  will have  $2^j N$  pixels ( $j < 0$ ), so that the total number of pixels in this new representation is equal to the number of pixels of the original image, to keep the volume of data maintained. This process can be summarized as, wavelet decompose an image into orthogonal sub-bands with low–low (LL), low–high (LH), high–low (HL) and high–high (HH) components which corresponding to approximation, horizontal, vertical and diagonal, respectively. The LL sub-band is further decomposed into another four sub-bands low–low–low–low (LLLL) component, which represents the image approximation at this level, and then it is decomposed once again and so on [150].

### 3.3 Curvelet Transform

Discrete curvelet transform is a new image representation approach that codes image edges more efficiently than wavelet transform [151]. Indeed, curvelet have useful geometric features that set them apart from wavelet. Curvelet is better than wavelet in the following cases [152]:

- 1) Optimally sparse representation of objects with edges.
- 2) Optimal image reconstruction in severely ill-posed problems.
- 3) Optimal sparse representation of wave propagators.

The curvelet transform coefficients of the object are used as a feature vector. Suppose we have a function  $f$  which has a discontinuity across a curve, and which is smooth otherwise, and consider approximating  $f$  from the best  $m$ -terms in the expansion. The squared error of such an  $m$ -term expansion obeys [152]:

$$\|f - f_{\tilde{F}}\|^2 \propto \frac{1}{\sqrt{m}}, m \rightarrow +\infty \quad (3.14)$$

( $f_{\tilde{F}}$  is the approximation from  $m$  best Fourier coefficients).

In a wavelet expansion, we have

$$\|f - f_{\tilde{W}}\|^2 \propto \frac{1}{m}, m \rightarrow +\infty \quad (3.15)$$

( $f_{\tilde{W}}$  is the approximation from  $m$  best wavelet coefficients).

In a curvelet expansion, we have

$$\|f - f_{\tilde{C}}\|^2 \propto \frac{1}{m^2} (\log m)^3, m \rightarrow +\infty \quad (3.16)$$

( $f_{\tilde{C}}$  is the approximation from  $m$  best curvelet coefficients).

This shows that the mean squared error will be reduced in curvelet. A fast and accurate discrete curvelet transform operating on digital data is required to use curvelet transform in various applications.

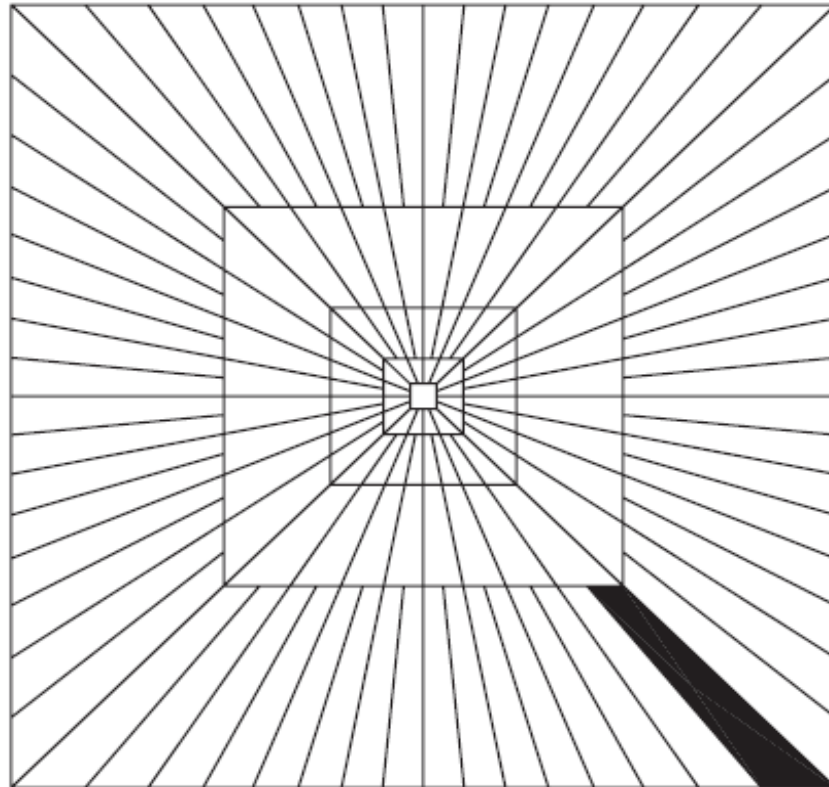


Figure 3.4 Curvelet basic digital tiling in two dimensions. The shaded region represents one such typical wedge.

Figure 3.4 illustrates the curvelet tiling. A Fast Discrete Curvelet Transform (FDCT) is described in [152] as it follows. The work is done throughout in two dimensions, i.e.,  $\mathbf{R}^2$  with  $x$  as spatial variable,  $\omega$  as frequency domain variable,  $r$  and  $\theta$  polar coordinates in the frequency domain. A pair of windows  $W(r)$  and  $V(t)$  are defined, which will be called the radial window and angular window, respectively. These are smooth, nonnegative and real-valued, with  $W$  taking positive real arguments and supported on  $r \in (1/2, 2)$  and  $V$  taking real arguments and supported on  $t \in [-1, 1]$ . These windows will always obey the admissibility conditions [148]:

$$\sum_{j=-\infty}^{\infty} W^2(2^j r) = 1, \quad r \in \left(\frac{3}{4}, \frac{3}{2}\right) \quad (3.17)$$

$$\sum_{l=-\infty}^{\infty} V^2(t - l) = 1, \quad t \in \left(-\frac{1}{2}, \frac{1}{2}\right) \quad (3.18)$$

For each  $j \geq j_0$ , a frequency window  $U_j$  defined in the Fourier domain by

$$U_j(r, \theta) = 2^{-\frac{3}{4}j} W(2^{-j}r) V\left(\frac{2^{\lfloor j/2 \rfloor} \theta}{2\pi}\right) \quad (3.19)$$

Where  $\lfloor j/2 \rfloor$  is the integer part of  $j/2$ . Thus the support of  $U_j$  is a polar wedge defined by the support of  $W$  and  $V$ , the radial and angular windows, applied with scale dependent window widths in each direction. The symmetrized version of (3.19), namely,  $U_j(r, \theta) + U_j(r, \theta + \pi)$  is used to obtain real valued curvelet.

Define the waveform  $\varphi_j(x)$  by means of its Fourier transform  $\widetilde{\varphi}_j(\omega) = U_j(\omega)$ . Let  $U_j(\omega_1, \omega_2)$  be the window defined in the polar coordinate system by equation (3.19).  $\varphi_j$  is the mother curvelet in the sense that all curvelets at scale  $2^{-j}$  are obtained by rotations and translations of  $\varphi_j$ . Introduce rotation angles  $\theta_l = 2\pi \cdot 2^{-\lfloor j/2 \rfloor} \cdot l$ , with  $l = 0, 1, \dots$  such that  $0 \leq \theta \leq 2\pi$ , the spacing between consecutive angles is scale dependent and the sequence of translation parameters  $k = (k_1, k_2) \in$



$\mathbf{Z}^2$ . The curvelets are defined (as a function of  $x = (x_1, x_2)$ ) at scale  $2^{-j}$ , orientation angle  $\theta_l$  and position  $x_k^{(j,l)} = R_{\theta_l}^{-1}(k_1 \cdot 2^{-j}, k_2 \cdot 2^{-j/2})$  by

$$\varphi_{j,l,k}(x) = \varphi_j \left( R_{\theta_l} \left( x - x_k^{(j,l)} \right) \right) \quad (3.20)$$

where  $R_\theta$  is the rotation by  $\theta$  radians and  $R_\theta^{-1}$  its inverse,

$$R_\theta = \begin{pmatrix} \cos \theta & \sin \theta \\ -\sin \theta & \cos \theta \end{pmatrix}, \quad R_\theta^{-1} = R_\theta^T = R_{-\theta}.$$

A curvelet coefficient is the inner product between an element  $f \in L^2(\mathbf{R}^2)$  and a curvelet  $\varphi_{j,l,k}$ ,

$$c(j, l, k) := \int_{\mathbf{R}^2} f(x) \overline{\varphi_{j,l,k}(x)} dx \quad (3.21)$$

Where  $\mathbf{R}$  denotes the real line. Curvelet transform obeys an anisotropy scaling relation,  $length \approx 2^{-j/2}$ ,  $width = 2^{-j}$ . i.e.  $width \approx length^2$ . This equation is called a curve scaling law [151].

### 3.4 Classifiers Used in the Work

In this work two different classifiers are investigated. One is KNN which is simple and fast classifier, the other is SVM which seek the optimal boundary between two classes.

#### 3.4.1 KNN Classifier

The KNN starts firstly by building the core of each class. The class core vector is calculated as the mean of set of training data. For each class, the class core vector is calculated using equation (3.22). For a new testing image, the distances between its feature vector and the classes' core vectors are calculated using equation (3.23). The system automatically classifies the feature vector in the class for which the distance obtained is the smallest.

$$V_{core}^i = \frac{1}{N} \sum_{j=1}^{j=N} V_j^i \quad (3.22)$$

$$Dist = \sqrt{\sum_{i=1}^k (V_{core}^i - V_{test}^i)^2} \quad (3.23)$$

Where  $V_{core}^i$  is the vector core of the corresponding class,  $V_j$  is the coefficient vectors for ROIs of the corresponding class,  $i$  is the index of the vector,  $N$  is the number of images used to produce the class core vector,  $Dist$  is the calculated distance between the tested image and the class core vector,  $k$  is the length of vector, and  $V_{test}^i$  is the feature vector of mammogram to be classified.

### 3.4.2 SVM Classifier

SVM is an algorithm for learning linear classifiers. It is motivated by the idea of maximizing margins [153]. Given  $n$  vectors  $\mathbf{v}_0, \mathbf{v}_1, \dots, \mathbf{v}_{n-1}$  from the vector space  $\mathbf{R}^m$  which are from two classes. The training data are  $\{(\mathbf{v}_j, y_j): j = 0, 1, \dots, n-1\}$  where  $y_j \in \{+1, -1\}$ . The goal is to learn a classification rule from the training data which only makes small classification errors. Given a weight vector  $\mathbf{w}$  and a bias  $b$ , it is assumed that these two classes can be separated by two margins parallel to the hyperplane:

$$\mathbf{w}^T \mathbf{v}_j + b \geq 1, \text{ for } y_j = +1 \quad (3.24)$$

$$\mathbf{w}^T \mathbf{v}_j + b \leq -1, \text{ for } y_j = -1 \quad (3.25)$$

for  $j = 0, 1, \dots, n-1$  and  $\mathbf{w} = (w_0, w_1, \dots, w_{m-1})^T$  is the column vector of  $m$ -elements. Inequalities (3.24) and (3.25) can be combined into a single Inequality

$$y_j(\mathbf{w}^T \mathbf{v}_j + b) \geq 1, \text{ for } j = 0, 1, \dots, n-1 \quad (3.26)$$

There exists a number of separating hyperplanes for an identical group of training data. The objective of the SVM is to determine the optimal weight  $\mathbf{w}^*$  and the optimal bias  $b^*$  such that the corresponding hyperplane separates the data of both classes with maximum margin. The equation for an arbitrary hyperplane is given by

$$\mathbf{w}^T \mathbf{x} + b = 0 \quad (3.27)$$

The distance between the two corresponding margins is

$$\gamma(\mathbf{w}^*, b^*) = \frac{2}{\|\mathbf{w}\|} \quad (3.28)$$

The saddle point of the Lagrange function

$$L_p(\mathbf{w}, b, \alpha) = \frac{1}{2} \mathbf{w}^T \mathbf{w} - \sum_{j=0}^{n-1} \alpha_j (y_j (\mathbf{w}^T \mathbf{v}_j + b) - 1) \quad (3.29)$$

Gives the solution to the minimization problem, where  $\alpha_j \geq 0$  are Lagrange multiplier. The solution of this optimization problem requires that the gradient of  $L_p(\mathbf{w}, b, \alpha)$  with respect to  $\mathbf{w}$  and  $b$  vanishes.

$$\left. \frac{\partial L_p}{\partial \mathbf{w}} \right|_{\mathbf{w}=\mathbf{w}^*} = 0, \quad \left. \frac{\partial L_p}{\partial b} \right|_{b=b^*} = 0$$

we obtain

$$\mathbf{w}^* = \sum_{j=0}^{n-1} \alpha_j y_j \mathbf{v}_j$$

and

$$\sum_{j=0}^{n-1} \alpha_j y_j = 0$$

inserting the obtained values into (3.29) yields

$$L_D(\alpha) = \sum_{i=0}^{n-1} \alpha_i - \frac{1}{2} \sum_{i=0}^{n-1} \sum_{j=0}^{n-1} \alpha_i \alpha_j y_i y_j \mathbf{v}_i^T \mathbf{v}_j \quad (3.30)$$

under the constraints

$$\sum_{j=0}^{n-1} \alpha_j y_j = 0, \quad \alpha_j \geq 0, \quad j = 0, 1, \dots, n-1$$

The points located on the two optimal margins will have nonzero coefficients  $\alpha_j$  among the solution of maximum  $L_D(\alpha)$  and the constraints. These vectors with nonzero coefficients  $\alpha_j$  are called support vectors. The bias  $b^*$  can be calculated as follows

$$b^* = -\frac{1}{2} \left( \min_{\{v_j | y_j = +1\}} \mathbf{w}^{*T} \mathbf{v}_j + \max_{\{v_j | y_j = -1\}} \mathbf{w}^{*T} \mathbf{v}_j \right) \quad (3.31)$$

After determination of the support vectors and bias, the decision function that separates the two classes can be calculated as follows [153],

$$f(\mathbf{x}) = \text{sgn} \left( \sum_{j=0}^{n-1} \alpha_j y_j \mathbf{v}_j^T \mathbf{x} + b^* \right) \quad (3.32)$$

### 3.5 Summary

This chapter gives the mathematical background for both multiresolution representations wavelet and curvelet. It presents how the wavelet can describe the signal in one and two dimensions for multilevel representation. Then, it describes multilevel representation of signals using curvelet transform. Finally it presents the classifiers used in the work: KNN and SVM.

## CHAPTER 4

### COMPUTER AIDED DIAGNOSIS SYSTEM DEVELOPMENT

#### **4.1 Overview**

The study is designed to develop a computer aided diagnosis (CAD) system for breast cancer in digital mammogram. The proposed system is applied to solve three mammogram classification problems:

- 1) The classification of normal versus abnormal class.
- 2) The classification of abnormalities (i.e. microcalcification clusters, spiculated masses, circumscribed masses, ill-defined masses, architectural distortion and bilateral asymmetry).
- 3) The classification of risk level of cancerous cells based on tumor nature (i.e. benign versus malignant).

The developed system starts by classifying between the normal and abnormal mammograms in the first step. In step two, the abnormal mammograms are classified according to the shape of the abnormality into microcalcification clusters, circumscribed mass, spiculated mass, ill-defined mass, architectural distortion and asymmetry. In step three, the developed system determines whether the abnormality is benign or malignant. Figure 4.1, illustrates the steps of the developed system.

The work in this study consists of two main parts. Part I contains the development of a computer aided diagnosis system. In this part, the regions of interest (ROIs) are extracted manually from the original mammogram images. The multiresolution representations curvelet and wavelet are then used to decompose the ROIs. Consequently, five feature extraction methods are presented to distinguish between the different classes of breast cancer. Finally, the classification accuracy rates are evaluated using K-nearest neighbor (KNN) and SVM classifiers. In part II, ROIs are detected automatically followed by curvelet decomposition and feature

extraction methods. The classification accuracy rates are calculated using KNN and SVM. The following Sections 4.2 and 4.3 describe the procedure for each part, respectively.

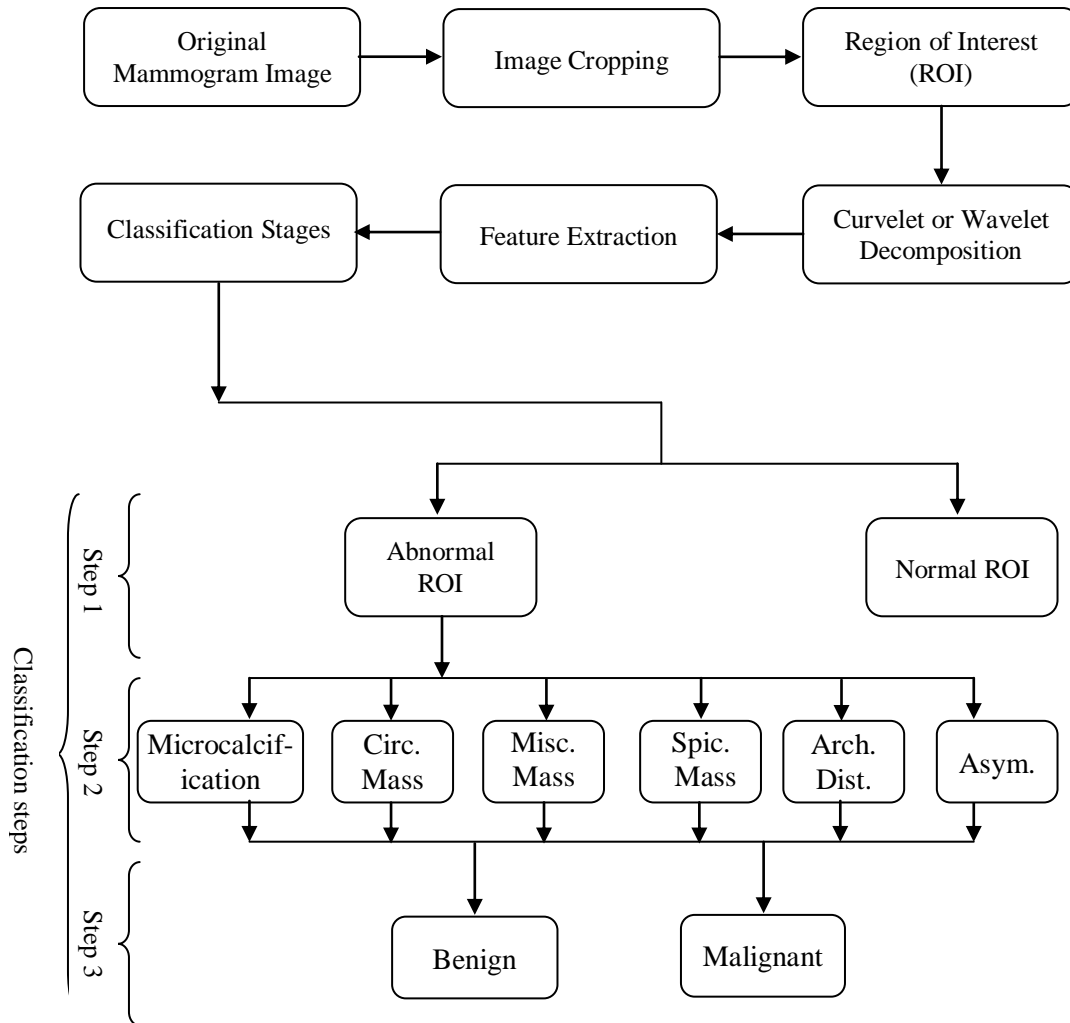


Figure 4.1 The proposed computer aided diagnosis system.

## 4.2 Part I: Computer Aided Diagnosis System

This part presents the method of developing computer aided diagnosis system via five methods for feature extraction from the multiresolution decompositions curvelet and wavelet. In this part, the ROIs are cropped manually as described in the following section.

### 4.2.1 Mammogram Cropping

The original mammograms are 1024 x 1024 pixels, and almost 50% of the image comprised of the background with a lot of noise such as label and pectoral muscle. Therefore a cropping operation is applied to the images to cut off the unwanted portions of the images. Regions of interest (ROI's) 128x128 are cropped. The cropping process was performed manually, where the given center of the abnormality area is selected to be the center of ROI. Thus, almost all the background information and most of the unwanted regions are eliminated. By this method we are sure that no abnormality was suppressed with the background. Figure 4.2, illustrates an example of cropping process that eliminates the label on the image and the black background. A sample of the obtained ROIs is presented in Figure 4.3. Once the ROIs are cropped, the wavelet or curvelet decompositions are applied in order to extract and select the most significant features to distinguish between different classes.

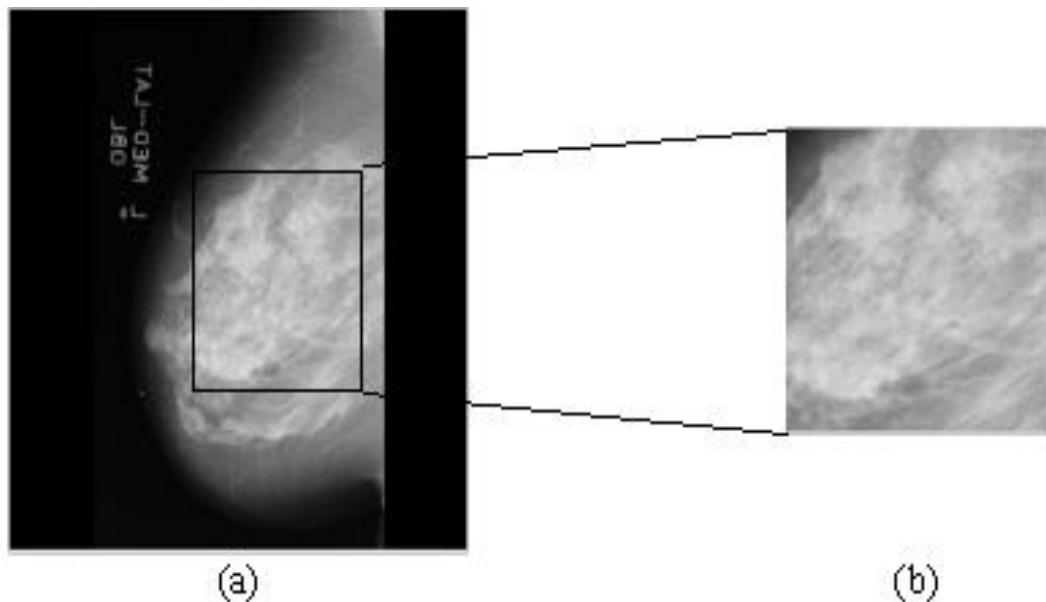


Figure 4.2 (a) Original image (1024 x 1024), (b) Cropped image (128 x 128).

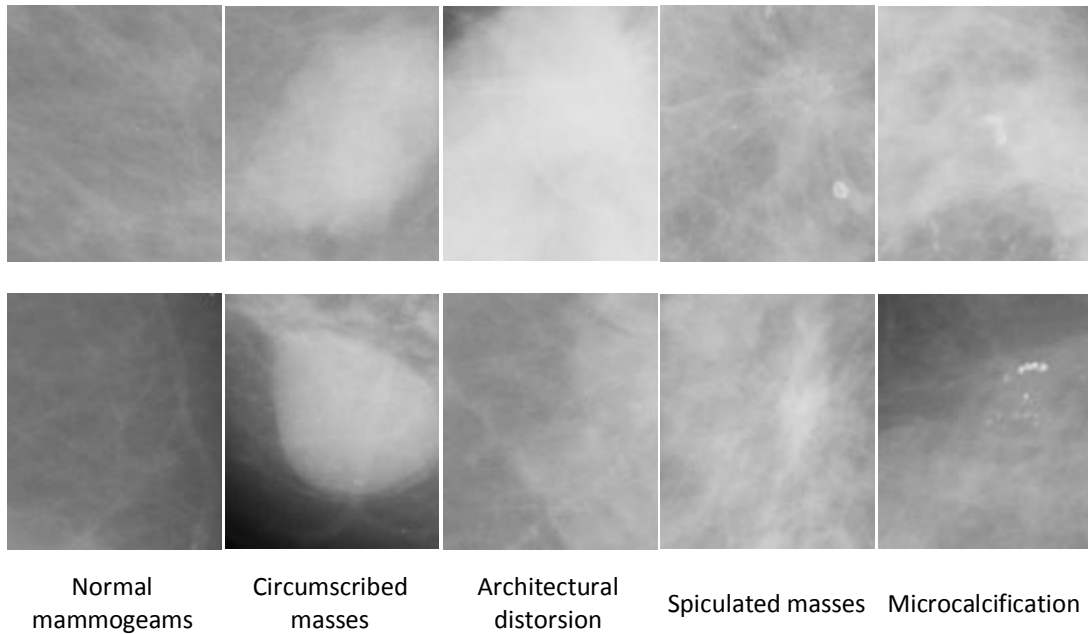


Figure 4.3 Samples of used ROIs of mammograms.

#### 4.2.2 Feature Extraction Techniques

Feature extraction is the main point that should be taken under consideration when implementing a computer aided diagnosis system for classifying between breast tissues. Extracting the most significant features that have the capability to describe and maximize the differences between different tissues in an ample way is an important factor that directly affects the classification result in mammogram classification. In this study, five methods for feature extraction are suggested and tested. The methods are described individually as follows.

##### 4.2.2.1 Feature Extraction Based on Extracting a Percentage of the Biggest Coefficients

The curvelet and wavelet are used to decompose the ROIs into four decomposition levels. Different ratios of the biggest coefficients from each decomposition level are used to be the feature vector of the corresponding mammogram. These ratios are taken between 10% and 90% of coefficients from each level. The selected ratios are collected in one vector to be presented to the classifier. The KNN classifier is



constructed based on the Euclidean distance. The procedure of the feature extraction and classification method is summarized in Figure 4.4.

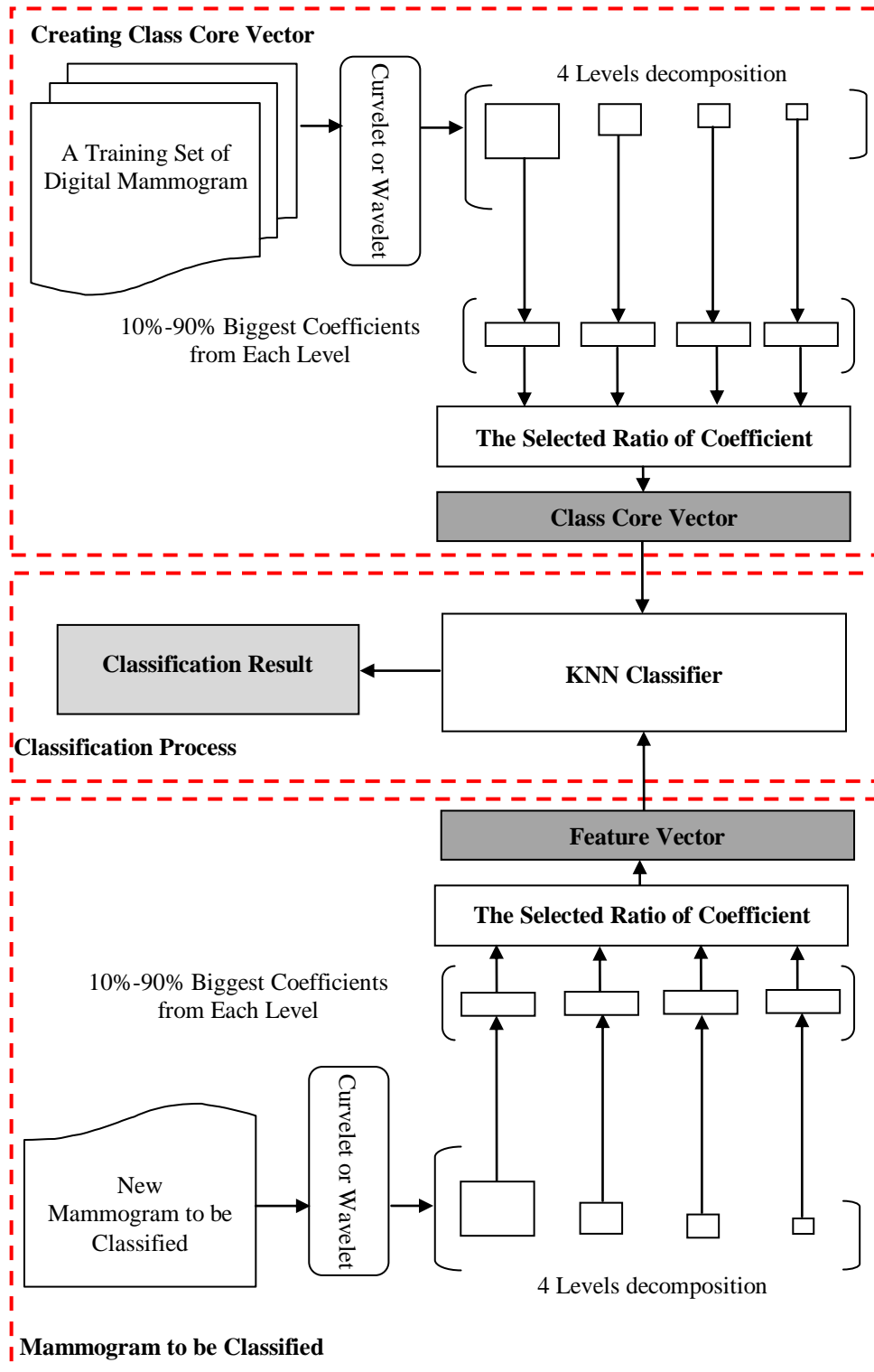


Figure 4.4 The proposed system for mammogram diagnosis by extracting a ratio of the biggest coefficients from each decomposition level.

#### 4.2.2.2 *Feature Extraction Based on Extracting the Biggest 100 Coefficients*

This is the second method considered to select a set of features from multiresolution representation. The method was presented before with wavelet coefficients, but here we present it with curvelet coefficients and compare the results obtained in both cases (wavelet and curvelet). Once the ROIs are cropped as described in Section 4.2.1, both wavelet and curvelet decompositions are applied separately to the ROIs. Features are extracted from the ROI based on a multiresolution transform. For wavelet, four different decomposition levels based on three different wavelet functions, Daubechies-8 (db8), symlet (sym8) and bi-orthogonal (bior3.7) are used. For both wavelet and curvelet in each decomposition level, the obtained coefficients are sorted in descending order. Then, the biggest 100 coefficients are selected to represent the corresponding mammogram (i.e., feature vector). This means that each mammogram image is represented by 400 coefficients. Then these coefficients are passed to classification steps. The classification steps are performed using KNN classifier. It starts by calculating the classes' core vectors then the distance between the new image vector and the calculated classes' core vectors is determined. The smallest distance shows that the tested image belongs to that class which produced the smallest distance. Figure 4.5 illustrates the steps for ROIs classification.

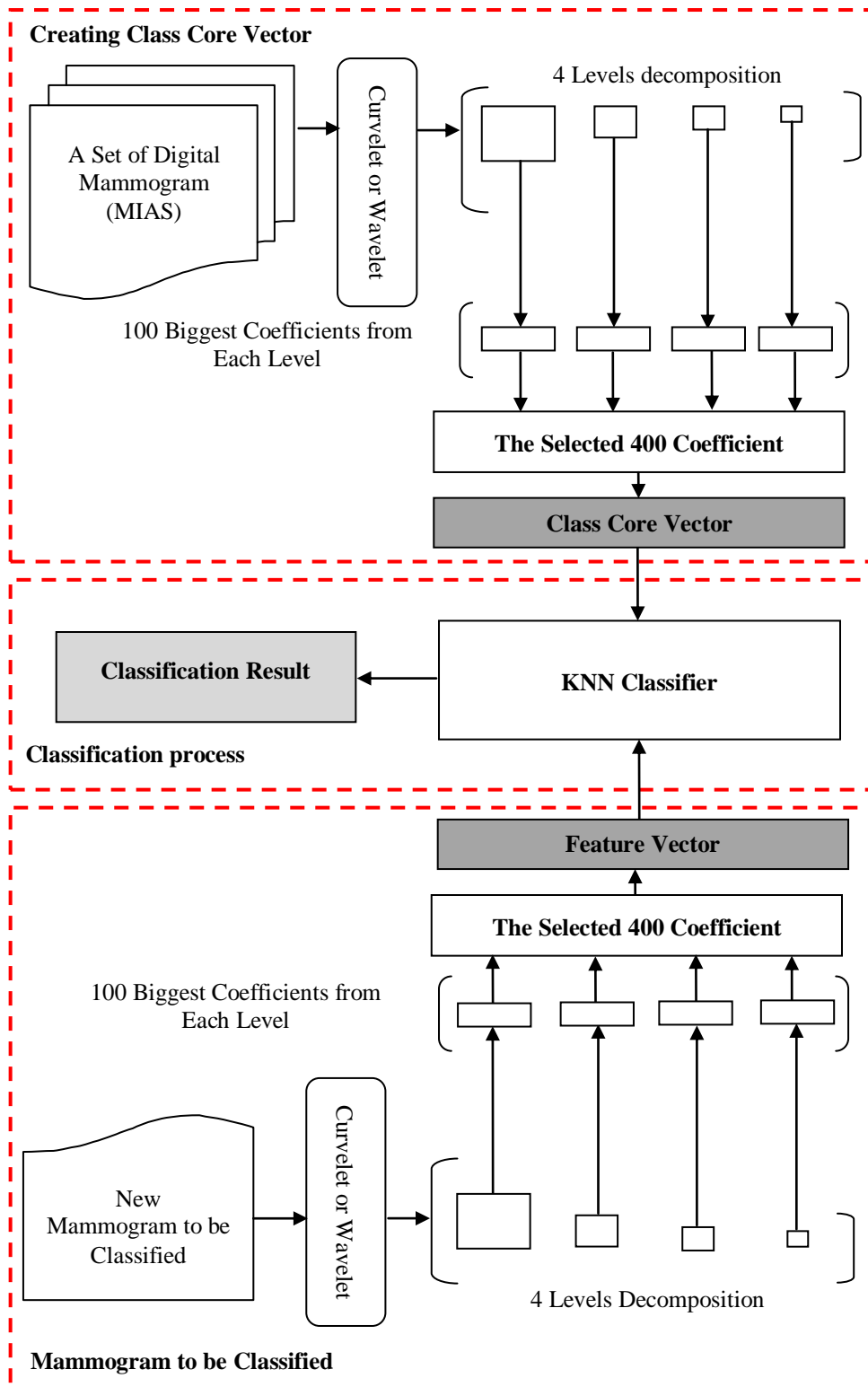


Figure 4.5 The proposed system for mammogram diagnosis by extracting the biggest 100 coefficients from each decomposition level.

### 4.2.2.3 Feature Extraction Using Standard Deviation of Means

This is the third method considered for feature extraction from multiresolution representation. The method requires an initial dataset, named building set. The building set contains ROIs from all classes that we are considered. The building set is used to construct the classifier as follows. Let  $K$  be the number of ROIs in the building set. All  $K$  images are decomposed using wavelet or curvelet transform. The obtained coefficients are used to construct a matrix  $K \times N$  ( $K$  rows,  $N$  columns), where,  $N$  is the number of coefficients obtained for each image. Typically  $N$  is a large number. For each class, a mean feature vector is obtained by calculating the mean of the coefficients of all images in that class column by column. Hence, a second matrix  $P \times N$  is constructed where  $P$  is the number of classes, i.e. each row corresponds to the mean of the classes' feature vectors. The standard deviation of the matrix  $P \times N$  is calculated. Now, each entry of the standard deviation vector indicates how the corresponding column separates the classes. A hard threshold is applied on the standard deviation vector. The column will be kept if the obtained standard deviation is greater than the threshold value, otherwise it will be suppressed. The threshold value is calculated using the formula  $\sqrt{2 \log(X)}$  as in [154], where  $X$  is the length of the coefficients vector. The resulting vector of coefficients will be the input to the classifier. The columns in  $K \times N$  matrix corresponding to the suppressed column are ignored. The resulting  $L$  columns are used as feature vector for each image. Figure 4.6 presents the proposed feature extraction method and how the overlapped coefficients are eliminated. Figure 4.7 explains an example to declare the method.

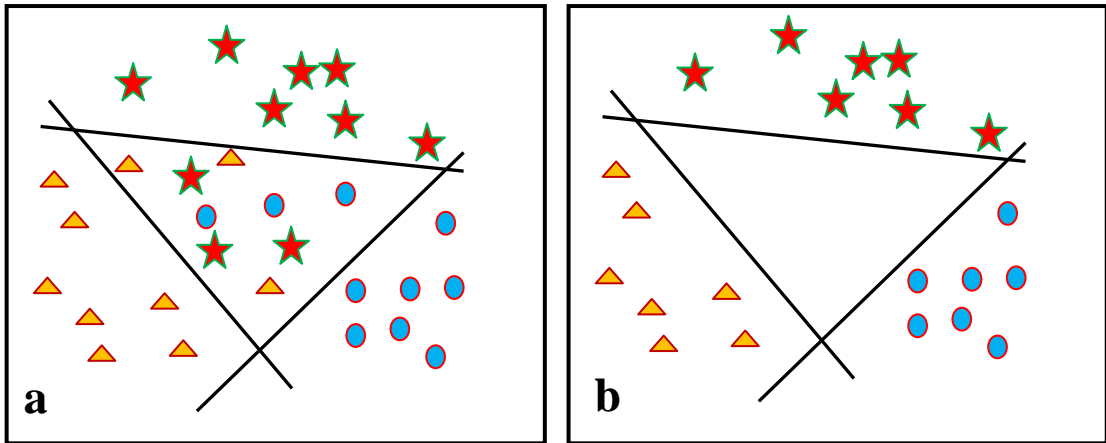


Figure 4.6 The proposed feature extraction technique. (a) Show the overlapping between the different classes' features. (b) The overlapped features are removed.

classes	Column1	Column2	Column3	Column4	Column5	Column6	Column7	Column8	Column9	Column10
Class A	1	3	4	5	3	2	6	7	8	4
	3	2	4	6	5	9	8	7	5	3
	7	1	2	5	7	8	9	5	5	7
Class B	6	7	5	7	8	4	1	2	7	4
	4	5	6	8	9	2	4	5	6	2
	7	1	3	5	7	9	2	4	6	8
Class C	8	2	3	5	7	5	3	1	8	3
	9	0	7	6	5	4	2	7	2	7
	7	8	5	3	4	7	2	1	7	0

Calculate the mean of each class

Mean(A)	3.67	2.00	3.33	5.33	5.00	6.33	7.67	6.33	6.00	4.67
Mean(B)	5.67	4.33	4.67	6.67	8.00	5.00	2.33	3.67	6.33	4.67
Mean(C)	8.00	3.33	5.00	4.67	5.33	5.33	2.33	3.00	5.67	3.33

Calculate the standard deviation of means

Stand Dev	2.17	1.17	0.88	1.02	1.64	0.69	3.08	1.76	0.33	0.77
-----------	------	------	------	------	------	------	------	------	------	------

Apply for example threshold (1.5)

Remains	2.17				1.64		3.08	1.76		
---------	------	--	--	--	------	--	------	------	--	--

The top table presents the matrix (K\*N) where k is the number of images, in this example k=9 distributed between three classes (A, B, C). N is the number of coefficients, in this example N=10. The mean of each class is calculated as shown in the second table. Then the standard deviation of the matrix of means is calculated. Let the threshold value applied in this example is (1.5), the remaining four columns (1, 5, 7 and 8) will be kept to present to the classifier.

Figure 4.7 An example illustrates the proposed feature extraction method using standard deviation of means.

Now, to classify a new ROI, it is first decomposed using wavelet or curvelet. From the obtained row vector of coefficients, all columns are suppressed except the  $L$  columns obtained from the building phase. The kept feature will be introduced to the KNN classifier. The KNN classifier is used to classify that ROI based on calculating the Euclidean distance between the obtained vector and the core vectors of the different classes. The proposed feature extraction method is illustrated in Figure 4.8.

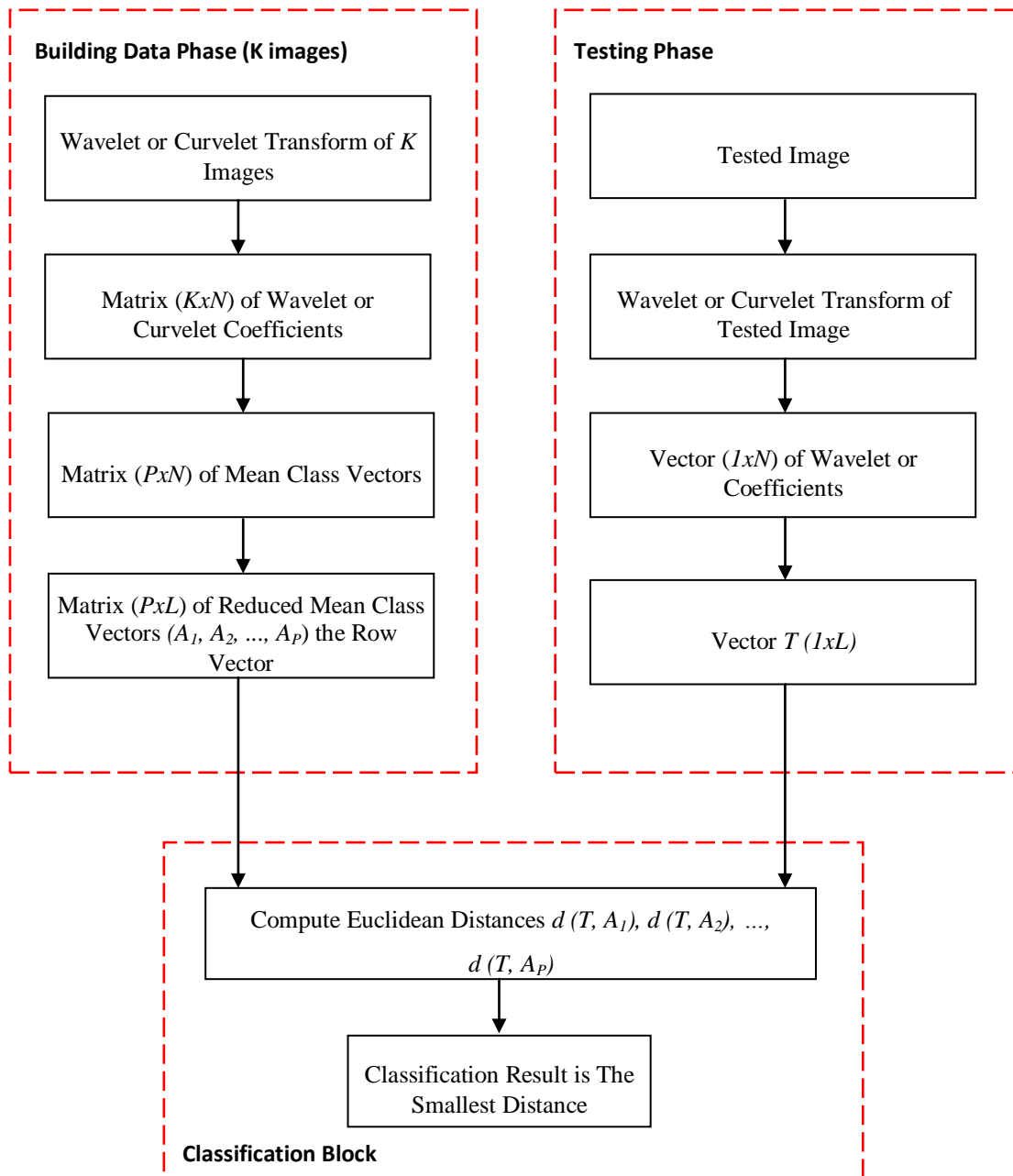


Figure 4.8 The proposed feature extraction method using the standard deviation of means to develop a computer aided system for mammogram diagnosis.

#### 4.2.2.4 Feature Extraction Based on Ranking Features Method

This is the fourth method for feature extraction. The method consists of decomposing a set of mammogram images. Then, the obtained coefficients are used to construct a matrix  $K \times N$ , where  $K$  is the number of images and  $N$  is the number of coefficients for each image. The features (columns) are treated individually, depending on its capability to separate different classes. This capability will be called  $C_T$ , then the features are ranked in descending order according to the value of  $C_T$ . The capability of features can be calculated as follows.

Denote two classes  $A$  and  $B$ . For each feature, we compute the means  $\mu_a$  and  $\mu_b$ , and standard deviations  $\sigma_a$  and  $\sigma_b$ . Then, the capability of the feature is calculated as follows [155]:

$$C_T = \frac{\mu_a - \mu_b}{\sqrt{\frac{\sigma_a^2}{n_a} + \frac{\sigma_b^2}{n_b}}} \quad (4.1)$$

where  $n_a$  and  $n_b$  are the number of images in class  $A$  and  $B$ , respectively. A threshold value is applied over the score of the features  $C_T$ . The most significant features are kept according to the applied threshold value. The obtained features are then presented to SVM classifier. In the classification step, the dataset was divided into two groups, training group 70% and testing group 30%. The training group is used to build SVM classifier and the testing group is used to calculate the performance of the classifier. To optimize the number of features with the maximum classification accuracy rate, a dynamic threshold is applied, i.e. the threshold value is changed and the classification is performed again using the new features set. This process is repeated until reaching with the classifier to the maximum performance with its corresponding number of coefficients. Then, 2x5 folds cross validation is applied to the optimized coefficients. The proposed method can be summarized as shown in Figure 4.9.

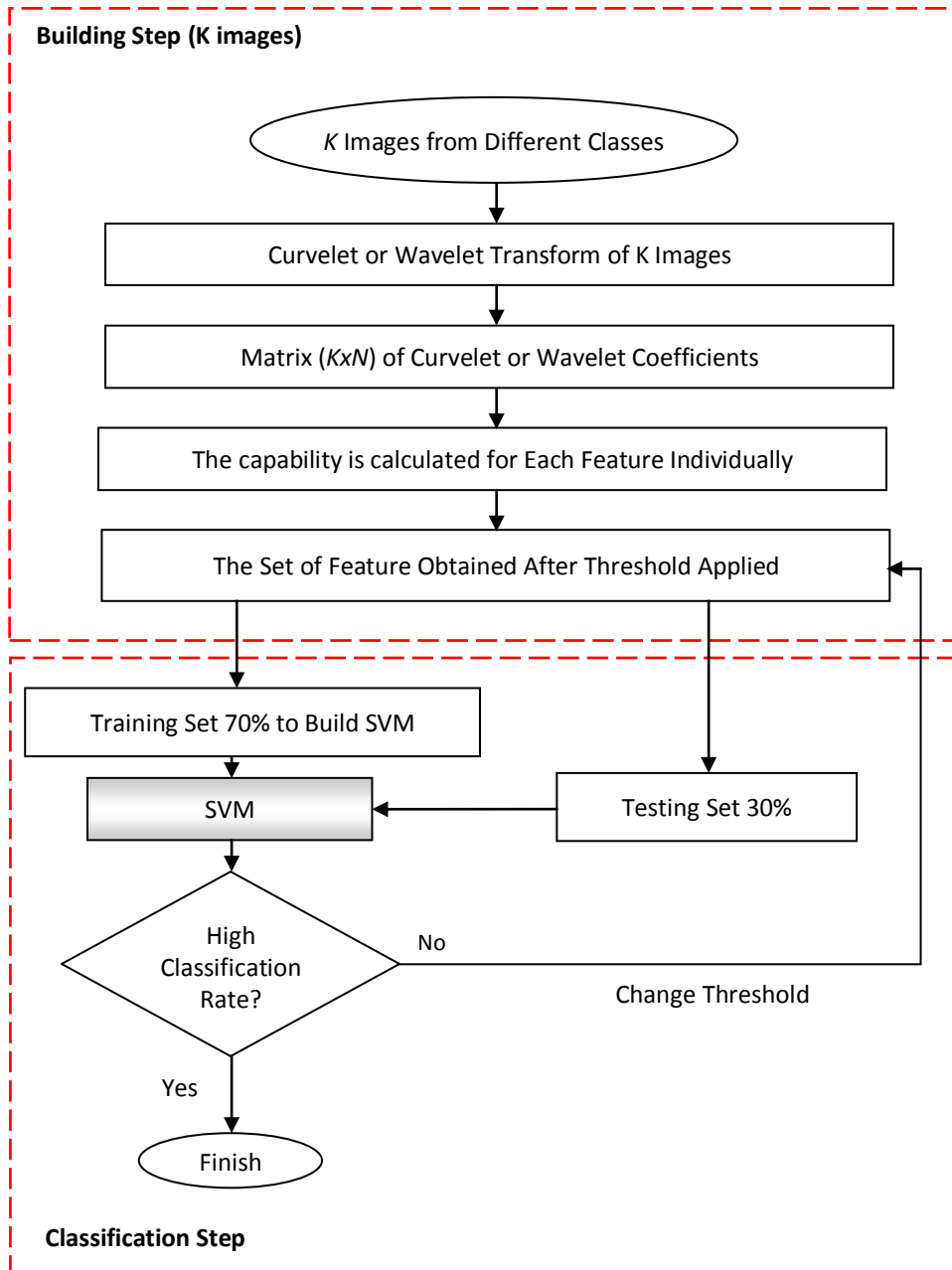


Figure 4.9 The proposed method for mammogram classification using feature ranking method.

#### 4.2.2.5 Curvelet Based Texture Feature Extraction Method

This is the fifth method for feature extraction presented in this work. Once the ROI are cropped as described previously in Section 4.2.1, the curvelet transform is applied on ROI. Then seven statistical properties for each wedge are calculated.



These properties are described in Table 4.1. In this study, curvelet is used with scale 4 and 16 angle, i.e. the ROI is decomposed into 81 wedges, and the features are calculated for each wedge, so that a total of 567 features are calculated to form a features vector. The most significant features are obtained by passing the features vectors to a standard deviation of mean feature extraction method. The method starts with calculating a mean features vector for each class. After that the standard deviation vector between the different means is calculated. A hard threshold is then applied on this standard deviation vector. The remaining features will be the features vector for the corresponding ROI. These selected features are used to classify between different classes. The number of features obtained after applying the feature extraction method is presented in Table 4.2.

Table 4.1 The seven texture features extracted from each wedge in curvelet decomposition

$$\text{Energy} = \sum_i^M \sum_j^N I^2 [i, j]$$

$$\text{Entropy} = - \sum_i^M \sum_j^N I [i, j] \log I [i, j]$$

$$\text{Mean} = \frac{1}{M*N} \sum_i^M \sum_j^N I [i, j]$$

$$\text{STD} = \sqrt{(I [i, j] - \bar{I} [i, j])^2}$$

$$\text{Max Probability} = \max I [i, j]$$

$$\text{Inverse Difference Moment} = \sum_i^M \sum_j^N \frac{I [i, j]}{|i-j|^2} \text{ where } i \neq j$$

$$\text{Homogeneity} = \sum_i^M \sum_j^N \frac{I [i, j]}{1+(i+j)^2}$$

Table 4.2 The obtained number of features before and after feature extraction method applied.

Function	total features	total features
	before feature extraction	after feature extraction
Normal vs. abnormal	567	220
Benign vs. malignant	567	222

The previous developed five methods for feature extraction were applied to ROIs that were manually cropped from the original mammograms. One of the objectives of the current study is to develop an automatic ROI segmentation algorithm. The following part considers this objective. It presents an automatic method to segment ROI, and then apply the proposed methods for feature extraction. Finally a comparison study between the manual and automatic segmentation is accomplished.

### 4.3 Part II: Automatic ROI Detection

A mammogram mainly contains two regions: the exposed breast region and the unexposed non-breast region. It is necessary to first identify the breast region for the reduction of the subsequent processing, then remove the non-exposed breast region. The computer aided detection systems for mass and architectural distortion generally provide lower performance compared to those developed to detect calcifications. The mass lesions are relatively more challenging because masses are often indistinguishable from the surrounding area, varying in size, shape and density. However, researchers have applied a number of different methods to prompt mass in mammogram. Architectural distortion detection methods are also difficult to identify from the surrounding tissue.

The work in this part consists of two stages. Firstly, an automatic thresholding algorithm is used to separate the area composed of the breast and the pectoral muscle from the background of the image. Subsequently, a region growing

algorithm is used to locate the muscle and suppress it from the breast. Secondly, the work concentrates in the region of interest (ROI) segmentation to detect the suspicious region. Two methods are suggested to accomplish the segmentation step; such methods are adaptive thresholding method and pattern matching method. Subsequently, curvelet and wavelet are used to decompose the suspicious regions and the feature extraction methods are performed. Finally, the classifier is used to determine whether the region is abnormal (mass or architectural distortion) or normal. The proposed scheme is fully automated; all the parameters are calculated based on the image under consideration. Hence, the proposed scheme can be used with any database of images without any customization or user interaction. Figure 4.10 presents the proposed system in part II.

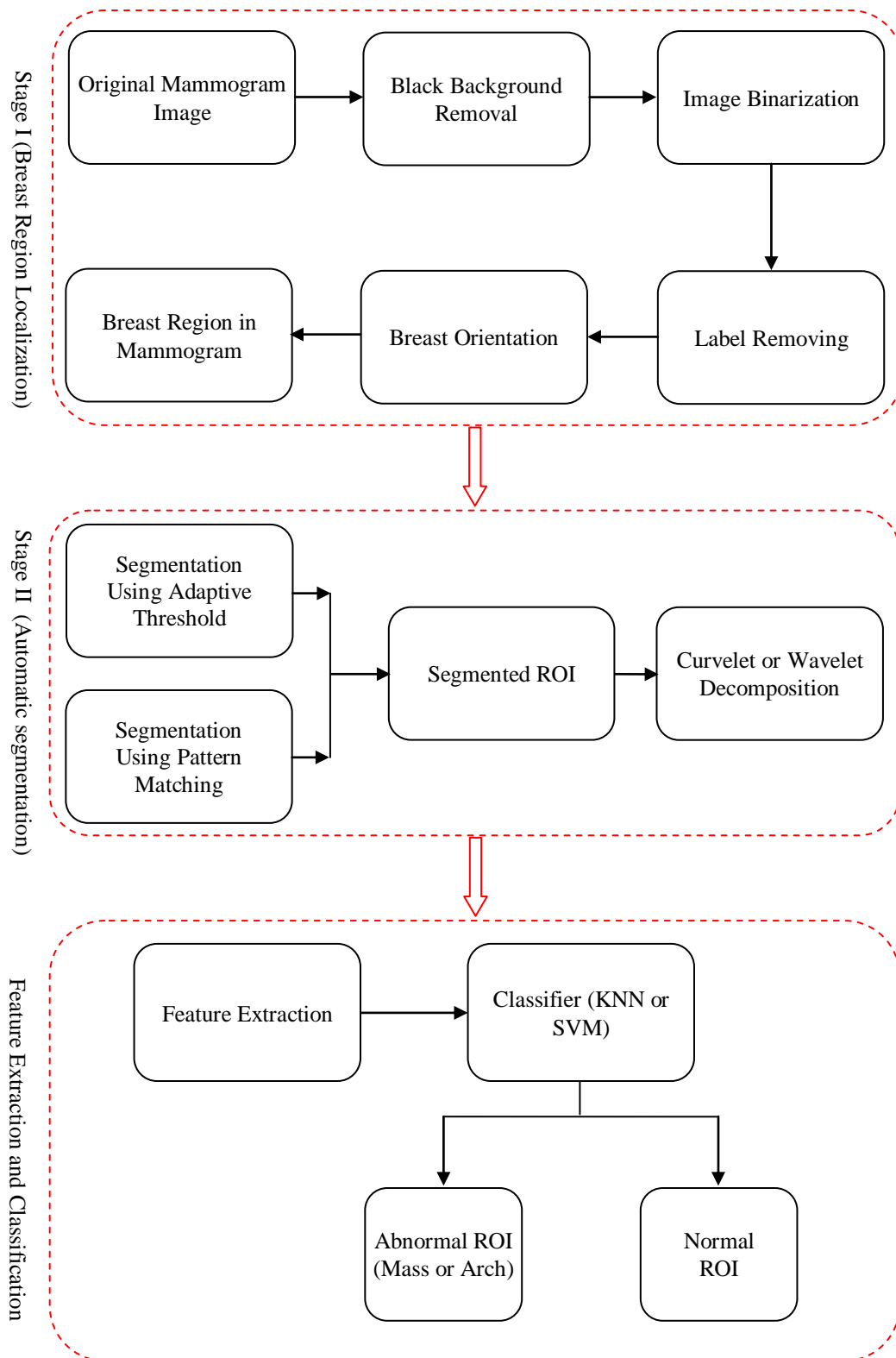


Figure 4.10 The proposed fully automatic detection and diagnosis of breast cancer in mammograms.

### 4.3.1 Stage One: Breast Region Localization

In this preprocessing step, the breast is segmented in order to limit the search for abnormalities from the background of the mammogram without undue influence in order to improve the quality of the image and reduce the noise. This stage consists of the following steps:

**Step 1: Black Background Removal:** For each mammogram image, the sums of columns are calculated. A threshold value is applied for the sum to eliminate the black background, i.e. the column will be removed if its sum is lower than the determined threshold value, as shown in formulae (4.2).

For each column:

$$\sum_{i=1}^{i=n} \sum_{j=1}^{j=m} I(i, j) \leq \varepsilon_1 \quad (4.2)$$

Where  $I(i, j)$  is the intensity of pixel  $(i, j)$ , and  $\varepsilon_1$  is a threshold values.  $n, m$  are the dimensions of the image.

**Step 2: Image Binarization:** A global image thresholding is performed with Otsu's method [156] to binarize the mammogram image.

**Step 3: label Removing:** In this step we obtained only the breast region and the label area. To remove the label area, the connected components method is applied. We keep the biggest region which corresponds to the breast and eliminate the others.

**Step 4: Breast Orientation:** To determine whether the mammogram image is right or left breast, we divide the image into two sides (right and left), then calculate the sum of both sides. The mammogram classified as right or left to the biggest sum obtained.

**Step 5: Pectoral Muscle Suppression:** Once the mammogram is classified to be right or left, a region growing method is used to estimate the pectoral muscle. It is then suppressed from the breast region.

### 4.3.2 Stage Two: ROI Segmentation

In this stage, the breast regions obtained from the first stage are used as the inputs to the second stage. The main objective of this stage is to segment the ROI automatically. This study includes two types of abnormalities (mass and architectural distortion). The detection of the ROI of these two types will be accomplished through two different suggested methods. Each method individually can achieve the task. These methods are the adaptive threshold method and the pattern matching method.

#### 4.3.2.1 ROI Segmentation Using an Adaptive Threshold Method

The abnormality regions in mass and architectural distortion are usually hidden in dense tissues with higher intensity values compared to the normal tissues, so the pixels with low intensity should not be considered as suspicious region. Therefore, only the regions whose pixels intensity is high will be considered as suspicious region. To suppress the normal tissues and keep only the highest intensity regions, a threshold value is applied. The method can be described as follows.

*Thresholding:* In this work the threshold value is calculated using the following formula [29].

$$T = \mu + k \sigma \quad (4.3)$$

where  $\mu$  is the mean of intensity values of image pixels,  $\sigma$  is the standard deviation of the corresponding mammogram image and  $k$  is a constant that is calculated empirically. The masses and architectural distortion images are divided into two sets. The first set is used to calculate  $k$  and the other set is used to validate the method. Once the  $k$  value is calculated, the threshold is applied over the data set to highlight the suspicious region.

*Suspicious Region Extraction:* after the threshold is applied to the breast region, the normal tissues are suppressed and the high intensity tissues are kept. In this step the connected components is applied to the thresholded image. Now, the kept

regions will be called the suspicious regions and every region should be separated perfectly from the breast image in order to extract its features.

#### 4.3.2.2 ROI Segmentation Using Pattern Matching Method

In this method, a region of typical mass region or architectural distortion region is used as a template region. The breast regions obtained from the first stage are used as an input to this stage. Each breast region is divided into windows equal to the size of the predefined abnormal template region. The correlation coefficient between the template region and the regions of the breast region image is calculated as in the following equation [157]:

$$R = \frac{\sum_m \sum_n (A_{mn} - \bar{A})(B_{mn} - \bar{B})}{\sqrt{(\sum_m \sum_n (A_{mn} - \bar{A})^2) * (\sum_m \sum_n (B_{mn} - \bar{B})^2)}} \quad (4.4)$$

where  $A$  is the template region and  $B$  is the breast region (window) under consideration from the whole breast region image. The correlation coefficient between the template region and the region under consideration from the breast region image is calculated and recorded. Then the maximum correlation coefficient value is calculated and the corresponding region will be called the suspicious region. Figure 4.11 illustrates the method of correlation coefficient calculation and the recording of its values.

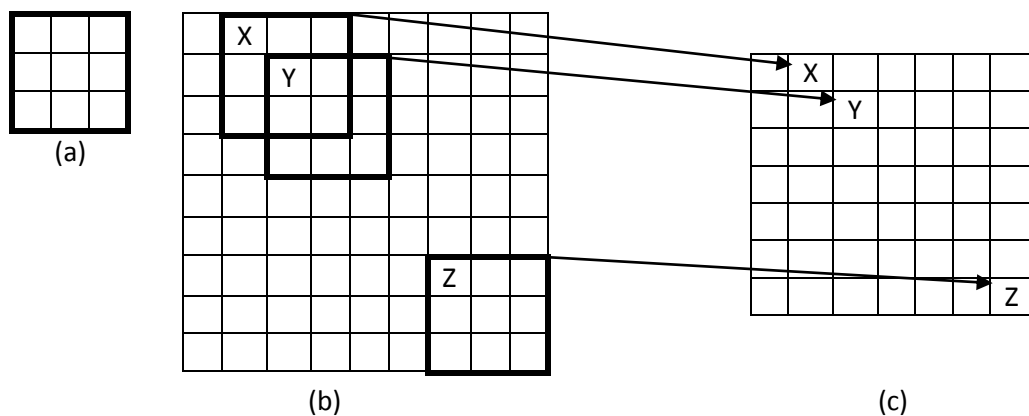


Figure 4.11 (a) The template region, (b) The dynamic window through the image, (c) The correlation matrix values of the corresponding window.

Once the maximum correlation coefficient value is determined, the corresponding region is cropped from the breast region. The regions should be separated perfectly from the breast region image in order to be used in the following step. Each suspicious region is passed to the classifier to determine whether it is abnormal (mass or architectural distortion) or normal tissue.

#### 4.3.2.3 *False Positive Reduction*

Now, the suspected regions are segmented. The next step will be to identify whether such regions are normal or abnormal. This task would be achieved through feature extraction and classification steps. So, the obtained suspected regions are decomposed using curvelet or wavelet in order to extract a set of features.

A. *Feature Extraction:* The suspicious regions detected from the previous step are decomposed using wavelet or curvelet transform. Two methods for feature extraction from the previously proposed methods are used to extract the most significant features.

- The first method for feature extraction is the standard deviation of means described in Section 4.2.2.3.
- The second method for feature extraction is the feature ranking method described in Section 4.2.2.4.

B. *Classification:* The classification stage here is performed using two classifiers, KNN and SVM.

## 4.4 **Summary**

This chapter presents the proposed methods to develop a computer aided system for breast cancer diagnosis in digital mammogram. The work is divided into two parts. In part I, a manual ROI segmentation is performed. Subsequently, curvelet and wavelet are used to decompose the ROI into four decomposition levels. The feature extraction step was performed through five methods. These methods are suggested to identify the most significant features. Then the classification stage was performed using KNN and SVM.



In part II, the ROIs of two abnormality types (mass and architectural distortion) were segmented automatically. First, the breast regions are localized in the original mammogram. Subsequently, two different methods for ROI detection were used. These methods are adaptive thresholding method and the pattern matching method. Once the ROIs are identified and segmented, the curvelet transform was applied and two methods for feature extraction from the previously proposed methods were used in order to differentiate between the normal or abnormal regions.

In the following chapter, the results are carried out according to the previous proposed methods and algorithms will be presented and comparison between the results obtained will be accomplished.

## CHAPTER 5

### RESULTS AND DISCUSSION

#### 5.1 Overview

This chapter presents the results and discussion of the proposed methods. It starts with presenting a description of the dataset used in the study, followed by the results of the first part of the work, which consists of assessing computer aided diagnosis system based on five different feature extraction methods. A comparison between curvelet and wavelet is accomplished. Subsequently, the results of automatic ROI segmentation in mammographic masses and architectural distortion are presented.

#### 5.2 Dataset

In the present study, a set of mammographic images provided by the Mammographic Image Analysis Society (MIAS) [158] is used in applying the proposed methods. These images were previously investigated and labeled by an expert radiologist based on technical experience and biopsy. The MIAS is a benchmark dataset. It is selected due to the various cases it includes. It is also widely used in similar research work [81], [96] - [97], [102] - [103]. The dataset is composed of 322 mammograms of right and left breast, from 161 patients, where 51 were diagnosed as malignant, 64 as benign and 207 as normal. The abnormalities are classified into microcalcifications, circumscribed masses, spiculated masses, ill-defined masses, architectural distortion and asymmetry. The odd number cases represent the left breast mammogram while the even number cases represent the corresponding right breast mammogram. The data set provides appropriate details as follows:

- 1) 1<sup>st</sup> column: MIAS database reference number.
- 2) 2<sup>nd</sup> column: Character of background tissue (Fatty, Fatty-glandular, or Dense-glandular).

- 3) 3<sup>rd</sup> column: Class of abnormality presents (microcalcification, circumscribed mass, ill-defined mass, spiculated mass, architecture distortion, asymmetry or normal).
- 4) 4<sup>th</sup> column: Severity of abnormality (Benign or Malignant).
- 5) 5<sup>th</sup> and 6<sup>th</sup> columns: X and Y image coordinates of center of abnormality.
- 6) 7<sup>th</sup> column: Approximate radius (in pixels) of a circle enclosing the abnormality.

In this study, 322 mammogram images were used. The dataset description and classification are given in Table 5.1.

Table 5.1 The distribution of (MIAS) dataset into different classes

Class	Benign	Malignant	Total
Microcalcification	12	13	25
Circumscribed masses	19	4	23
Ill-defined masses	7	7	14
Spiculated masses	11	8	19
Architectural distortion	9	10	19
Asymmetry lesion	6	9	15
Normal tissue	-	-	207
Total	64	51	322

The original mammograms are 1024x1024 pixels, and almost 50% of the whole image comprised of the background with a lot of noise. Therefore a cropping operation is applied to the images to cut off the unwanted portions of the images. Regions of interest (ROIs) 128x128 are cropped. The cropping process was performed manually, where the given center of the abnormality area is selected to be the center of ROI. Thus, almost all the background information and most of the noise such as label are eliminated. By this method we are sure that no abnormality was suppressed with the background.

### **5.3 Part I: Computer Aided Diagnosis System**

This part consists of the following steps. The first step is to crop the ROIs manually from the original mammogram. Secondly, five feature extraction methods are used to identify the most significant features. Subsequently the obtained features are presented to the classifiers. The results of this part are presented as follows.

#### **5.3.1 Results of Computer Aided Diagnosis System by Extracting a Percentage of the Biggest Coefficients**

Curvelet and wavelet are used to analyze the cropped ROIs from mammogram images. This decomposition step is performed as a pre-process for ROIs classification. Both wavelet and curvelet are applied to 4 levels. From each decomposition level, a ratio of the biggest coefficients is used to be the feature vector of the corresponding mammogram. This means that, each ROI will be presented in 4 percentages, each percentage selected from different scale. The percentages are selected from 10% to 90%. The constructed feature vectors are presented to KNN to distinguish between different classes. The obtained results from KNN classifier to distinguish between abnormal and normal classes are presented in Table 5.2. It shows that the highest average classification accuracy rate obtained with curvelet coefficients was 99.05% using 60% of coefficients, while it was 96.62% using 80% of coefficients with wavelet coefficients. The comparison between the classification accuracy rate based on features extracted from curvelet or wavelet decomposition is illustrated in Figure 5.1. These results prove the effectiveness of curvelet in edges representation and mammogram images analysis.

Table 5.2 The classification accuracy rates between abnormal and normal classes by extracting different percentages from each decomposition level of curvelet and wavelet.

Method	class	10%	20%	30%	40%	50%	60%	70%	80%	90%
Curvelet	Abnormal	97.50	95.95	98.01	96.41	98.46	97.35	97.11	97.35	93.97
	Normal	92.59	96.30	96.30	92.59	88.89	100.00	96.30	96.30	96.30
	W. Average	94.34	96.18	96.91	93.95	92.31	99.05	96.59	96.68	95.47
Wavelet	Abnormal	95.86	85.09	89.83	87.90	95.83	87.73	89.86	90.53	93.62
	Normal	77.78	100.00	100.00	96.30	88.89	100.00	88.89	100.00	77.78
	W. Average	84.24	94.68	96.37	93.30	91.37	95.62	89.24	96.62	83.44

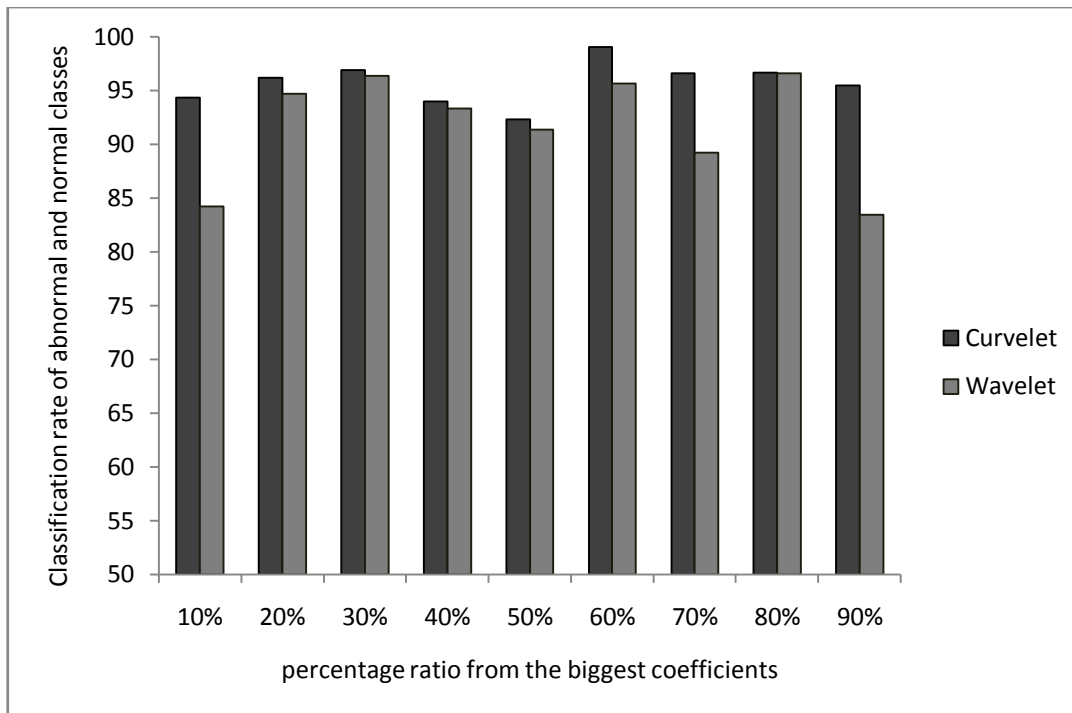


Figure 5.1 The average classification accuracy rates for normal and abnormal classes obtained using curvelet and wavelet decompositions with different percentage ratios of coefficients.

Table 5.3 presents the classification accuracy rates achieved in differentiating between the abnormalities classes based on their shapes. For each percentage, an average of accuracy rate is calculated and a comparison is accomplished between curvelet and wavelet. Figure 5.2 illustrates the comparison between curvelet and wavelet at different percentages. It shows that curvelet outperforms wavelet for the current mammogram classification problem.

It can be concluded that the obtained results by extracting a percentage of the biggest coefficients from 4 scales decomposition of curvelet and wavelet show that several percentages make the classifier achieves high accuracy rates. The comparison between wavelet and curvelet decomposition proves that curvelet gives a better multiresolution representation.

Table 5.3 The classification accuracy rate between different abnormality types by extracting different percentages from each decomposition level of curvelet and wavelet.

Method	Class	10%	20%	30%	40%	50%	60%	70%	80%	90%
Curvelet	Calc	96.00	92.00	100.00	100.00	96.00	96.00	96.00	96.00	92.00
	Circ	95.65	95.65	100	95.65	100.00	100.00	100.00	100.00	95.65
	Ill-def	100.00	100.00	100.00	100.00	100.00	100.00	100.00	100.00	100.00
	Spic	100.00	100.00	94.74	94.74	94.74	94.74	100.00	94.74	94.74
	Arch	100.00	94.74	100.00	94.74	100.00	100.00	100.00	100.00	94.74
	Asym	93.33	93.33	93.33	93.33	100.00	93.33	86.67	93.33	86.67
	W. Average	97.39	95.65	98.26	96.52	98.26	97.39	97.39	97.39	93.91
Wavelet	Calc	100.00	64.00	60.00	80.00	100.00	100.00	76.00	80.00	88.00
	Circ	100.00	95.65	100.00	100.00	95.65	86.96	100.00	100.00	100.00
	Ill-def	85.71	100.00	100.00	100.00	100.00	85.71	100.00	100.00	100.00
	Spic	89.47	84.21	84.21	84.21	52.63	100.00	73.68	100.00	94.74
	Arch	100.00	100.00	94.74	63.16	100.00	73.68	89.47	63.16	78.95
	Asym	100.00	66.67	100.00	100.00	126.67	80.00	100.00	100.00	100.00
	W. Average	96.52	84.35	87.83	86.96	94.78	88.70	88.69	89.57	93.04

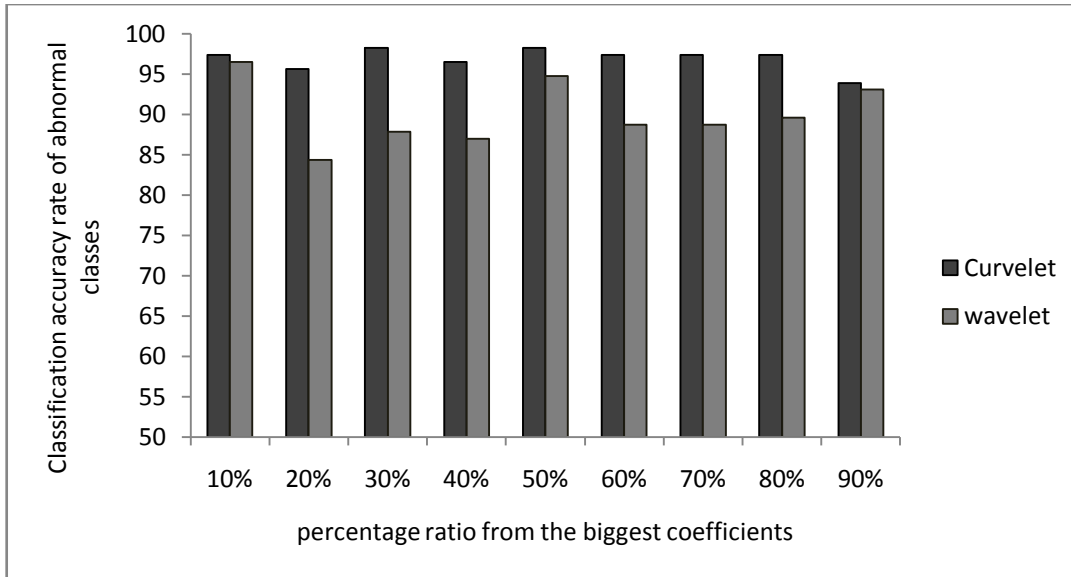


Figure 5.2 The classification accuracy rates for abnormal classes obtained using curvelet and wavelet decompositions with different percentage ratios of coefficients.

The classification accuracy rates achieved to differentiate between the benign and malignant classes are presented in Table 5.4. The average of the ability of each percentage is calculated and a comparison is accomplished between curvelet and wavelet at each percentage. The comparison between curvelet and wavelet at different percentages is illustrated in Figure 5.3. It shows that curvelet outperforms wavelet in classifying mammogram images between benign and malignant.

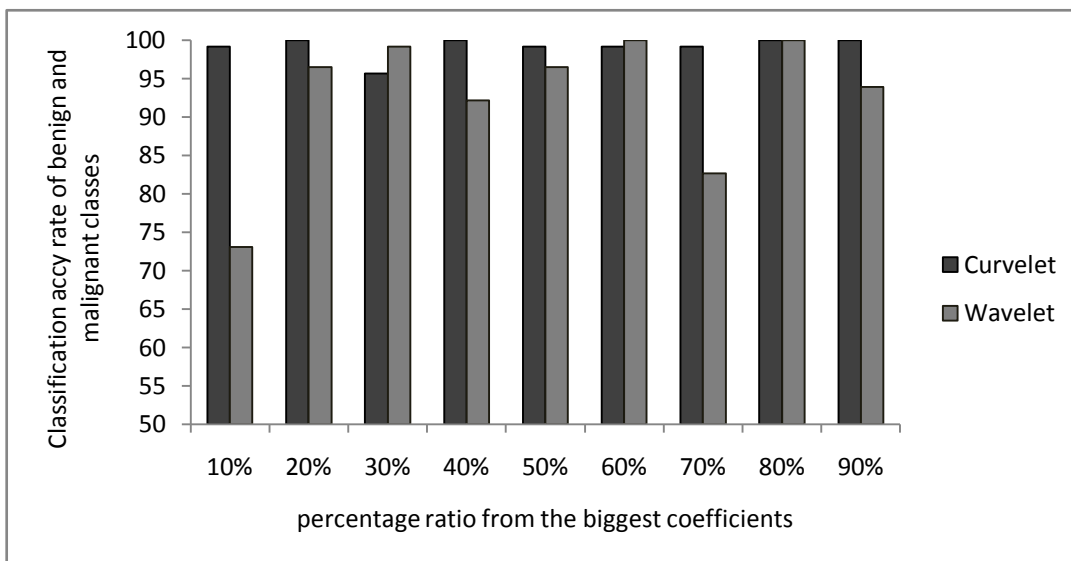


Figure 5.3 The classification accuracy rates for abnormal classes obtained using curvelet and wavelet decompositions with different percentage ratios of coefficients.



Table 5.4 The classification accuracy rates between benign and malignant types by extracting different percentages from each decomposition level of curvelet and wavelet.

Method	class	10%	20%	30%	40%	50%	60%	70%	80%	90%
Curvelet	Benign	98.44	100.00	100.00	100.00	100.00	98.44	98.44	100.00	100.00
	Malign	100.00	100.00	90.20	100.00	98.04	100.00	100.00	100.00	100.00
	W. Average	99.13	100.00	95.65	100.00	99.13	99.13	99.13	100.00	100.00
Wavelet	Benign	51.56	100.00	98.44	85.94	93.75	100.00	68.75	100.00	89.06
	Malign	100.00	92.16	100.00	100.00	100.00	100.00	100.00	100.00	100.00
	W. Average	73.04	96.52	99.13	92.18	96.52	100.00	82.61	100.00	93.91

### 5.3.2 Results of Computer Aided Diagnosis System by Extracting the 100 Biggest Coefficients

Features are extracted from the ROIs based on a multiresolution decomposition using wavelet and curvelet. For wavelet, four different decomposition levels based on three different wavelet functions, Daubechies-8 (db8), symlet (sym8) and bi-orthogonal (bior3.7) are used, The used levels of decomposition and wavelet functions are selected based on previous work [81], [97], the number of decomposition levels used for curvelet transform is 4, based on the work of Candes [159]. The four levels are obtained from the formula  $\log_2(S) - 3$ , where  $S$  is the size of the image, in this work  $S = 128$ .

In each decomposition level, the obtained coefficients are sorted in descending order. Then, the biggest 100 coefficients from each level are extracted to represent the corresponding mammogram i.e. each ROI is represented by 400 coefficients. Then this vector of coefficients is passed to the classification step. The Euclidean distance is used to construct the KNN classifier. The dataset is divided into 5 samples two times, i.e. 2x5-folds cross validation. Then 10 experiments are performed. In each experiment a single sample is used to build the classes' core vectors as described in equation (3.22) and the remaining samples are used to test the model. Each method is then assessed via a weighted average (W. Average) of 10 experiments followed by  $t$ -test statistical significance analysis. Table 5.5 presents the obtained results to distinguish between the normal and abnormal classes. It shows the successful classification rate of mammogram images with the overall classification accuracy based on 2x5-folds cross validation. The weighted average rate for each fold is calculated and then the average for each multiresolution representation method is calculated by averaging the 2x5-folds cross validation. Table 5.5 illustrates that the average classification rate achieved for normal and abnormal is 95.15% with curvelet coefficients, while the highest average rate achieved by wavelet functions (db8, Biro3.7 and sym8) is 90.76%. The average of the classification accuracy rates achieved for normal and abnormal is shown in figure 5.4. The error bar presents the standard deviation for 2x5 folds cross validation.

Table 5.5 The classification accuracy rates obtained over the 2x5-folds to classify the normal and abnormal classes by extracting the biggest 100 coefficients for each decomposition level.

Method	Class	Partitions 1					Partitions 2					Average
		Fold 1	Fold 2	Fold 3	Fold 4	Fold 5	Fold 1	Fold 2	Fold 3	Fold 4	Fold 5	
Curvelet	Abnormal	94.69	89.96	91.02	93.27	95.12	88.54	92.31	98.08	94.23	89.23	92.65
	Normal	98.20	94.08	98.50	100.00	90.91	92.27	96.58	100.00	100.00	94.85	96.54
	W. Average	96.95	92.61	95.83	97.60	92.41	90.94	95.06	99.31	97.94	92.84	95.15
Db8	Abnormal	92.69	91.53	92.31	83.33	85.37	80.77	75.38	91.61	89.54	100.00	88.25
	Normal	81.82	86.36	98.24	90.91	96.37	90.51	100.00	100.00	100.00	77.27	92.15
	W. Average	85.70	88.21	96.12	88.20	92.44	87.03	91.21	97.00	96.26	85.39	90.76
Bior3.7	Abnormal	82.69	92.31	79.93	88.46	76.93	75.38	81.15	88.46	90.39	86.54	84.22
	Normal	81.82	90.91	100.00	100.00	100.00	68.18	100.00	100.00	100.00	77.27	91.82
	W. Average	82.13	91.41	92.83	95.88	91.76	70.75	93.27	95.88	96.57	80.58	89.11
Sym8	Abnormal	100.00	94.23	55.49	81.15	80.77	74.42	70.88	72.80	91.47	100.00	82.12
	Normal	68.18	100.00	100.00	100.00	100.00	81.82	100.00	100.00	100.00	72.73	92.27
	W. Average	79.54	97.94	84.10	93.27	93.13	79.18	89.60	90.29	96.95	82.47	88.65

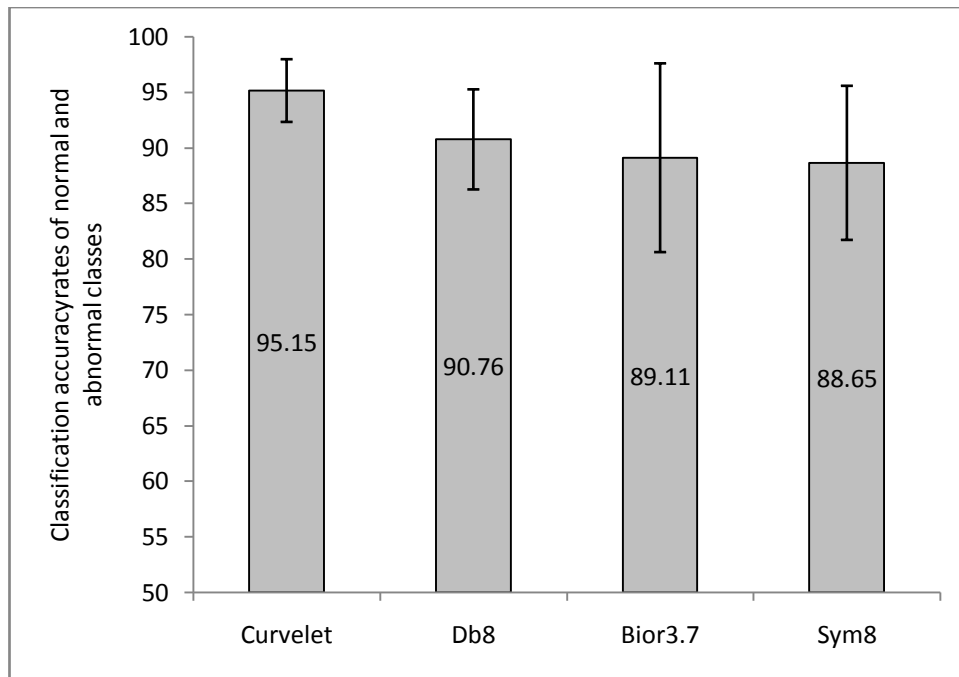


Figure 5.4 The average of the results of 2x5 folds obtained for classifying the normal and abnormal classes by extracting the biggest 100 coefficients.

For the second step, the classification rates of the abnormalities (microcalcifications, circumscribed masses, spiculated masses, ill-defined masses, architectural distortion and asymmetry) of 2x5-folds cross validation are listed in Table 5.6. The weighted average rate for each fold is calculated then the average for each representation method (curvelet and wavelet (db8, bior3.7 and sym8)) is calculated as well. Table 5.6 shows that, the average successful classification rate for all classes is 94.02% using curvelet transform coefficients. For wavelet functions (db8, Biro3.7 and sym8) the highest average rate obtained is 87.23%. Figure 5.5 presents average of classification accuracy rates achieved for this step of the work. It shows also that the error bar in case of curvelet is less than that in case of wavelet. From the obtained results, it can be concluded that curvelet based features yielded accuracy rates higher than those of wavelet based features. This was expected since the curvelet transform is able to capture the multidimensional features in wedges, while in case of wavelet it can only capture points.

Table 5.6 The classification accuracy rates obtained over the 2x5-folds to differentiate between abnormality types by extracting the biggest 100 coefficients from each decomposition level.

Method	Class	Partitions 1					Partitions 2					Average
		Fold 1	Fold 2	Fold 3	Fold 4	Fold 5	Fold 1	Fold 2	Fold 3	Fold 4	Fold 5	
Curvelet	Calc	95.24	85.71	85.71	100.00	100.00	100.00	100.00	100.00	95.24	85.71	94.76
	Circ	95.00	85.00	90.00	95.00	95.00	90.00	100.00	95.00	95.00	95.00	93.50
	Spic	93.75	93.75	100.00	93.75	87.50	100.00	93.75	93.75	93.75	81.25	93.13
	Ill-def	100.00	100.00	100.00	100.00	90.91	100.00	100.00	100.00	100.00	100.00	99.09
	Arch	87.50	87.50	93.75	100.00	87.50	81.25	81.25	81.25	93.75	100.00	89.38
	Asym	100.00	91.67	100.00	100.00	91.67	75.00	100.00	100.00	100.00	100.00	95.83
	W. Average	94.87	89.71	93.86	97.97	92.68	91.64	95.87	94.87	95.90	92.80	94.02
Db8	Calc	100.00	78.95	100.00	84.21	89.47	100.00	100.00	100.00	73.68	52.63	87.89
	Circ	66.67	72.22	66.67	100.00	83.33	83.33	83.33	83.33	100.00	83.33	82.22
	Spic	73.33	80.00	66.67	93.33	86.67	60.00	93.33	73.33	73.33	73.33	77.33
	Ill-def	90.91	100.00	100.00	90.91	90.91	100.00	100.00	100.00	100.00	100.00	97.27
	Arch	73.33	66.67	73.33	100.00	66.67	86.67	100.00	100.00	100.00	73.33	84.00
	Asym	100.00	100.00	83.33	83.33	75.00	83.33	83.33	100.00	100.00	100.00	90.83
	W. Average	83.41	81.06	81.25	92.18	82.30	85.68	93.39	92.26	89.87	77.56	85.89

Table 5.6 The classification accuracy rates obtained over the 2x5-folds to differentiate between abnormality types by extracting the biggest 100 coefficients from each decomposition level (Continued).

Method	Class	Partitions 1					Partitions 2					Average
		Fold 1	Fold 2	Fold 3	Fold 4	Fold 5	Fold 1	Fold 2	Fold 3	Fold 4	Fold 5	
Bior3.7	Calc	63.16	73.68	78.95	78.95	68.42	57.89	84.21	73.68	73.68	73.68	72.63
	Circ	77.78	66.67	83.33	72.22	88.89	100.00	100.00	94.44	94.44	94.44	87.22
	Spic	73.33	73.33	73.33	66.67	80.00	100.00	53.33	100.00	100.00	100.00	82.00
	Ill-def	81.82	81.82	81.82	72.73	90.91	90.91	100.00	100.00	100.00	100.00	90.00
	Arch	80.00	53.33	73.33	73.33	66.67	100.00	100.00	100.00	66.67	100.00	81.33
	Asym	91.67	100.00	91.67	91.67	83.33	75.00	75.00	75.00	100.00	100.00	88.33
	W. Average	76.54	73.28	79.98	75.55	78.82	86.48	85.60	89.91	87.66	93.17	82.70
Sym8	Calc	100.00	73.68	100.00	100.00	94.74	100.00	100.00	100.00	73.68	52.63	89.47
	Circ	100.00	72.22	83.33	72.22	77.78	100.00	83.33	83.33	83.33	83.33	83.89
	Spic	66.67	60.00	93.33	66.67	80.00	66.67	73.33	73.33	100.00	100.00	78.00
	Ill-def	100.00	81.82	100.00	100.00	90.91	100.00	100.00	100.00	100.00	100.00	97.27
	Arch	100.00	80.00	100.00	100.00	73.33	86.67	100.00	100.00	66.67	60.00	86.67
	Asym	91.67	100.00	91.67	100.00	83.33	83.33	83.33	83.33	100.00	100.00	91.67
	W. Average	93.41	76.60	94.48	88.94	83.42	90.12	90.09	90.09	85.44	79.76	87.23

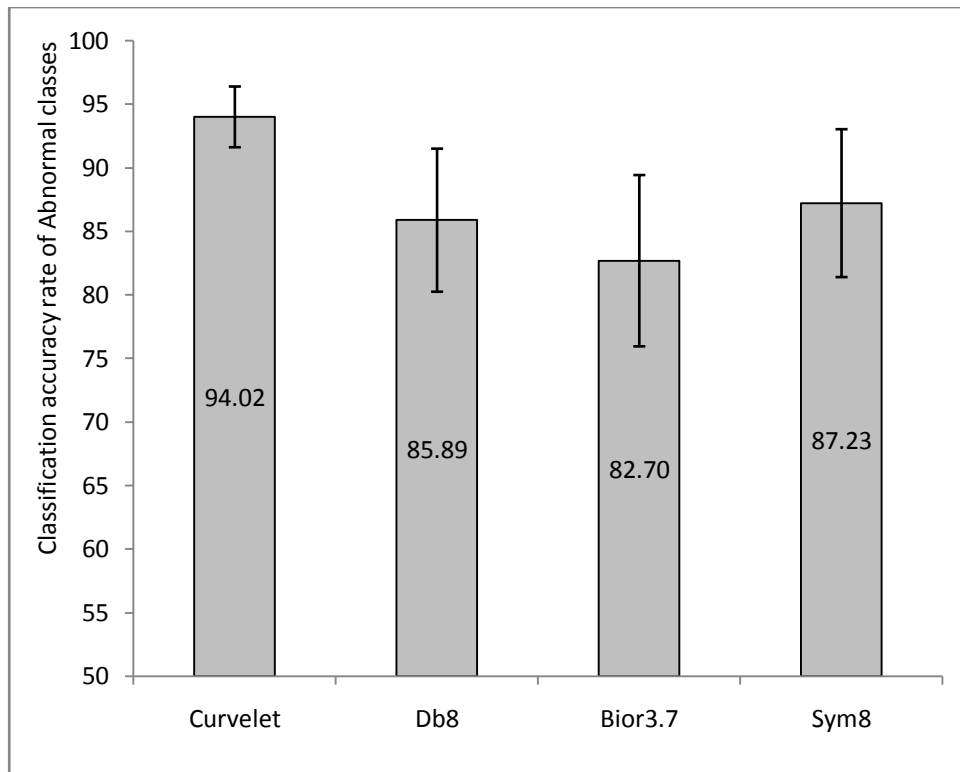


Figure 5.5 The average of the results of 2x5 folds obtained for classification of abnormal classes by extracting the biggest 100 coefficients.

In the third step, the proposed computer aided diagnosis system is used to distinguish between benign and malignant lesion. The obtained results for this classification problem is presented in Table 5.7. It shows that curvelet is still doing better than wavelet in the analysis of the mammogram images. The average classification accuracy rates obtained for 2x5 folds cross validation is presented in Figure 5.6. It shows that the standard deviation error in case of curvelet is also still better than its value in case of wavelet. The advantage of curvelet returns to its ability to describe the curvature better than wavelet.

Table 5.7 The classification accuracy rates obtained over the 2x5-folds to classify the benign and the malignant classes by extracting the biggest 100 coefficients from each decomposition level.

Method	Class	Partitions 1					Partitions 2					Average
		Fold 1	Fold 2	Fold 3	Fold 4	Fold 5	Fold 1	Fold 2	Fold 3	Fold 4	Fold 5	
Curvelet	Benign	100.00	86.54	94.23	86.54	100.00	88.08	84.62	96.15	88.46	100.00	92.46
	Malignant	85.37	85.37	87.80	100.00	90.24	100.00	100.00	100.00	100.00	100.00	94.88
	W. Average	93.51	86.02	91.38	92.51	95.67	93.37	91.44	97.86	93.58	100.00	93.53
Db8	Benign	90.22	90.38	84.62	78.85	100.00	61.54	65.38	80.77	96.15	100.00	84.79
	Malignant	85.37	92.68	96.45	87.80	70.73	100.00	85.37	102.44	82.93	100.00	90.38
	W. Average	88.07	91.40	89.87	82.82	87.02	78.60	74.25	90.38	90.29	100.00	87.27
Bior3.7	Benign	65.38	84.62	76.92	76.92	53.85	65.38	76.92	76.92	80.77	73.08	73.08
	Malignant	100.00	100.00	82.93	100.00	100.00	85.37	85.37	100.00	100.00	100.00	95.37
	W. Average	80.73	91.44	79.59	87.16	74.32	74.25	80.67	87.16	89.30	85.02	82.97
Sym8	Benign	100.00	88.46	60.00	76.92	61.54	63.46	80.77	84.62	100.00	100.00	81.58
	Malignant	100.00	100.00	70.00	85.37	100.00	85.37	60.98	60.98	82.93	100.00	84.56
	W. Average	100.00	93.58	64.43	80.67	78.60	73.18	71.99	74.14	92.43	100.00	82.90



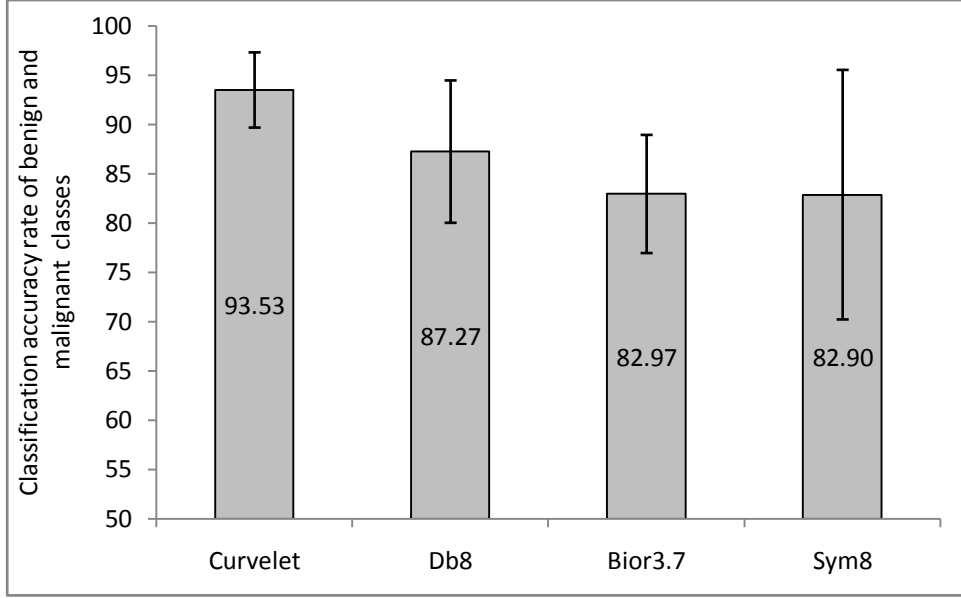


Figure 5.6 The average of the results of 2x5 folds obtained for classification of benign and malignant classes by extracting the biggest 100 coefficients.

For the three classification problems considered in this study, the obtained results suggest that curvelet features based system performs better than wavelet features based system. This goes in the same line with the expectations since curvelet transform is able to capture multidimensional features in wedges as opposed to points in wavelet transform. A hypothesis test is performed to evaluate the significance of the difference between the performances of both, curvelet and wavelet. To test whether the classification rates for curvelet are significantly higher than those of wavelet, a paired  $t$ -test is performed on the results of the 2x5-folds cross validation. Let  $\mu_c$  and  $\mu_w$  be respectively the mean accuracies of curvelet and wavelet. The null hypothesis is that the difference between the means of the two techniques is equal to zero ( $H_0 : \mu_c - \mu_w = 0$ ), and the alternative hypothesis is that the difference is positive ( $H_a : \mu_c - \mu_w > 0$ ). For a trial  $i$  of the cross validation, let  $A_w^i$  and  $A_c^i$  be respectively the results obtained by using wavelet and curvelet. The test statistic is computed as follows [160]:

$$t = \frac{\bar{A} \cdot \sqrt{n}}{\sqrt{\frac{\sum_i^n (A^i - \bar{A})^2}{n-1}}} \quad (5.1)$$

where  $\bar{A} = \frac{1}{n} \sum_{i=1}^n A^i$ ,  $A^i = A_c^i - A_w^i$  and  $n$  is the number of runs (10 for this experiment). The  $P$ -value is obtained from a  $t$ -distribution table at the degree of freedom  $(n-1)$ , and is compared to the critical value 0.05 (i.e. 5% significance level). If the  $P$ -value is smaller than 0.05, the null hypothesis is rejected at 0.05 significance level. The results of calculating  $P$ -value and  $T$ -value at 5% significance level are summarized in Table 5.8. The results show that, the null hypothesis is rejected at 0.05 significance level for all three mammogram classification problems. The comparison study is accomplished between curvelet and three different wavelet functions. It shows that the classification rates obtained using curvelet are higher than those obtained using wavelet and the differences are statistically significant.

Table 5.8 The results of  $t$ -test at significance level  $\alpha = 5\%$  to compare curvelet and wavelet decompositions.

Function	Method	$T$ -value	$P$ -value	Null Hypothesis ( $H_0$ )
Abnormal vs. Normal	Curvelet vs. Db8	2.6141	0.0176	Rejected
	Curvelet vs. Bior3.7	2.1348	0.0468	Rejected
	Curvelet vs. Sym8	2.7487	0.0132	Rejected
Abnormal Classes	Curvelet vs. Db8	4.1961	$5.4295 \times 10^{-4}$	Rejected
	Curvelet vs. Bior3.7	5.0023	$9.2371 \times 10^{-5}$	Rejected
	Curvelet vs. Sym8	3.4078	0.0031	Rejected
Benign vs. Malignant	Curvelet vs. Db8	2.4230	0.0262	Rejected
	Curvelet vs. Bior3.7	4.6991	$1.7880 \times 10^{-4}$	Rejected
	Curvelet vs. Sym8	2.5406	0.0205	Rejected

For the previous two methods, they start by sorting the coefficients of each scale and then extract a set of the biggest coefficients. This means that both methods are not considering the position of the coefficients after multiresolution decomposition, which represents a drawback. The following proposed methods will consider the position of the coefficients.

### **5.3.3 Results of Computer Aided Diagnosis System by Extracting Features Using Standard Deviation of Means**

The dataset is divided into two equal sets. Each set contains a number of images from all available classes in the dataset. The first set is used to construct the feature vectors, while the second set is used to test the proposed method. Wavelet and curvelet transforms are used to represent the ROIs of mammogram images in order to extract a set of coefficients to be presented to the classifier. In this work, four decomposition levels are used for both wavelet and curvelet.

After obtaining a multiresolution decomposition with either curvelet or wavelet of each image of the first set, a matrix of coefficients is constructed. Each row represents the vector of coefficients of an image. Subsequently, the mean of each class of images is calculated to produce a matrix, where each row vector is the mean vector of one class and the number of columns remains the length of the obtained feature vector from the multiresolution decomposition. Then the standard deviation of the matrix of means of classes is calculated to produce a vector representing the standard deviations column by column. The hard threshold value is calculated using the formula  $\sqrt{2 \log(X)}$  as in [154], where  $X$  is the length of the coefficients vector. A hard threshold is applied on the standard deviation vector. The features which have a standard deviation of means value less than the threshold will be removed, while the kept features will be passed to the classifier in order to differentiate between different classes. Table 5.9 presents the number of coefficients before and after applying the threshold.

Table 5.9 The obtained coefficients from wavelet and curvelet before and after applying threshold

Problem	Wavelet		Curvelet	
	before threshold (N)	after threshold (L)	before threshold (N)	after threshold (L)
Normal vs. abnormal	25129	722	46080	1619
Abnormality types	25129	2141	46080	2066
Benign vs. malignant	25129	1144	46080	1091

The proposed method is applied to solve the three mammogram classification problems as follows. The first step is the classification of normal versus abnormal classes. The second step is the classification of abnormality indicator based on their shape. The third step is to differentiate between benign and malignant tumors. In this work, the average of classification accuracy rates is calculated based on 2x5-folds cross validation. The proposed method is compared to the method of biggest 100 coefficients presented previously in Section 5.3.2.

Table 5.10 presents the classification accuracy rates achieved in differentiating between normal and abnormal classes. It shows that 100% of abnormal tissues have been detected, i.e. the true positive rate reached 100%. The detection of normal class reached 94.29%. The results show that the method of the standard deviation of means outperforms the method of biggest 100 coefficients in both wavelet and curvelet. Figure 5.7 illustrates the comparison results of the two methods.

Table 5.10 The classification accuracy rates obtained over the 2x5-folds to differentiate between the normal and abnormal classes using standard deviation of means feature extraction method.

Method	Class	Partitions 1					Partitions 2					Average	
		Fold 1	Fold 2	Fold 3	Fold 4	Fold 5	Fold 1	Fold 2	Fold 3	Fold 4	Fold 5		
Curvelet	Abnormal	100.00	100.00	100.00	100.00	100.00	100.00	100.00	100.00	100.00	100.00	100.00	100.00
	Normal	95.06	93.72	93.72	94.20	94.20	93.72	94.20	94.20	95.65	94.20	94.29	
	W. Average	96.82	95.96	95.96	96.27	96.27	95.96	96.27	96.27	97.20	96.27	96.33	
Wavelet	Abnormal	100.00	100.00	100.00	100.00	100.00	100.00	100.00	100.00	100.00	100.00	100.00	
	Normal	91.30	90.82	91.79	91.3	91.79	91.79	92.75	91.79	91.30	90.82	91.55	
	W. Average	94.41	94.10	94.72	94.41	94.72	94.72	95.34	94.72	94.41	94.10	94.57	

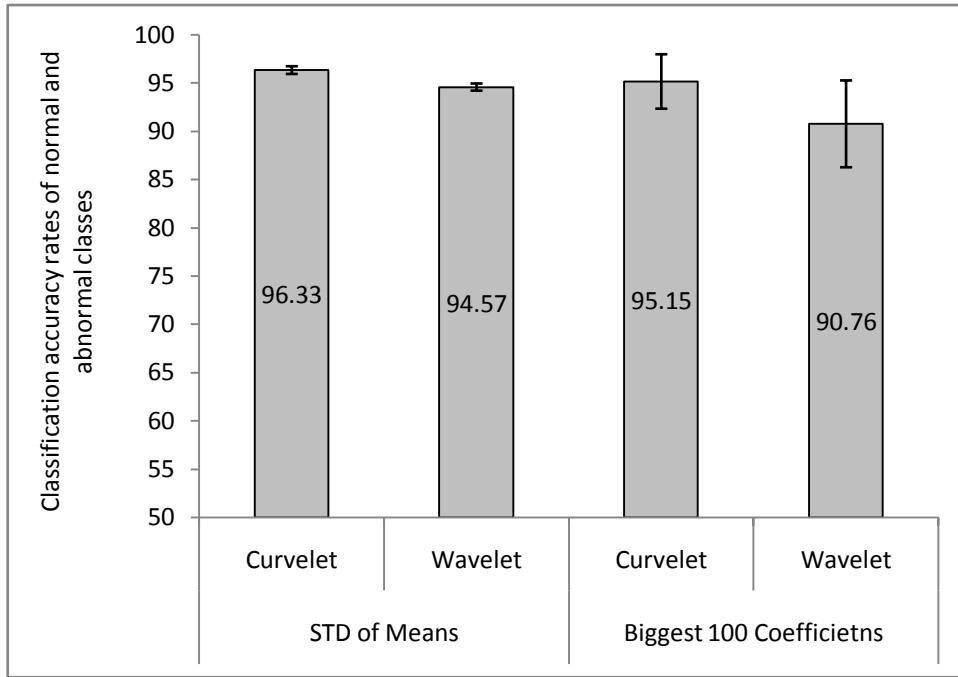


Figure 5.7 The average of the classification rates of 2x5 folds obtained for classification of normal and abnormal classes using standard deviation of means feature extraction method.

Table 5.11 presents the classification accuracy rates of abnormality types according to their shapes. It shows that the set of coefficients extracted from curvelet transform achieves higher classification rate compared to wavelet coefficients. It shows as well that the proposed method performs better than the method of extracting the biggest 100 coefficients from different decomposition levels presented in Section 5.3.2. The comparison between the current proposed method and the method of extracting the biggest 100 coefficients from different decomposition levels is illustrated in Figure 5.8.

Table 5.11 The classification accuracy rates obtained over the 2x5-folds to differentiate between abnormality types using standard deviation of means feature extraction method.

Method	Class	Partitions 1					Partitions 2					Average
		Fold 1	Fold 2	Fold 3	Fold 4	Fold 5	Fold 1	Fold 2	Fold 3	Fold 4	Fold 5	
Curvelet	Calc	100.00	100.00	100.00	100.00	92.00	100.00	100.00	96.00	96.00	96.00	98.00
	Circ	91.30	91.30	91.30	86.96	86.96	95.65	95.65	95.65	95.65	91.30	92.17
	Misc	100.00	100.00	100.00	100.00	92.86	100.00	100.00	100.00	100.00	100.00	99.29
	Spic	100.00	100.00	94.74	100.00	100.00	94.74	94.74	94.74	94.74	94.74	96.84
	Arch	89.47	89.47	84.21	89.47	89.47	94.74	94.74	94.74	89.47	100.00	91.58
	Asym	100.00	100.00	100.00	100.00	100.00	100.00	100.00	100.00	100.00	100.00	100.00
	W. Average	96.52	96.52	94.78	95.65	93.04	97.39	97.39	96.52	95.65	96.52	96.00
Wavelet	Calc	92.00	96.00	100.00	92.00	100.00	96.00	100.00	100.00	96.00	96.00	96.80
	Circ	86.96	91.30	95.65	91.30	86.96	95.65	100.00	95.65	95.65	95.65	93.48
	Misc	92.86	92.86	100.00	92.86	100.00	100.00	100.00	85.71	100.00	100.00	96.43
	Spic	100.00	78.95	94.74	89.47	100.00	84.21	89.47	94.74	94.74	89.47	91.58
	Arch	94.74	100.00	89.47	84.21	94.74	78.95	100.00	89.47	94.74	100.00	92.63
	Asym	100.00	100.00	100.00	100.00	100.00	100.00	100.00	100.00	100.00	100.00	100.00
	W. Average	93.91	93.04	96.52	91.30	96.52	92.17	98.26	94.78	96.52	96.52	94.96

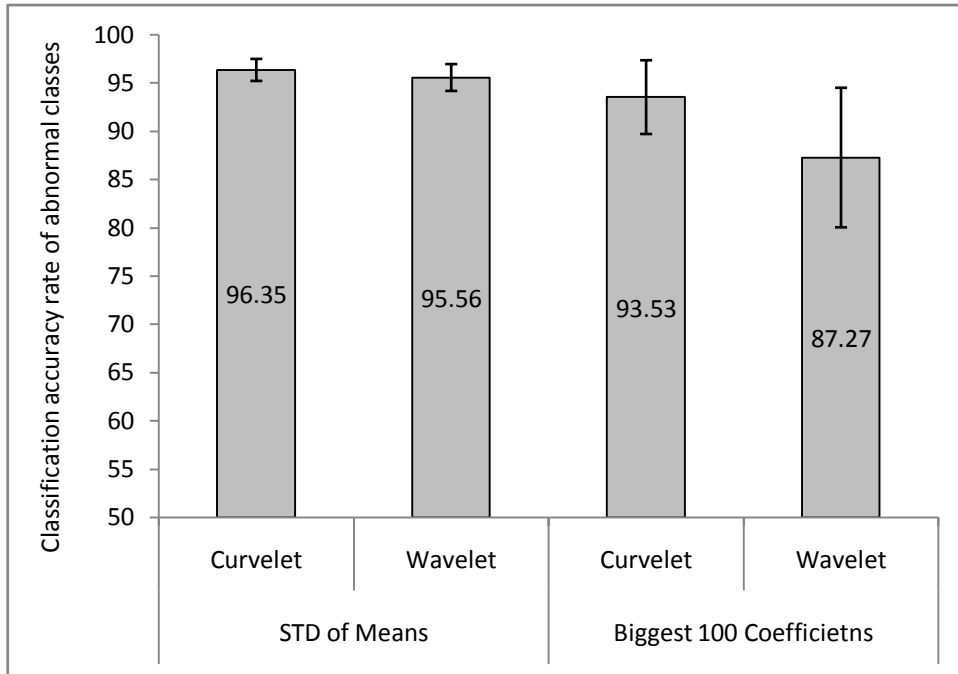


Figure 5.8 The average of the classification rates of 2x5 folds obtained for classification of abnormal classes using standard deviations of means feature extraction method.

Table 5.12 shows that the malignant class has been classified completely, and curvelet still outperforms wavelet. The proposed method gives classification rates higher than the work presented in Section 5.3.2. Figure 5.9 illustrates the comparison results between the proposed method of extracting features using the standard deviation of means and the method of extracting the biggest 100 coefficients from different decomposition levels to differentiate between benign and malignant in mammogram images.



Table 5.12 The classification accuracy rates obtained over the 2x5-folds to differentiate between benign and malignant classes using standard deviation of means feature extraction method.

Method	Class	Partitions 1					Partitions 2					Average
		Fold 1	Fold 2	Fold 3	Fold 4	Fold 5	Fold 1	Fold 2	Fold 3	Fold 4	Fold 5	
Curvelet	Benign	95.31	93.75	95.31	92.19	93.75	95.31	92.19	95.31	89.06	92.19	93.44
	Malignant	100.00	100.00	100.00	100.00	100.00	100.00	100.00	100.00	100.00	100.00	100.00
	W. Average	97.39	96.52	97.39	95.65	96.52	97.39	95.65	97.39	93.91	95.65	96.35
Wavelet	Benign	93.75	92.19	95.31	90.63	90.63	93.75	90.63	95.31	87.50	90.63	92.03
	Malignant	100.00	100.00	100.00	100.00	100.00	100.00	100.00	100.00	100.00	100.00	100.00
	W. Average	96.52	95.65	97.39	94.79	94.79	96.52	94.79	97.39	93.04	94.79	95.56

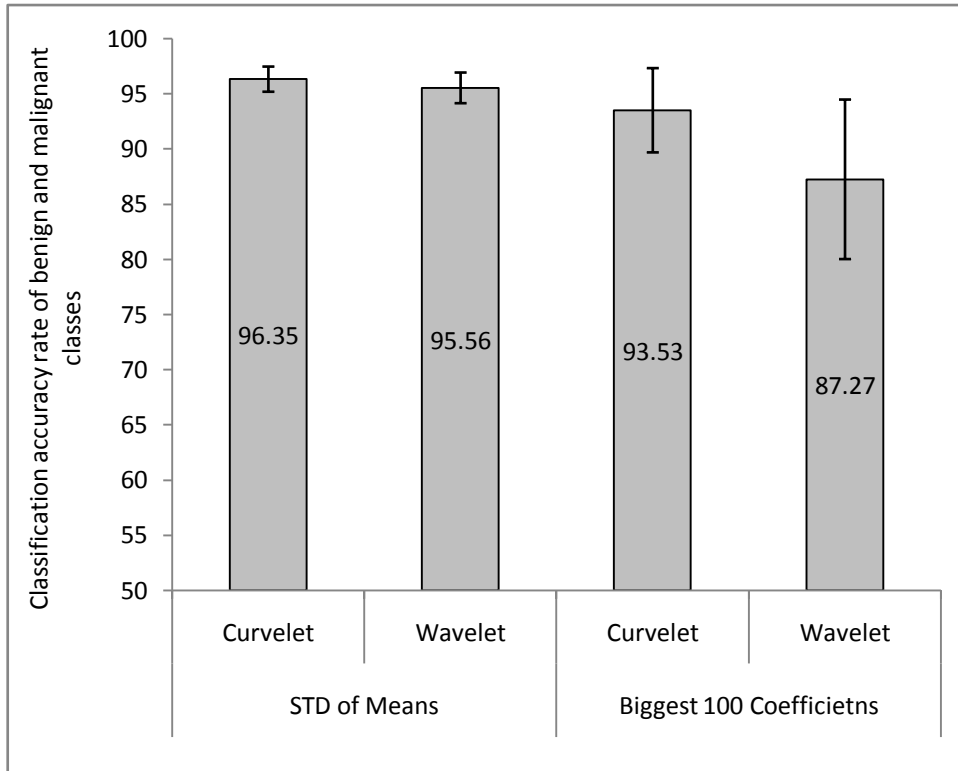


Figure 5.9 The average of the classification rates of 2x5 folds obtained for classification of benign and malignant classes using standard deviations of means feature extraction method.

To test whether the difference between the classifications rates of the method of standard deviation of means and the method of extracting the biggest 100 coefficients presented in Section 5.3.2 is statistically significant, a paired  $t$ -test is performed on the results of the 2x5-folds cross validation.

Let  $\mu_1$  and  $\mu_2$  be respectively the mean accuracies of the current proposed method and the method of biggest 100 coefficients, respectively. The null hypothesis is that the difference between the means of the two methods is zero, i.e. ( $H_0 : \mu_1 - \mu_2 = 0$ ), and the alternative hypothesis is that the difference is positive, i.e. ( $H_a : \mu_1 - \mu_2 > 0$ ). For a trial  $i$  of the cross validation, let  $A_1^i$  and  $A_2^i$  be respectively the results obtained by using the proposed method and the method of 100 biggest coefficient in each level. The  $t$ -test statistic is computed as given in Section 5.3.2. The  $P$ -value is obtained from a  $t$ -distribution Table at the degree of freedom ( $n-1$ ), and is compared to the critical value 0.05 (i.e. 5% significance level).

If the  $P$ -value is less than 0.05, the null hypothesis is rejected at 5% significance level. The results at 5% significance level are summarized in Table 5.13.

Table 5.13 The results of  $t$ -test at significance level  $\alpha=5\%$  between the standard deviation of means and the biggest 100 coefficients feature extraction methods.

Problem	Method	$T$ -value	$P$ -value	Null Hypothesis ( $H_0$ )
Abnormal vs. Normal	Curvelet	1.3036	0.2088	Accepted
	Wavelet	2.6672	0.0157	Rejected
Abnormality types	Curvelet	2.2961	0.0339	Rejected
	Wavelet	4.7148	$1.7276 \times 10^{-4}$	Rejected
Benign vs. Malignant	Curvelet	2.2273	0.0389	Rejected
	Wavelet	3.5663	0.0022	Rejected

The null hypothesis is rejected at 5% significance level all over the three classification steps except in case of using curvelet to differentiate between abnormal and normal. It means that the classification rates obtained using the current proposed method are higher than those obtained using the method presented in Section 5.3.2, and the difference is statistically significant.

#### 5.3.4 Results of Computer Aided Diagnosis System by Extracting Features Based on Feature Ranking Method

In this method, a matrix of coefficients is constructed by the obtained features vectors from wavelet or curvelet decomposition of the ROIs images. Subsequently, a ranked list of features is built based on the criterion used to assess the capability of every feature for separating two labeled classes. Then, a dynamic threshold is applied to extract the most significant features. The dataset decomposed into training and testing data. The training data are used to build the SVM classifier, while the testing data are used to calculate the classification accuracy rate. This method is repeated until reaching the best classification rate with the minimum number of coefficients.

The evaluation of the system can be carried out using two mammogram classification steps. The first step is the classification of normal versus abnormal tissues. The second step is to distinguish whether the abnormal tissue is benign or malignant. Firstly, we apply the wavelet to the dataset, followed by the proposed method for feature extraction. Then SVM is constructed and the classification accuracy rate is calculated. Figure 5.10 illustrates the performance of the SVM classifier to distinguish between normal and abnormal corresponding to the number of extracted feature with different threshold values. It shows that the maximum accuracy obtained is 94.79% with 1238 features. It can be noted that there are several points which reached the highest performance but we choose the point where the number of features is the minimum and the classification accuracy rate is the maximum.

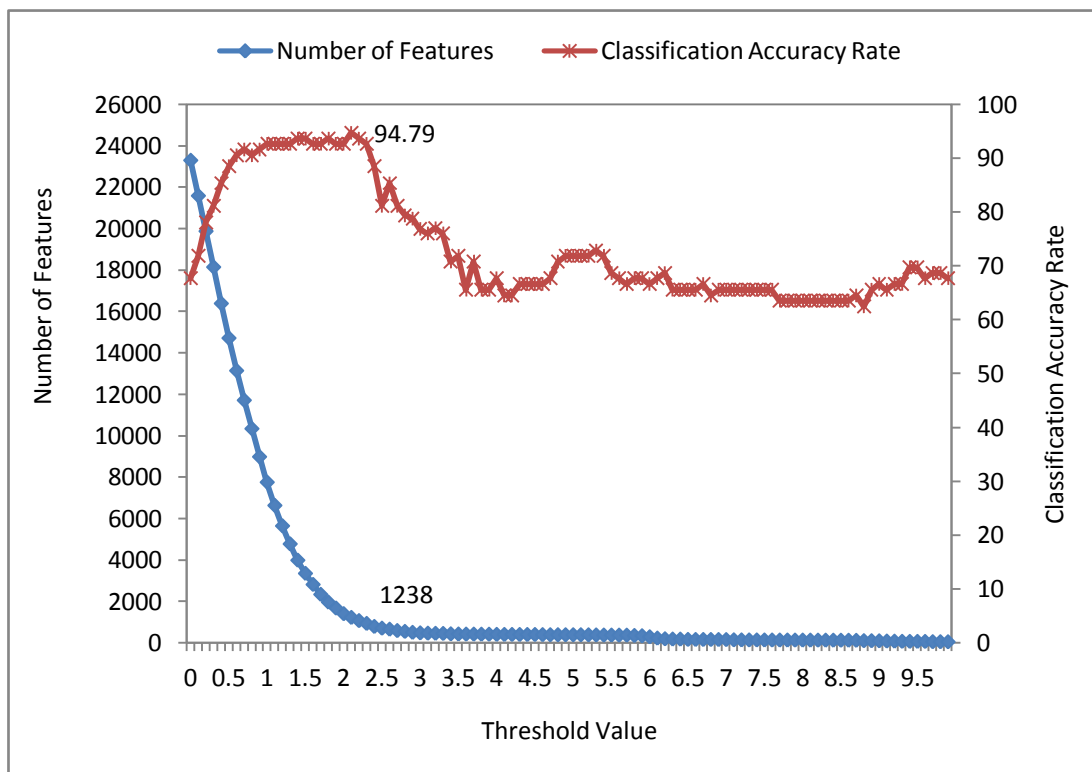


Figure 5.10 The classification accuracy rates for normal and abnormal classes corresponding to the number of features with different thresholds using wavelet coefficients.

Subsequently, the system is used to distinguish between benign and malignant tumors. Figure 5.11 illustrates the performance of the SVM classifier corresponding to the number of extracted features with different threshold values. The classifier achieved 100% at several points; the minimum number of features that achieved 100% classification rate is 150 features.

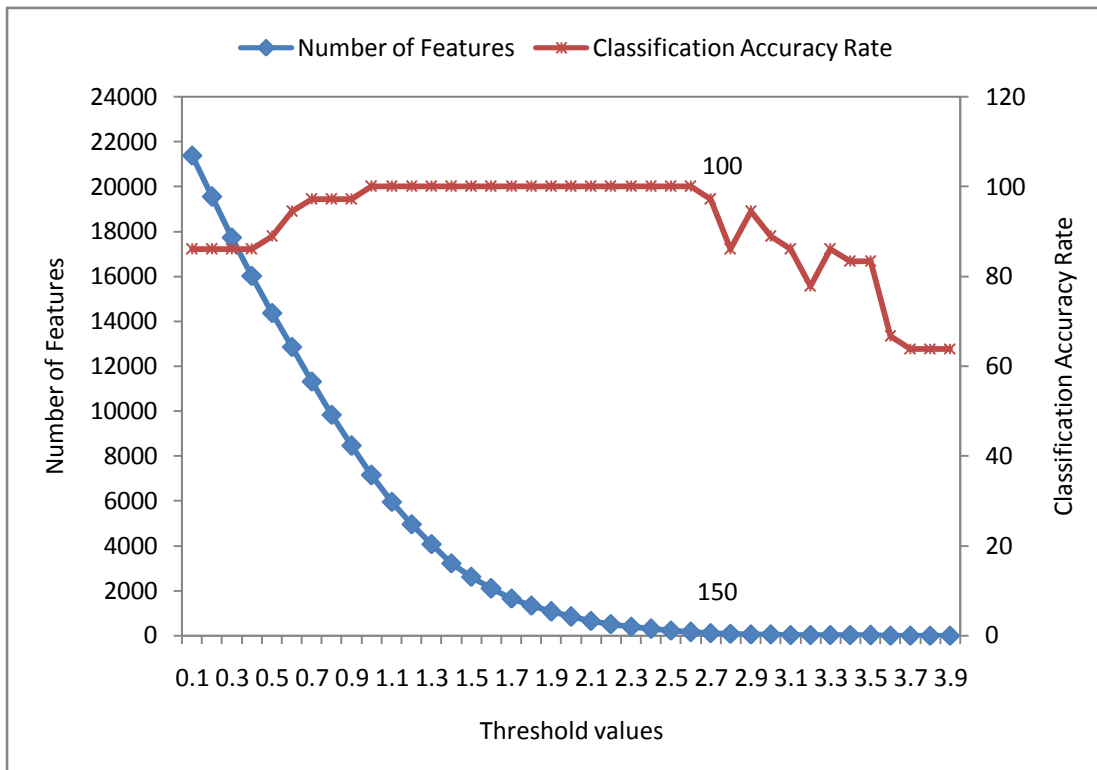


Figure 5.11 The classification accuracy rates for benign and malignant classes corresponding to the number of features with different thresholds using wavelet coefficients.

Secondly, curvelet is applied to the dataset, followed by the proposed method for feature extraction and SVM classifier. Figure 5.12 and Figure 5.13 illustrate the performance of the classifier in case of using features provided by curvelet transform. They show that the classification accuracy rate reached 95.67% using 5663 coefficients to classify between normal and abnormal, while it reached 100% in case of classifying benign and malignant using 333 coefficients.

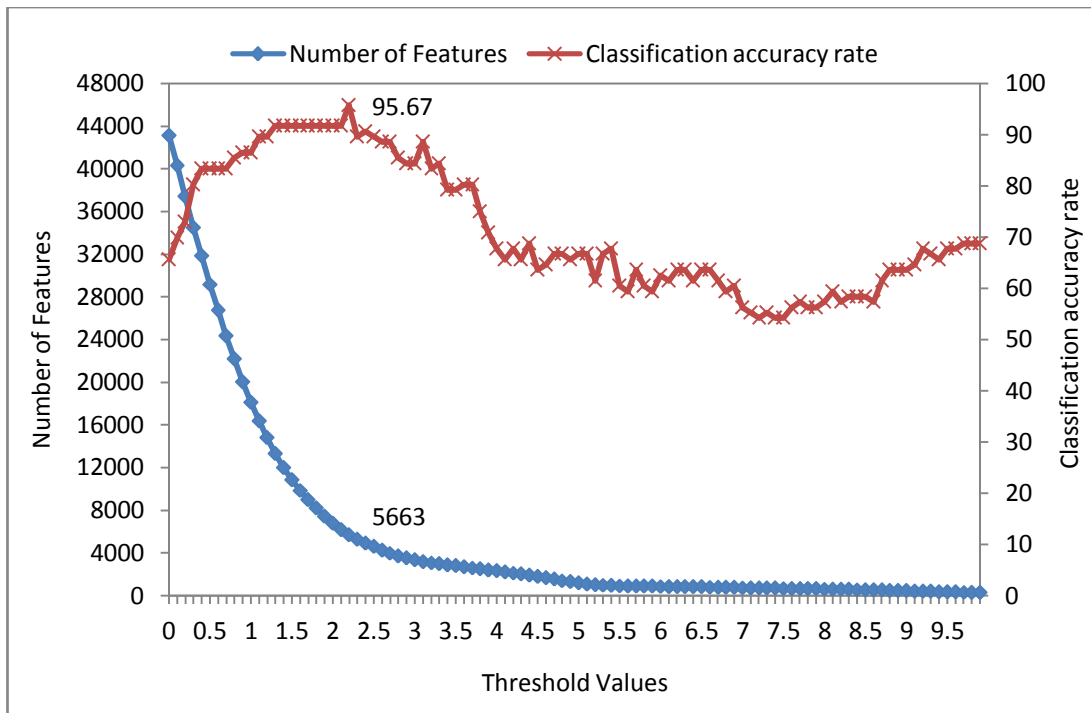


Figure 5.12 The classification accuracy rates for normal and abnormal classes corresponding to the number of features with different thresholds using curvelet coefficients.

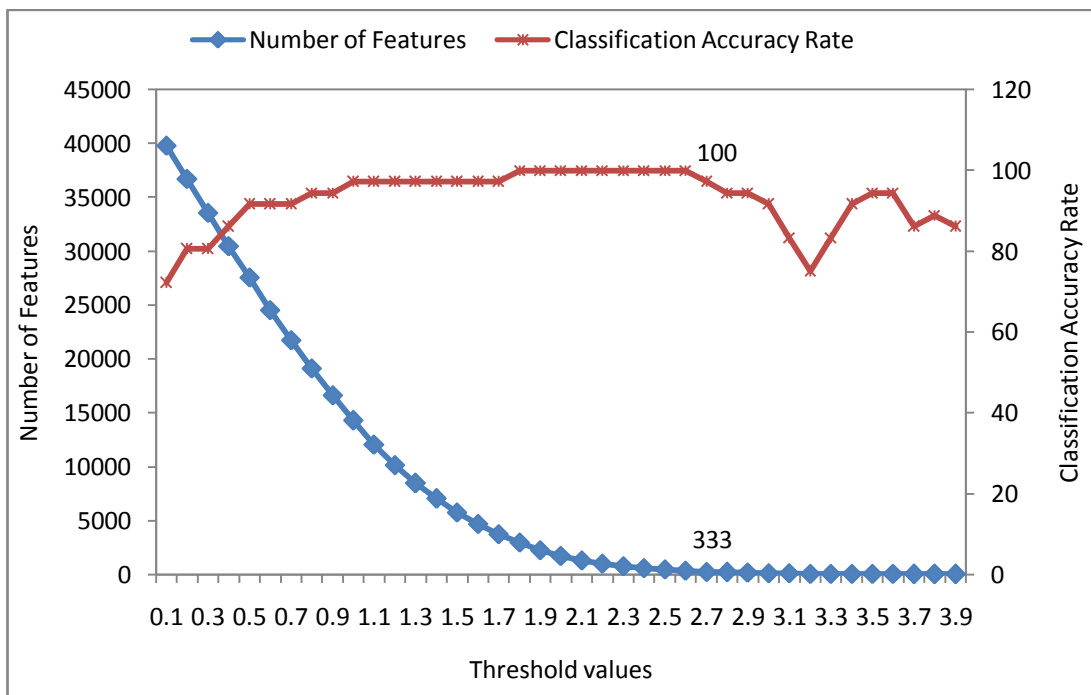


Figure 5.13 The classification accuracy rates for benign and malignant classes corresponding to the number of features with different thresholds using curvelet coefficients.

To validate the results, 2x5-folds cross validation method is applied at the optimized threshold point. The classification accuracy rates are calculated using the obtained coefficients from the applied threshold. The result of 2x5-folds cross validation are presented in Figure 5.14. The error bar represents the standard deviation between different folds.

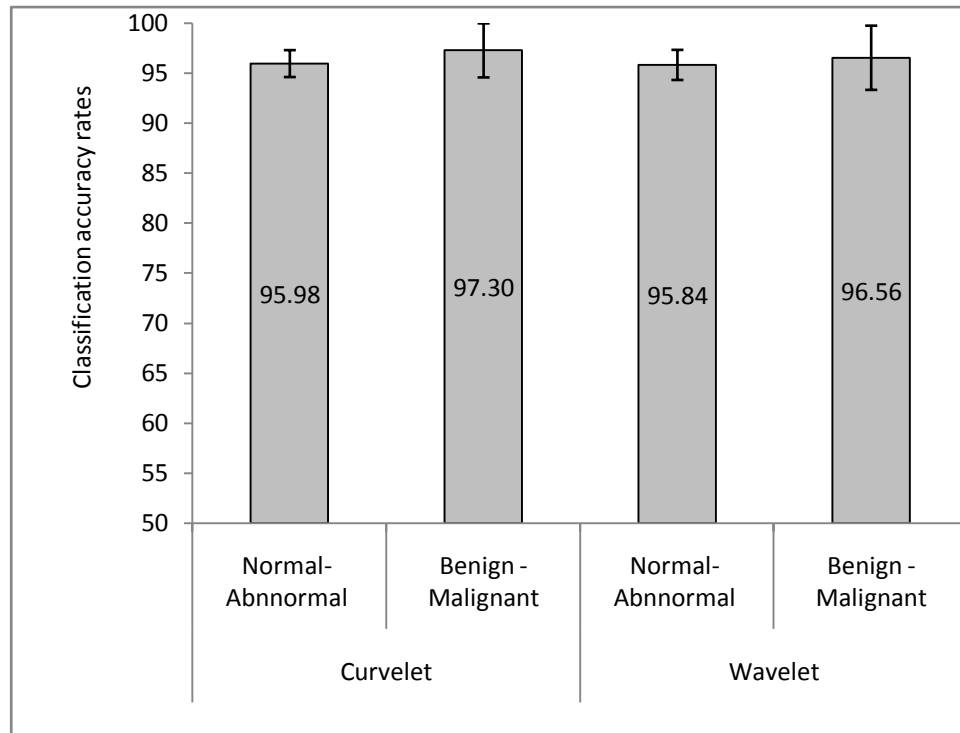


Figure 5.14 Classification accuracy rates obtained through 2x5-folds cross validation.

The proposed method proves a good capability to classify between different classes. The number of features decreases drastically from 25,129 coefficients to only 1238 and 150 with accepted classification rates in wavelet, while, in case of curvelet it decreases from 46,080 coefficients to 5663 and 333 with the two classification stages, respectively.

A comparison study between the current method of feature extraction and the previously presented methods of extracting the biggest 100 coefficients or using the standard deviation of means is accomplished. A *t*-test is performed to compare the current method and each of the previously presented methods. Table 5.14 presents the results of *t*-test between the feature ranking and the biggest 100 coefficients method.

Table 5.14 The results of *t*-test at significance level  $\alpha=5\%$ , between the feature ranking method and the biggest 100 coefficients method.

Function	Method	<i>T</i> -value	<i>P</i> -value	Null Hypothesis ( $H_0$ )
Abnormal vs. Normal	Curvelet	0.8387	0.4126	Accepted
	Wavelet	3.4418	0.0029	Rejected
Benign vs. Malignant	Curvelet	4.1913	$5.4867 \times 10^{-4}$	Rejected
	Wavelet	3.7733	0.0014	Rejected

Table 5.14 shows that the current proposed method gives a statistically significant improvement compared to the method of extracting the biggest 100 coefficients; except when using curvelet to differentiate between normal and abnormal. The acceptance of null hypothesis in that case is due to the high accuracy obtained with extracting 100 coefficients using curvelet decomposition. By the same way, a statistical analysis is accomplished between the feature ranking method and the method of standard deviation of means as given in Table 5.15.

Table 5.15 The results of *t*-test at significance level  $\alpha=5\%$  between the feature ranking method and the standard deviation of means method.

Problem	Method	<i>T</i> -value	<i>P</i> -value	Null Hypothesis ( $H_0$ )
Abnormal vs. normal	Curvelet	0.7657	0.4538	Accepted
	Wavelet	3.0736	0.0065	Rejected
Benign vs. Malignant	Curvelet	1.2741	0.2188	Accepted
	Wavelet	0.9916	0.3345	Accepted

Table 5.15 shows that there is no statistically significant difference between the feature ranking method and the standard deviation of means method except in the case of wavelet with normal and abnormal. For that unique case, the method of standard deviation of means performs better than the feature ranking method and the difference is statistically significant. It can be concluded that the method of standard



deviation of means for feature extraction has the best performance among the discussed methods.

### 5.3.5 Results of Computer Aided Diagnosis System Using Curvelet Based Texture Feature Extraction Technique

In this section, the texture features are used to identify different types of breast cancer. The ROIs are cropped with size 128x128, where the given centers of the abnormality areas were selected to be the centers of ROIs. The dataset was divided into two groups. The first is used to calculate the extracted feature and construct the classifier. The second group is used to test the proposed method.

Once the images are cropped as described earlier, the curvelet transform is applied to the obtained ROI. Then seven statistical properties for each wedge are calculated. In this study, curvelet is used with scale 4 and 16 angle, i.e. the ROI is decomposed into 81 wedges, and the features are calculated for each wedge, so that a total of 567 features are calculated to form a feature vector.

The most significant features are extracted by using the method of standard deviation of means presented in Section 4.2.2.3. These extracted features are used to classify between different classes. The number of features obtained after applying the feature extraction method is presented in Table 5.16.

Table 5.16 The obtained features before and after feature extraction method applied

Problem	Total features	Total features
	before feature extraction	after feature extraction
Normal vs. Abnormal	567	220
Benign vs. Malignant	567	222

In the classification level two main problems are covered, to distinguish between normal and abnormal, and then the abnormalities are classified into benign or malignant. The classification step is performed using the KNN classifier. The

classifier is constructed using the Euclidean distance as a measurement between the correspondent coefficients.

Table 5.17 shows the successful classification rate of mammogram images with the overall classification accuracy based on 2x5-folds cross validation. The average rate for each fold is calculated, and then the average of 2x5-folds is calculated. It shows that, the average of successful classification rates of mammogram images for normal and abnormal reaches 96.20%. A rate of 90.85% for classification between benign and malignant tumors is obtained as shown in Table 5.18. Figure 5.15 presents the results for both classification problems.

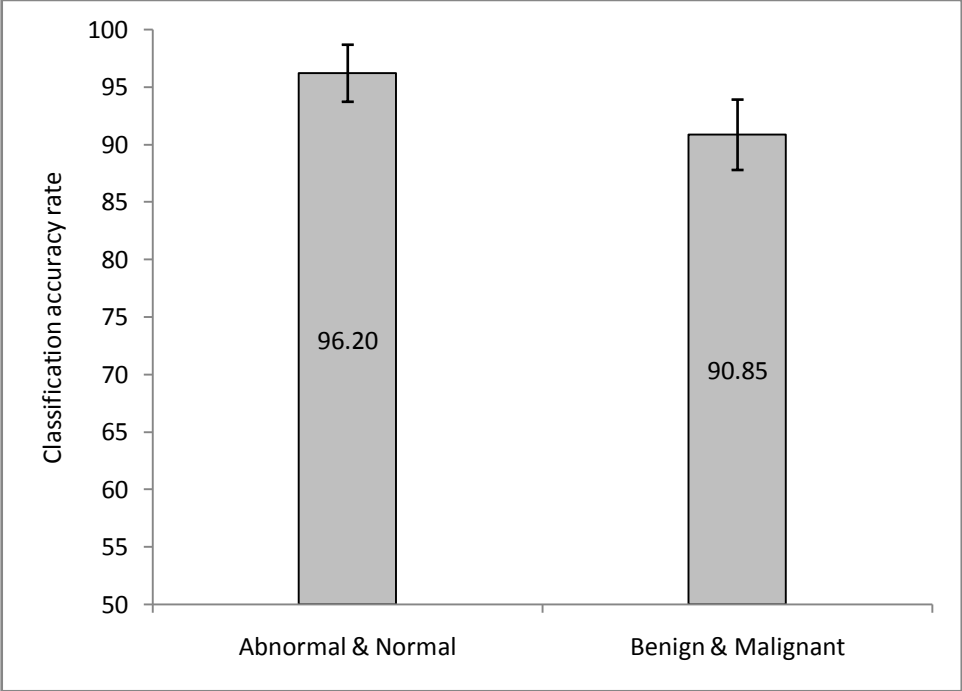


Figure 5.15 The average classification accuracy rate for two mammogram classification problems using texture feature method.

Table 5.17 The classification accuracy rates obtained over the 2x5-folds to classify between normal and abnormal classes using texture features method.

Class	Partitions 1					Partitions 2					Average
	Fold 1	Fold 2	Fold 3	Fold 4	Fold 5	Fold 1	Fold 2	Fold 3	Fold 4	Fold 5	
Abnormal	100.00	100.00	97.10	98.07	100.00	93.20	94.68	92.46	89.59	91.54	95.66
Normal	95.65	93.04	100.00	100.00	100.00	94.65	94.26	93.45	98.12	95.82	96.50
W. Average	97.20	95.53	98.96	99.31	100.00	94.13	94.41	93.10	95.07	94.29	96.20

Table 5.18 The classification accuracy rates obtained over the 2x5-folds to classify between benign and malignant classes using texture features method.

Class	Partitions 1					Partitions 2					Average
	Fold 1	Fold 2	Fold 3	Fold 4	Fold 5	Fold 1	Fold 2	Fold 3	Fold 4	Fold 5	
Benign	87.50	89.25	86.56	100.00	81.25	87.56	90.63	87.50	81.25	84.38	87.59
Malignant	100.00	100.00	100.00	90.20	100.00	88.24	94.12	90.20	92.15	94.38	94.93
W. Average	93.04	94.02	92.52	95.65	89.57	87.86	92.18	88.70	86.08	88.81	90.85

## **5.4 Part II: Automatic ROI Detection**

This part concerns with the segmentation of the ROIs automatically. It consists of two stages. Firstly, it starts by identifying the breast region area by removing the black background. Subsequently, the pectoral muscle is suppressed using region growing algorithm. Secondly, two methods are applied to detect the suspicious regions in the image. Then, the suspicious regions are analyzed using curvelet and wavelet in order to extract and select a set of feature to differentiate between the cancerous regions and the normal regions. In this part, the study considers two types of abnormality (mammographic mass and architectural distortion). The following sections give the obtained results from each stage.

### **5.4.1 Stage One: Breast Region Segmentation**

In the preprocessing step, the breast is segmented in order to limit the search for abnormalities from the background of the mammogram without undue influence, in order reduce the processing time. This stage consists of the following steps:

#### *5.4.1.1 Step 1: Black Background Removal*

A threshold values is applied to the sums of rows and columns to eliminate the black background. Figure 5.16 illustrates the removing of black background from the original image.

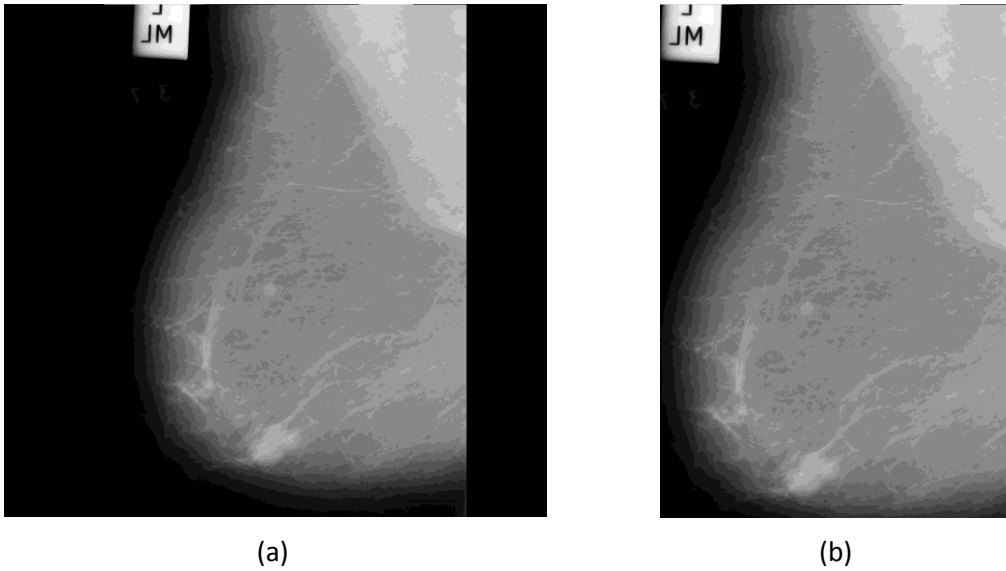


Figure 5.16 The black background removal. (a) Original mammogram image, (b) The captured region of the original mammogram.

#### 5.4.1.2 Step 2: Image Binarization

A global image thresholding is performed with Otsu's method [156] to binarize the mammogram image. The goal of this step is to determine the regions of the processed image; the label region and the breast region. Figure 5.17 illustrates the binarized image.



Figure 5.17 The binarized image to define the label of the image and the breast region.

#### 5.4.1.3 Step 3: Label Removal

In this step we obtained only the breast region and the label area. To remove the label area, the connected components thresholding is applied. We keep the biggest region which corresponds to the breast and eliminate the others. Figure 5.18 illustrates the removal of the label and keeping only the breast region.

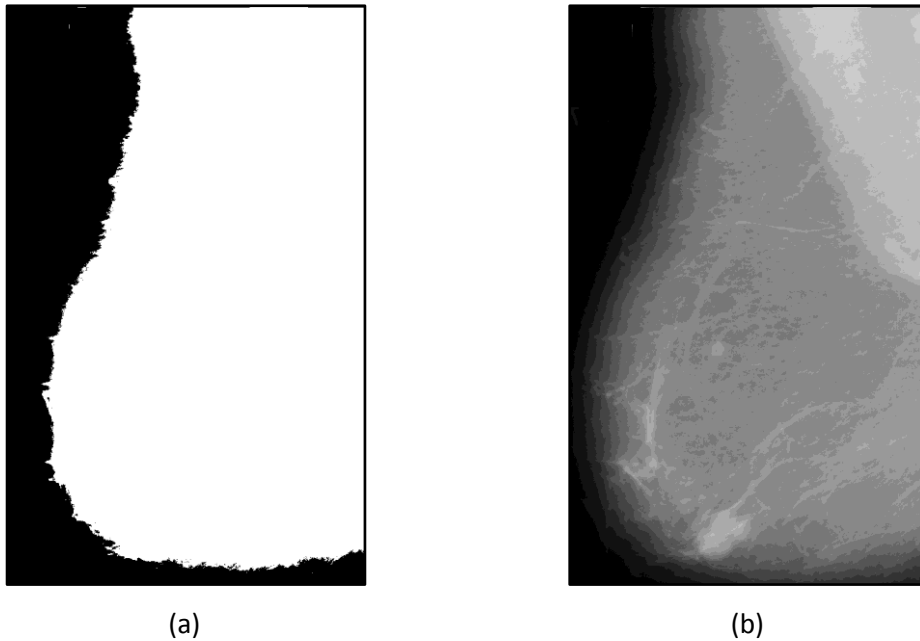


Figure 5.18 The label removal step. (a) The binarized image after removing the label. (b) The obtained area from the original mammogram image.

#### 5.4.1.4 Step 4: Breast Orientation

The objective of this step is to determine whether the mammogram image is right or left. To define the mammogram as right or left breast, we divide the image into two sides (left and right) as shown in Figure 5.19. We, then calculate the sum of both sides. The mammogram is classified as right or left according to the biggest sum obtained.

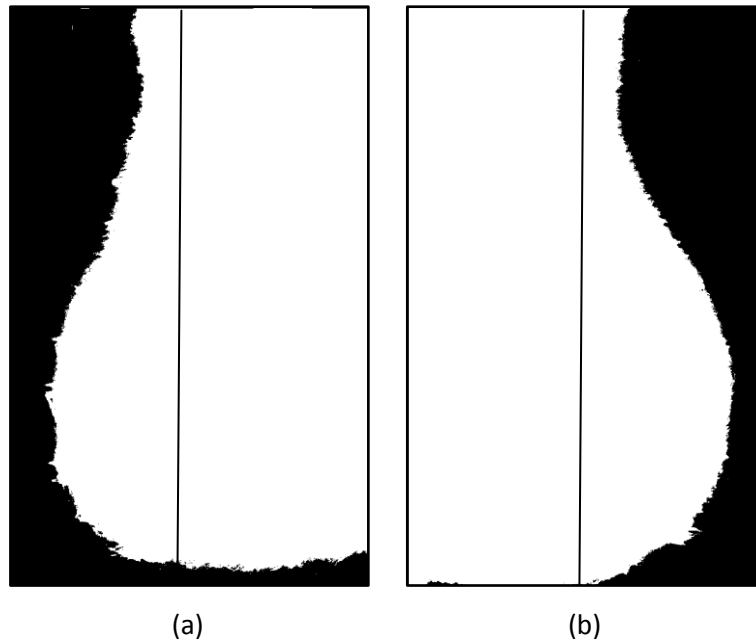


Figure 5.19 The orientation of the breast. (a) Left mammogram (b) Right mammogram.

#### 5.4.1.5 Step 5: Pectoral Muscle Suppression

The mammogram is already classified as right or left breast. Then, a region growing method is used to estimate the pectoral muscle. The region growing algorithm needs a seed point and a thresholded value. The seed point can be determined easily from the orientation of the breast, because the pectoral muscle is always in one of the upper corners. Once the seed point is determined, the region growing algorithm starts to grow in all directions. Then, the mean of the region is calculated. The new pixel will be added to the region if the difference between that pixel value and the calculated mean is within the predefined threshold value. If all differences of the neighbor pixel values are higher than the threshold value, the region growing algorithm will stop immediately. Subsequently, the determined region which is the pectoral muscle is suppressed from the breast region. Figure 5.20 illustrates two mammogram images with suppressed pectoral muscles.

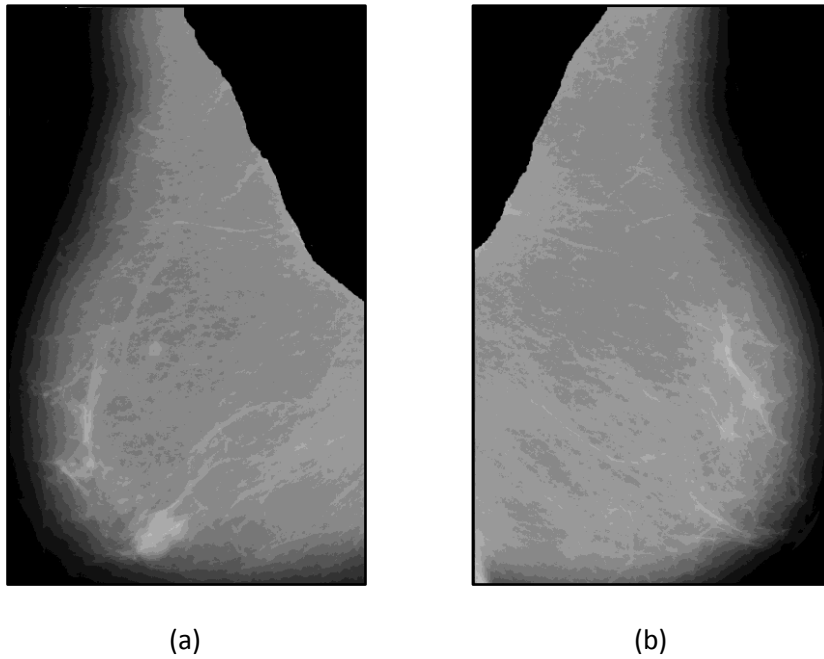


Figure 5.20 Region growing result of two different mammogram images.

Now, the study successfully determines and extracts the breast region from the original mammogram image. This process is applied to 322 images from MIAS dataset. The method was successful in extracting 310 breast regions from the whole dataset. It achieved detection accuracy of 96.27%.

#### **5.4.2 Stage Two: Region of Interest (ROI) Segmentation**

In this stage the goal is to identify the suspicious regions in the breast region detected in stage one. Subsequently, a false positive reduction method is used to identify the abnormal regions from the normal regions. So, this stage can be divided into two steps. The first step is to detect the suspicious region. The second step is to reduce the false positive regions. To accomplish these goals, there are two suggested methods to detect the suspicious region. The first method is based on developing an adaptive threshold method, and the second is based on developing a pattern matching method. The results obtained by using these methods are described as follows.



#### 5.4.2.1 An Adaptive Threshold Method to Identify the Suspicious Region

*A- Thresholding:* The threshold value is determined according to a calculated value of  $k$  in the threshold equation  $T = \mu + k \sigma$  given in Section 4.3.2.1. To calculate the value of the constant  $k$ , the dataset is divided into two sets. The first set is used to determine the value of  $k$  experimentally. The second set is used to validate the calculated  $k$  value. Figure 5.21 and Figure 5.22 illustrate the breast region after applying the adaptive thresholding method for both masses and architectural distortion, respectively. They show that the obtained image after applying the threshold value has several different regions as in columns (b). Firstly, a connected component thresholding method is applied to remove the small regions as in columns (c). Secondly, the remaining regions will be used as suspicious regions.

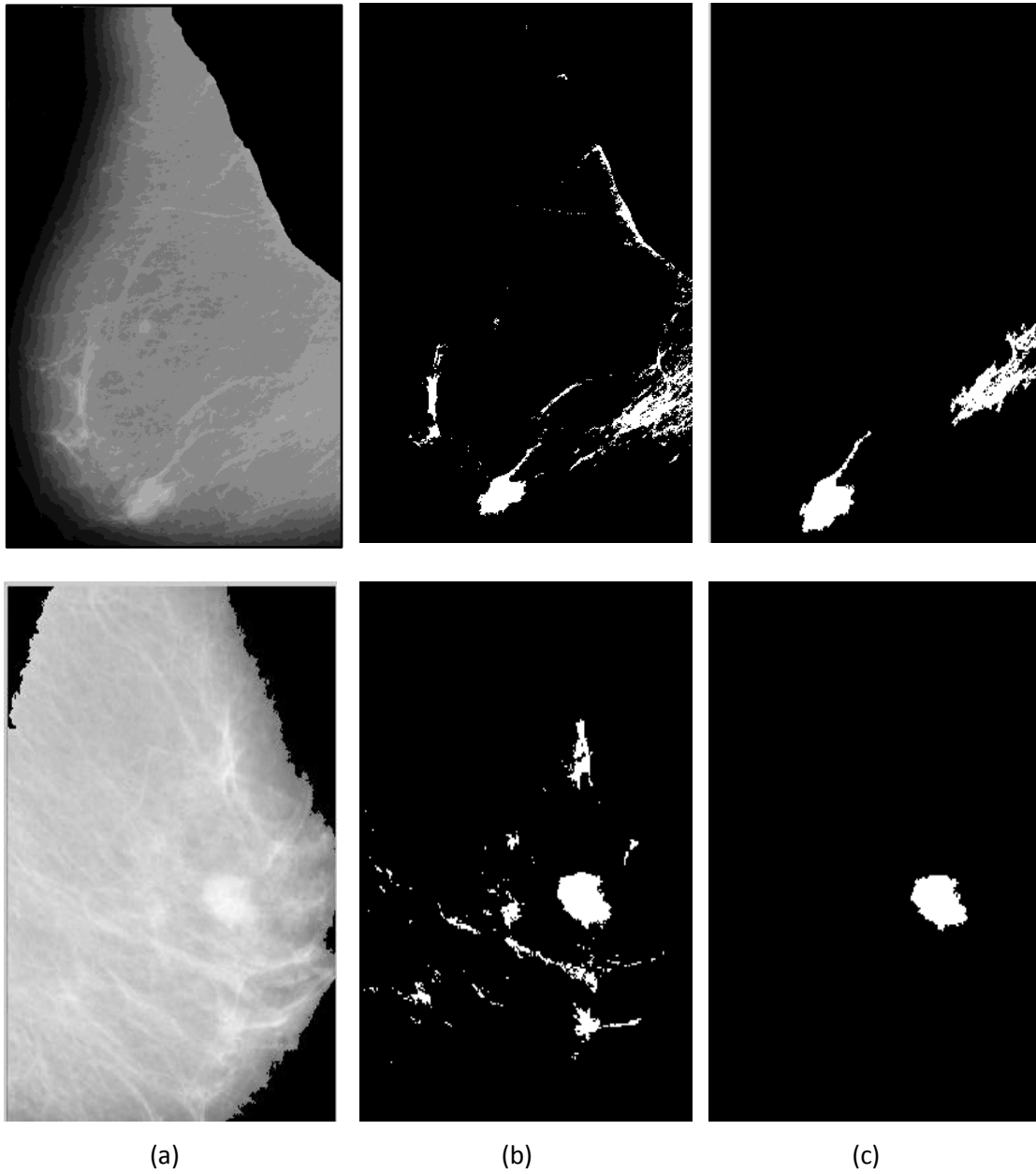


Figure 5.21 Thresholding the mammogram breast region to extract the suspicious regions in mammographic mass. (a) The original breast region image. (b) The thresholded image (c) The suspicious regions appear after suppression of the small regions.

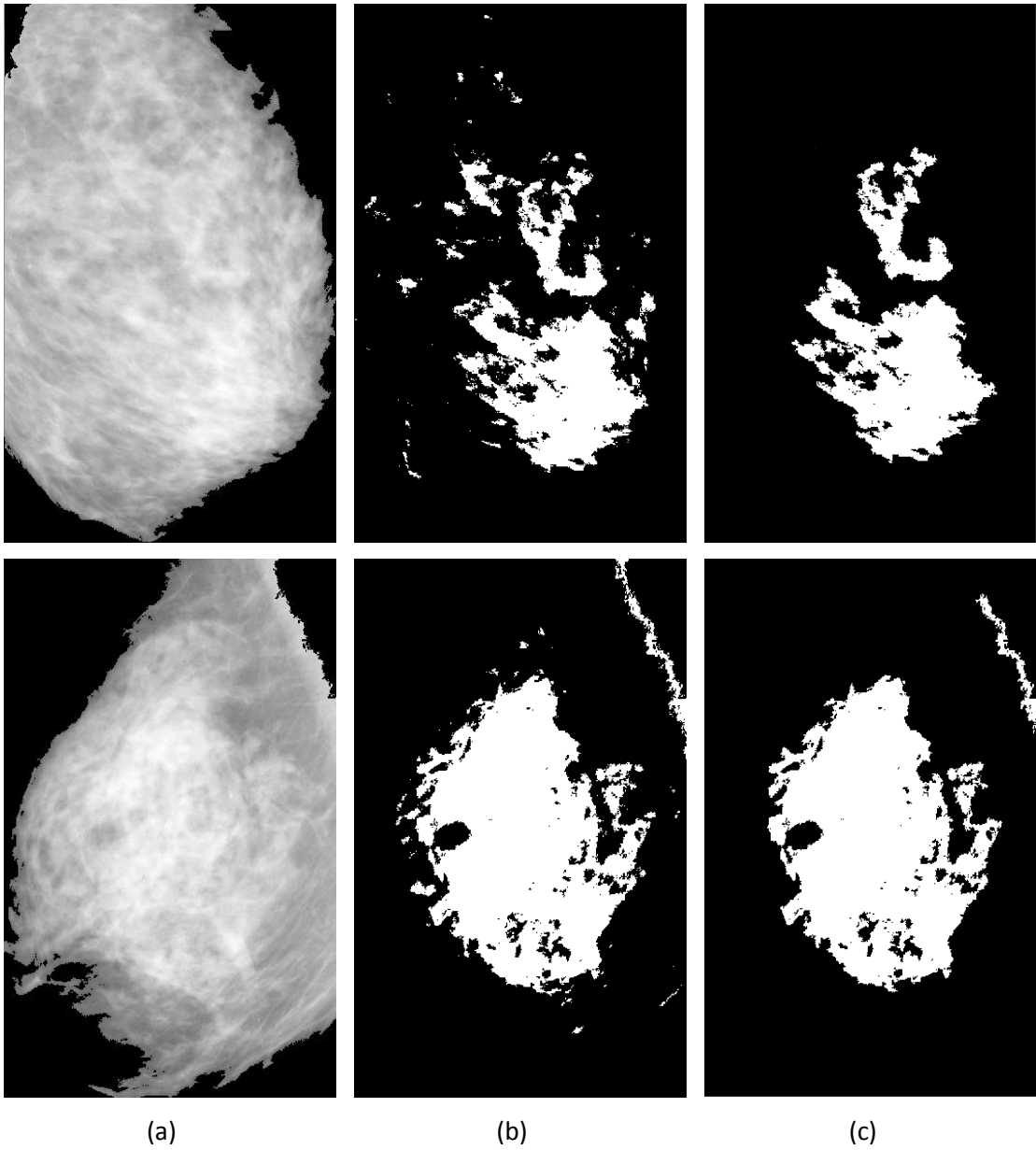


Figure 5.22 Thresholding the mammogram breast region to extract the suspicious regions in architectural distortion. (a) The original breast region image. (b) The thresholded image (c) The suspicious regions appear after suppression of the small regions.

*B- Suspicious Region Extraction:* after the connected component threshold is applied to the thresholded image, the kept regions will be called the suspicious regions and every region should be separated perfectly from the breast image in order to extract its features. Figure 5.23 illustrates the separated regions from the mammographic mass image. Figure 5.24 illustrates the separated regions from the mammographic architectural distortion.

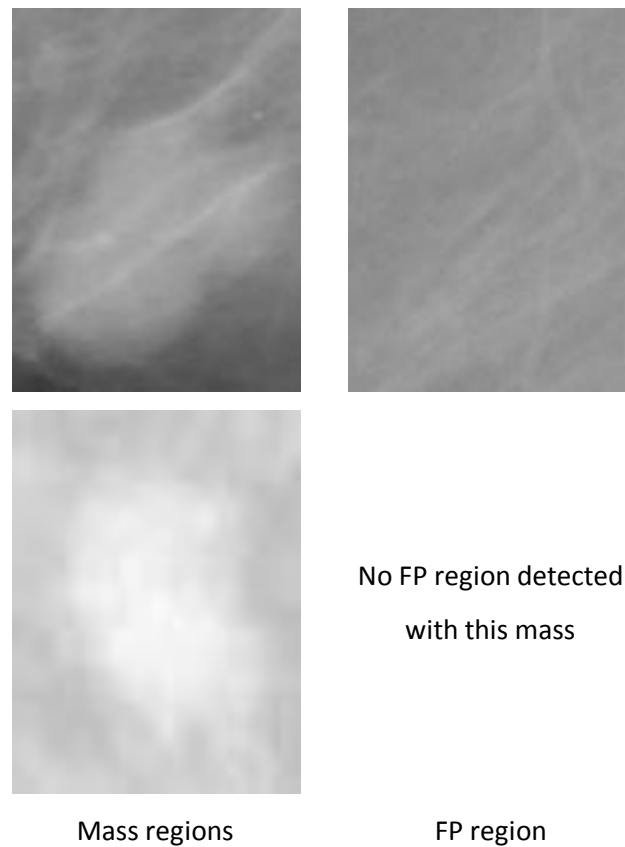


Figure 5.23 Set of suspicious mammographic mass regions segmented automatically.

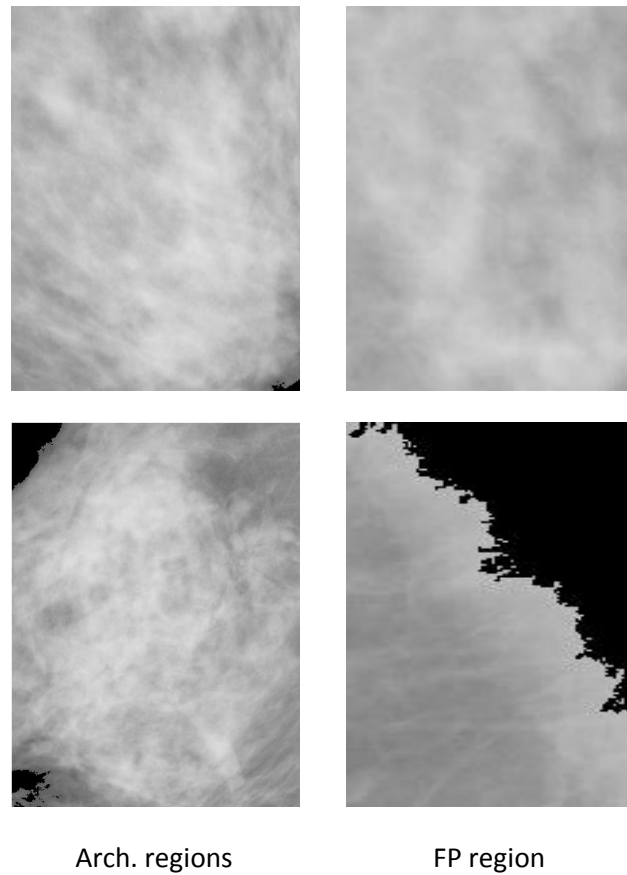


Figure 5.24 Set of suspicious mammographic architectural distortion regions segmented automatically.

The suspicious regions detected from the previous steps are decomposed using wavelet or curvelet transform into 4 decomposition levels. Two methods are applied to extract and select the most significant features; The method of standard deviation of means as presented in Section 4.2.2.3 and the method of features ranking as presented in Section 4.2.2.4.

*C- Classification:* The classification step is performed using two classifiers, KNN and SVM. The study firstly starts with the differentiation between the mass and normal tissues. Secondly, the classification step is repeated to differentiate between the architectural distortion and normal tissues.

### *1- Mammographic Mass Identification Using Adaptive Threshold*

This section presents the results of the experiments carried out to a set of 118 mammogram images (50 masses and 68 normal). The 50 masses produced 53 regions containing mass (There are three images containing two masses (mdb005, mdb132 and mdb144) and 91 false positives (FPs). The 68 normal images produce 130 FPs, i.e. 274 suspicious regions are extracted. The obtained results show that for mass detection, the algorithm exhibits a sensitivity of 100% with average of 1.87 FP detections per image. Once the suspicious regions are extracted from the mammogram images, curvelet or wavelet transform is applied to these regions. Subsequently, both feature extraction methods are applied followed by the classification step of whether the region is mass or normal tissue.

Figure 5.25 illustrates the classification accuracy rate achieved by KNN and SVM classifiers; 2x5-folds cross validation using the method of standard deviation of means. The figure shows that KNN classifier slightly outperforms SVM and the curvelet performs well better than wavelet in analysis of mammogram images. The error bar shows the standard deviation between the 2x5-folds cross validation.

Figure 5.26 presents the classification accuracy rate using 2x5-folds cross validation in case of using features ranking method for feature extraction. The comparison between both figures shows that the method of standard deviation of means performs better with curvelet than wavelet, while the features ranking method gives better classification rate compared to the standard deviation of means method in case of wavelet. It can be seen that the error bar in Figure 5.25 in case of SVM is smaller than its value in case of KNN, while in Figure 5.26 the error bar in SVM is greater than its value in case of KNN. These differences in error bar are due to the difference in representing the different classes through the training data and testing data. This drawback might be solved when the used dataset becomes larger.

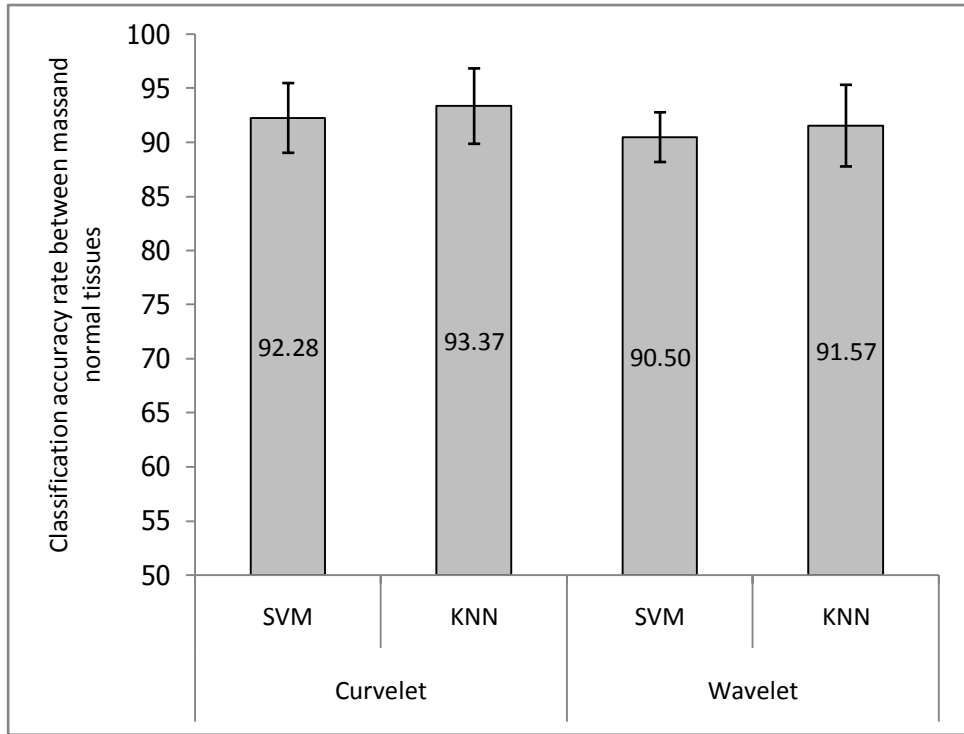


Figure 5.25 The classification accuracy rate when extracting features by the standard deviation of means method to differentiate between mass and normal tissue.

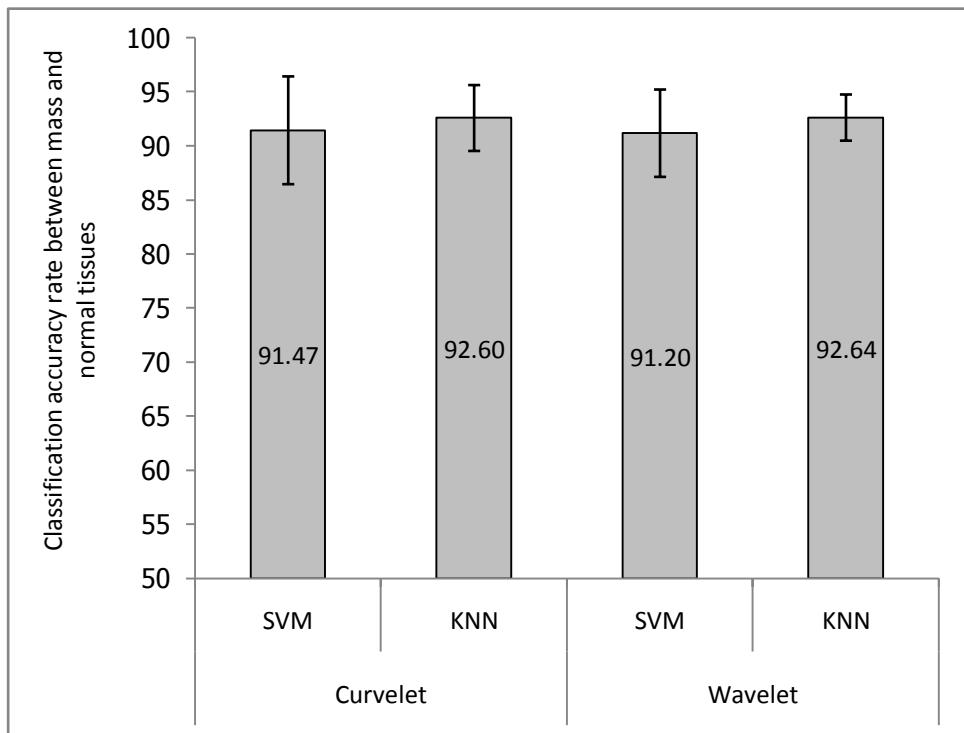


Figure 5.26 The classification accuracy rate when extracting features by feature ranking method to differentiate between mass and normal tissue.

The classification rates obtained in this study from KNN and SVM are near to the results obtained when we work into the ROIs extracted manually by using the given data. It can be concluded that we successfully obtained the ROIs automatically and the classifier succeeded to reduce the FPs by discriminating between masses and normal regions.

## *2- Mammographic Architectural Distortion Identification Using Adaptive Threshold*

The proposed method was applied to a set of 55 mammogram images (19 architectural distortions and 36 normal). The 19 architectural distortion mammograms produced 19 regions containing architectural distortion and 40 FPs. The 36 normal images produced 56 FPs, i.e. 115 suspicious regions are extracted. For architectural distortion detection, the obtained results show that the algorithm exhibits a sensitivity of 100% with average of 1.75 FPs detections per image. Once the suspicious regions are extracted from the mammogram images, curvelet and wavelet transform is applied to these regions. Subsequently, both feature extraction methods are applied followed by the classification to determine whether the region is architectural distortion or normal tissue. Figure 5.27 illustrates the classification accuracy rate obtained by SVM and KNN classifiers. 2x5-folds cross validation using the standard deviation of means feature extraction method. The figure shows that SVM classifier slightly outperforms KNN and curvelet performs well better than wavelet in analysis of mammogram images. The error bar shows the standard deviation between the 2x5-folds cross validation. It shows that error value in KNN is less than in case of SVM. Figure 5.28 presents the classification accuracy rates using 2x5-folds cross validation in case of applying feature ranking method for feature extraction from curvelet and wavelet. The comparison between both figures shows that the feature ranking method outperforms the method of standard deviation of means. In this case, the error bar value in KNN is smaller than its value in case of SVM. As discussed earlier, these differences in error bars are due to the difference in representing the different classes through the training data and testing data. This drawback might be eliminated when a larger dataset is used.



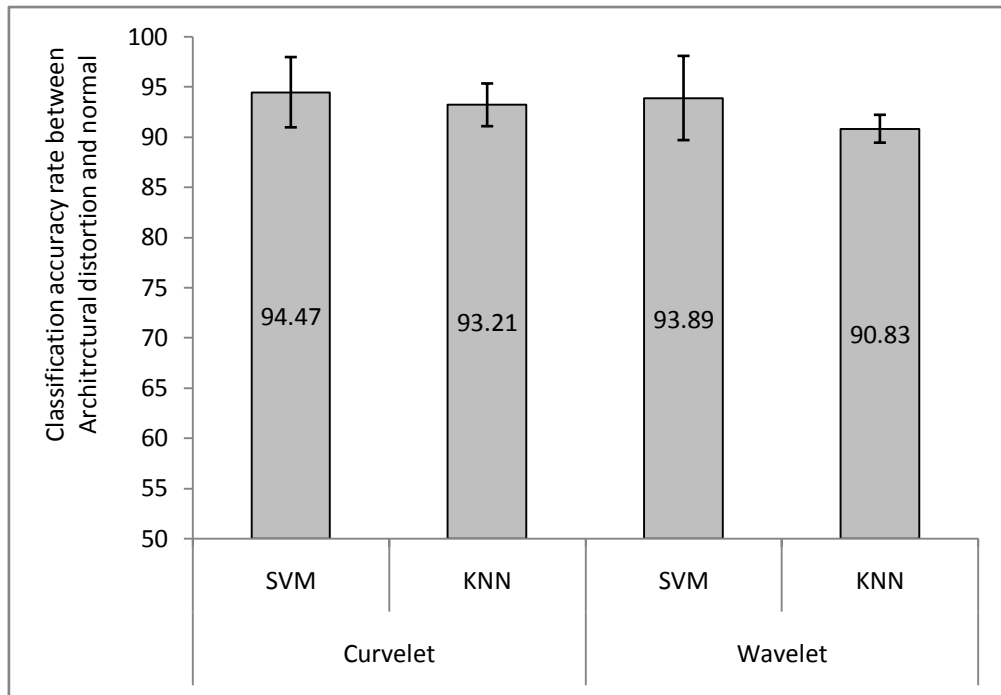


Figure 5.27 The classification accuracy rate when extracting features by the standard deviation of means method to differentiate between architectural distortion and normal tissue.

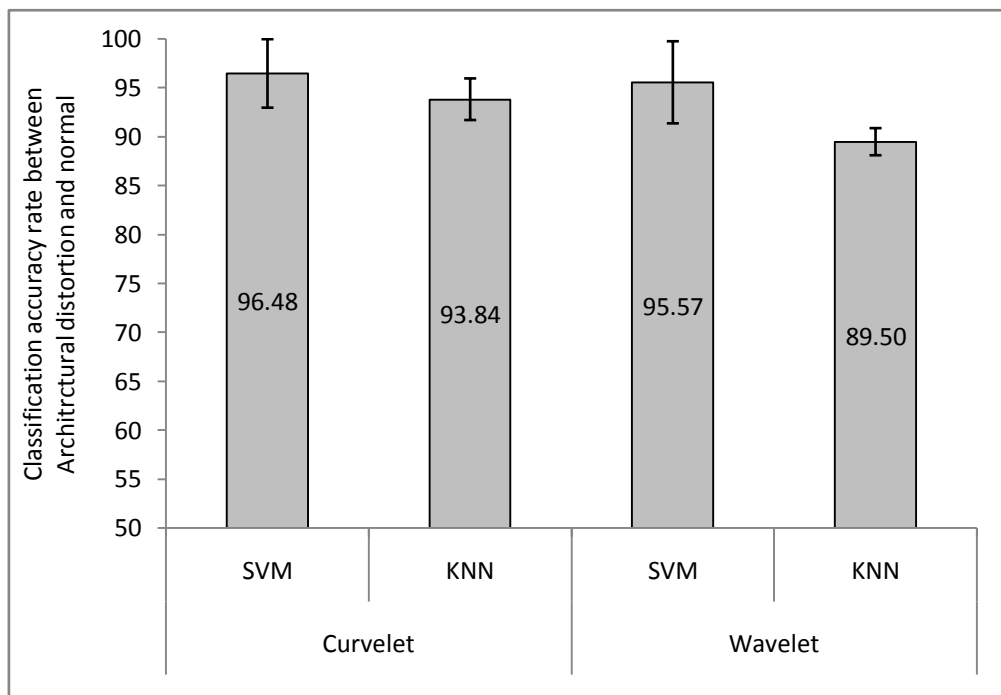


Figure 5.28 The classification accuracy rate of 2x5 folds cross validation when extracting features by feature ranking method to differentiate between architectural distortion and normal tissue.

#### 5.4.2.2 *The Results Obtained by Developing a Pattern Matching Method to Identify the Suspicious Region*

In this step, a region of typical abnormal region (whether it is mass or architectural distortion) is used as a template. The breast regions obtained from the first stage are used to be the input to the second stage. Each ROI is divided into windows equal to the size of the predefined template abnormal region. The correlation coefficient between the template region and the regions of the breast region image is calculated as in the following equation [157]:

$$R = \frac{\sum_m \sum_n (A_{mn} - \bar{A})(B_{mn} - \bar{B})}{\sqrt{(\sum_m \sum_n (A_{mn} - \bar{A})^2) * (\sum_m \sum_n (B_{mn} - \bar{B})^2)}} \quad (5.2)$$

where  $A$  is the template abnormal region (mass or architectural distortion), and  $B$  is the breast region (window) under consideration from the whole breast region image. The correlation coefficient between the template region and the region under consideration from the breast region image is calculated and recorded. Then the maximum correlation coefficient value is calculated and the corresponding region will be called the suspicious region. Once the maximum correlation coefficient value is determined, the corresponding region is cropped from the breast region. Region should be separated perfectly from the breast region image in order to be used in the following steps. Each suspicious region is passed to the classifier to determine whether it is abnormal or a normal region.

#### A- *Mammographic Mass Identification Using Pattern Matching Method*

The method is applied to a set of 116 mammogram images (56 masses and 60 normal). Once the suspicious regions are extracted from the mammogram images, the curvelet transform is applied to these regions. Subsequently, a feature extraction method is applied followed by the classification step of mass or normal tissue. In this case, the method of standard deviation of means is used to select a set of feature followed by KNN to classify between mass and normal tissues. The classification accuracy rate is calculated using 2x5-folds cross validation. It shows that the average

classification accuracy rate reaches 94.66%. The proposed method successfully detected 50 masses regions from 56 regions, i.e. a sensitivity rate obtained 89.28%. It was noted that all missed masses were spiculated masses. The other masses were perfectly detected.

#### *B- Mammographic Architectural Distortion Identification Using Pattern Matching Method*

The method is applied to a set of 79 mammogram images (19 containing architectural distortion and 60 normal). Once the suspicious regions are extracted from the mammogram images, the curvelet transform is applied to these regions. Subsequently, the method of standard deviation of means is applied followed by KNN classifier to classify the suspicious region as architectural distortion or normal tissue. The classification accuracy rate is calculated using 2x5-folds cross validation. It shows that the average classification accuracy rate achieved 93.16%. The proposed method successfully detected 16 regions of architectural distortion from 19 regions, i.e. a sensitivity rate obtained 84.21%. Figure 5.29 presents the obtained results for 2x5-folds cross validation for mammographic mass and architectural distortion.

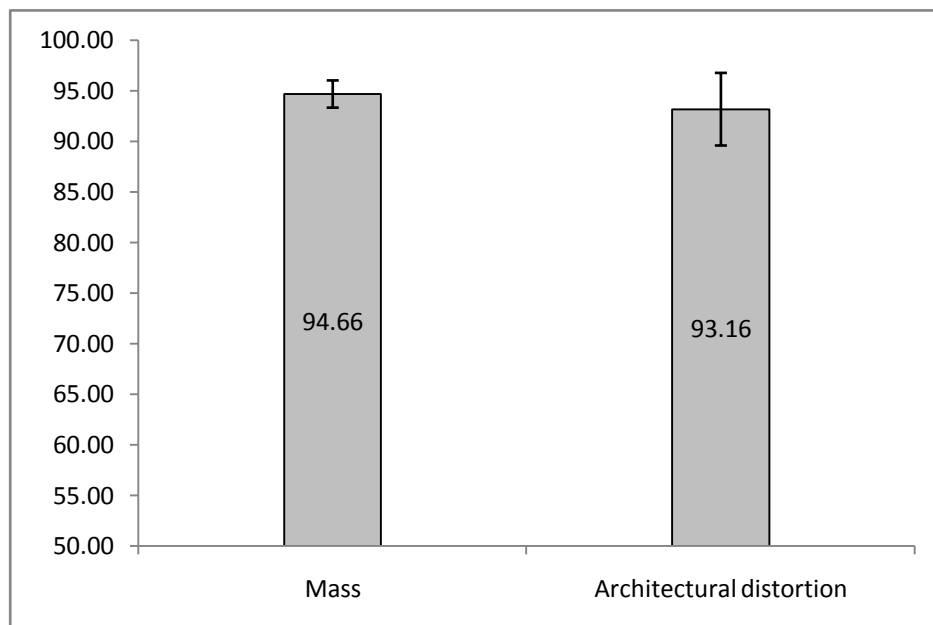


Figure 5.29 The classification accuracy rate of 2x5 folds cross validation using the automatically detected ROIs by pattern matching method.

## 5.5 Summary

This chapter presents the results obtained by applying the two proposed parts of study. In part I, the ROIs are segmented manually then it followed by five feature extraction methods. Such methods are based on extracting the most significant features which have the ability to differentiate between different classes. In this study, the feature extraction methods are based on extracting the feature from the multiresolution representations curvelet and wavelet. The KNN and SVM are used to classify between the different classes using the selected feature from the feature extraction step. A comparison study is presented between curvelet and wavelet in mammogram decomposition. The comparison shows that curvelet performs better than wavelet in mammogram analysis and the difference is statistically significant. A comparison study is also accomplished between the different feature extraction methods. The study shows that the method of extracting features based on standard deviation of means of different classes is better than the method of extracting a number of biggest coefficients from different decomposition levels. The method of extracting feature based on features ranking method is better than the method of extracting a number of biggest coefficients from different decomposition levels. The method of standard deviation of means is better than the method feature ranking method.

In part II, the ROIs are segmented automatically in order to identify whether this region is normal or abnormal. This part consists of two stages. The first stage is used to identify the breast region from the original mammogram. The second stage considers the detection of abnormal region in the identified breast region obtained from the first stage. Two methods are suggested to segment the suspicious region: adaptive thresholded method and pattern matching method. Then such methods are followed by false positive reduction method through classifying between the normal and abnormal tissues. This part concentrates in mass and architectural distortion abnormalities. The obtained results from part two show that the methods succeeded in automatic detection of ROIs.

## CHAPTER 6

### CONCLUSIONS AND FUTURE WORK

In this chapter, all research work presented in this thesis will be summarized in Section 6.1 and its overall contributions will be presented in Section 6.2. In Section 6.3 some aspects for future work that could improve the performance of the proposed computer aided system for breast cancer diagnosis will be presented.

#### **6.1 Conclusions of the Proposed Systems**

The point at issue in this thesis is to design a computer aided system for breast cancer diagnosis in digital mammogram based on advances of curvelet transform and multiresolution representations. The motivation for using curvelet is its ability to represent the edges in images. The work in this thesis consists of two parts.

##### **6.1.1 Part I: Developing Computer Aided Diagnosis System**

We focused our attention on developing the computer aided diagnosis system by developing five methods for feature extraction. The regions of interest (ROIs) were extracted manually from the original mammogram image. The multiresolution representations curvelet and wavelet were used to decompose the ROIs. The extracted features are then presented to the classification step. In this work two different classifiers KNN and SVM are used to differentiate between different classes.

- 1) The first method of feature extraction is based on extracting different ratios of the biggest coefficients from each decomposition level to be the feature vector of the corresponding mammogram. These ratios are taken between 10% and 90% of coefficients from each level. The extracted ratios are collected to be presented to the classifier. The highest classification accuracy rate of 99.05% was achieved

via using 60% of the biggest coefficients of curvelet to differentiate between normal and abnormal classes. While it is 98.26% when using 30% or 50% of the biggest coefficients of curvelet to classify between different classes according to their shapes and reached to 100% when using 20% of the biggest coefficients of curvelet to classify between benign and malignant. The overall results from this method show that curvelet outperforms wavelet.

- 2) The second method is based on extracting the biggest 100 coefficients from each decomposition level. The average classification accuracy rate achieved for 2x5 folds cross validation is 95.15% to classify between normal and abnormal classes using the coefficients vector of curvelet while the highest of wavelet is 90.76%. The same conclusion can be given to the other two classification problem: abnormal classes based on their shape and the problem of classifying between benign and malignant. The statistical comparison between the results obtained using curvelets and wavelets show that curvelets outperform wavelets and the difference is statistically significant.
- 3) The third method is called the standard deviation of means. This method calculates the mean of each class followed by calculating the standard deviation of these means. Each entry of the standard deviation vector indicates how the corresponding column separates the classes. A column will be kept if the obtained standard deviation is greater than a fixed threshold value, otherwise it is suppressed. The hard threshold value is applied to remove the features that make overlapping between classes and keep the features that maximize the difference between each class. The average classification accuracy rate for 2x5 folds cross validation reached 96.33%. The comparison study between using the standard deviation of means and using the biggest 100 coefficients shows that the former outperforms the latter and the difference is statistically significant.
- 4) The fourth method is called the feature ranking method. In this method the features are ranked depending on their capability to separate different classes. Then a dynamic threshold is applied over the score of the ranked features. The most significant features are kept according to the applied threshold value. The obtained features are then presented to SVM classifier. The proposed method makes the SVM classifier achieved 95.98% average classification accuracy rate

for 2x5 folds cross validation to classify between normal and abnormal classes and 97.30% between benign and malignant when using curvelet coefficients. A comparison study between the current method of feature extraction and the previously presented methods of extracting the biggest 100 coefficients or using the standard deviation of means is accomplished. A t-test is performed to compare the current method and each of the previously presented methods. The statistical analysis shows that the proposed method gives a statistically significant improvement compared to the method of extracting the biggest 100 coefficients; except when using curvelet to differentiate between normal and abnormal. The acceptance of null hypothesis in that case is due to the high accuracy obtained when extracting 100 coefficients using curvelet decomposition.

The comparison study between the method of feature ranking and standard deviation of means shows that there is no statistically significant difference between the feature ranking method and the standard deviation of means method except in the case of wavelet with normal and abnormal. For that unique case, the method of standard deviation of means performs better than the feature ranking method and the difference is statistically significant. It can be concluded that the method of standard deviation of means for feature extraction has the best performance among the discussed methods.

- 5) The fifth method is based on extracting a set of texture features from the curvelet transform. In this method, curvelet is used with scale 4 and 16 angle, i.e. the ROI is decomposed into 81 wedges, and seven texture features are calculated for each wedge, so that a total of 567 features are calculated to form a features vector for each mammogram image. The most significant features are obtained by passing the features vectors to a standard deviation of means feature extraction method. The remaining features will be the feature vector for the corresponding ROI. These extracted features are used to classify between different classes. The average classification accuracy rate for 2x5 folds cross validation reaches 96.20% to classify between normal and abnormal and it is 90.85% to distinguish between benign and malignant.

### 6.1.2 Part II: Automatic ROI Detection

- 1) Stage one: The aim of stage one is to determine the breast region in the original mammogram. Firstly, an automatic thresholding algorithm is used to separate the area composed of the breast and the pectoral muscle from the background of the image. Subsequently, a region growing algorithm is used to locate the muscle and suppress it from the breast. The study successfully determines and extracts the breast region from the original mammogram image. This process is applied to 322 images from MIAS dataset. The method was succeeded in extracting 310 breast regions from the whole dataset, i.e. It achieved detection accuracy of 96.27%.
- 2) Stage two: The work concentrates in the ROI segmentation to detect the suspicious region. Two methods are suggested to accomplish the segmentation step; such methods are adaptive thresholding method and pattern matching method. Subsequently, curvelet and wavelet are used to decompose the suspicious regions and the feature extraction method is performed. Finally, the classifier is used to determine whether the region is abnormal (mass or architectural distortion) or normal. The proposed scheme is fully automated to determine the suspicious region. Then a false positive reduction method is applied via classification step to determine whether the region is normal or abnormal. Both curvelet and wavelet transforms are applied. Two methods for features extraction are used: standard deviation of means and feature ranking method followed by applying the KNN and SVM to accomplish the classification step. The classification rates obtained in this study from KNN and SVM are encouraging compared to the results obtained when we worked with the ROIs extracted manually by using the given data. It can be concluded that we successfully determined the ROIs automatically and the classifier succeeded to reduce the FPs by discriminating between abnormal and normal regions. As a result, we find that the curvelet transform outperforms the wavelet transform. The method of standard deviation of means performs better than the remaining methods for feature extraction.



## 6.2 Contributions of the Work

The main contribution of this work is to implement the curvelet transform as a multiresolution representation method to decompose the ROI in order to identify its nature. The specific contributions of this thesis are summarized as follows:

- 1) Five feature extraction methods from multiresolution representation.
  - Extracting a percentage of the biggest coefficients from each decomposition level.
  - Extracting the biggest 100 coefficients from each decomposition level.
  - Standard deviation of means method.
  - Features ranking method.
  - Curvelet based texture features method.
- 2) The proposed feature extraction methods are compared and a statistical analysis is accomplished. The comparison study suggests that curvelet outperforms wavelet and the difference is statistically significant. The obtained results show that the developed computer aided diagnosis system achieved high classification rate compared to the previous work.
- 3) A mammogram image segmentation algorithm that effectively and efficiently divides mammogram images into distinct components, breast region, background, labels and pectoral muscle is presented.
- 4) Automatic systems for masses and architectural distortion detection that identifies and extracts the suspicious areas in mammogram images using two different methods are presented. The methods are as follows:
  - The adaptive thresholding method.
  - The pattern matching method.

The limitation of the work is that it depends only on a single dataset. It might be better to apply the proposed systems to a different dataset.

### **6.3 Recommendations for Future Work**

The following approaches are recommended for future studies:

- 1) Reconstruction of the extracted coefficients of curvelet and wavelet for ROI detection might be suitable to detect the abnormality in the original mammogram.
- 2) Applying the multiresolution decomposition using curvelet and wavelet to the ROI. Haralick's descriptors are calculated from the representation of regions followed by applying the rough set theory to identify the most significant features that have high capability to distinguish between different classes in breast cancer.
- 3) Distinguishing the different classes using an ensemble of SVM classifier.
- 4) Integrating other imaging modalities, such as ultrasound, magnetic resonance imaging (MRI) and computed tomography (CT) with X-ray mammography. This may lead to a novel effective system for breast cancer control.
- 5) The proposed system is built using a single dataset. It might be interesting to apply it to a different dataset.

## REFERENCES

- [1] WHO, “Cancer facts sheet, 2010,” <http://www.who.int/mediacentre/factsheets/fs297/en/> (Accessed, February 2011).
- [2] P. Gomez, “Breast cancer, early detection, saves lives,” [www.pantaicancersupport.com](http://www.pantaicancersupport.com), (Accessed, April 2010).
- [3] R.M. Rangayyan, F.J. Ayres, J.E.L. Desautels, “A review of computer aided diagnosis of breast cancer: Toward the detection of subtle signs,” *Journal of the Franklin Institute* 344, 312-348, 2007.
- [4] M. Bhosle, S. Samuel, V. Vosuri, E. Paskett, R. Balkrishnan, “Physician and patient characteristics associated with outpatient breast cancer screening recommendations in the United States: analysis of the National Ambulatory Medical Care Survey Data 1996–2004,” *Breast Cancer Res. Treat.* vol. 103, pp. 53–59, 2007.
- [5] J. Bozek, M. Mustra, K. Delac, M. Grgic, “A survey of image processing algorithms in digital mammography,” *Rec. Advan. in Mult. Sig. Process. and Commun.*, SCI 231, Springer-Verlag Berlin Heidelberg, pp. 631–657, 2009.
- [6] Y. Zheng, “Breast Cancer Detection with Gabor Features from Digital Mammograms,” *Journal of Algorithms*, vol. 3, no. 1, pp. 44-62, 2010.
- [7] <http://www.mammoimage.org/signs-of-disease/>, (accessed May 2010).
- [8] R.M. Rangayyan, “*Biomedical Image Analysis*,” CRC press, Boca Raton, 2005.
- [9] U.K. Nagah, “A mammogram and breast ultrasound-base expert system with image processing features for breast diseases,” Ph.D thesis, USM, Penang, Malaysia, 2007.
- [10] [www.ahedegypt.org/pubs/pmmssc/pmmssc\\_breastcancer.pdf](http://www.ahedegypt.org/pubs/pmmssc/pmmssc_breastcancer.pdf), (Accessed, April 2010).
- [11] A. Mukhdoomi, “On the problem of segmenting fibroglandular tissue in mammograms, M.S. thesis, Department of Computing Science, Umea University, Sweden, 2006.

- [12] E.A. Sickles, "The Spectrum of Breast Asymmetries: Imaging Features, Work-Up, Management," In *Radiologic clinics of North America*, vol. 45, Issue 5, September 2007.
- [13] P.E. Shile, J.A. Guingrich. "Detecting "missed" breast cancers: A comparison of CAD systems", *Supplement to Applied Radiology*, available at: [http://appliedradiology.mobi/uploadedfiles/Issues/2002/10/Supplements/AR\\_October\\_Shile\\_CADX.pdf](http://appliedradiology.mobi/uploadedfiles/Issues/2002/10/Supplements/AR_October_Shile_CADX.pdf), 2002.
- [14] C.M. Erickson, "Automated detection of breast cancer using SAXS data and wavelet features," M.S. thesis, University of Saskatchewan, Saskatoon, Canada, 2005.
- [15] M. Helvie, "Improving mammographic interpretation: double reading and computer-aided diagnosis," In *Radiologic clinics of North America*, vol. 45, Issue 5, September 2007.
- [16] I. Christoyianni, E. Dermatas, G. Kokkinakis, "Fast detection of masses in computer aided mammography," *Journal IEEE Signal Process. Mag.*, vol. 17, no. 1, pp. 54–64, 2000.
- [17] B. Zheng, R. Shah, L. Wallace, C. Hakim, M.A. Ganott, G. David, "Computer aided detection in mammography: An assessment of performance on current and prior images," *Journal of Acad Radiol*, vol. 9, No. 11, pp. 1245–1250, 2002.
- [18] T.W. Freer, M.J. Ullissey, "Screening mammography with computer-aided detection: prospective study of 12,860 patients in a community breast center," *Journal of Radiology*, vol. 220, pp.781–786, 2001.
- [19] D. Gur, J.H. Sumkin, H.E. Rockette, M. Ganott , C. Hakim , L. Hardesty, et al. "Changes in breast cancer detection and mammography recall rates after the introduction of a computer-aided detection system," *Journal Natl. Cancer Inst.* vol. 96, no. 3, pp.185–190, 2004.
- [20] M.A. Helvie, L. Hadjiiski, E. Makariou, H.P. Chan, N. Petrick, B. Sahiner, et al. "Sensitivity of noncommercial computer-aided detection system for mammographic breast cancer detection: pilot clinical trial," *Journal of Radiology* vol. 231, pp. 208–214, 2004.

- [21] R.L. Birdwell, P. Bandodkar, D.M. Ikeda, "Computer aided detection with screening mammography in a university hospital setting," *Journal of Radiology* vol. 236, pp. 451–457, 2005.
- [22] T.E. Cupples, J.E. Cunningham, J.C. Reynolds, "Impact of computer-aided detection in a regional screening mammography program," *Am. J. of Roentgenol.*, vol. 185, pp. 944–950, 2005.
- [23] M.J. Morton, D.H. Whaley, K.R. Brandt, K.K. Amrami, "Screening mammograms: interpretation with computer-aided detection—prospective evaluation," *Journal of Radiology* vol. 239, pp.375–383, 2006.
- [24] J.C. Dean, C.C. Ilvento, "Improved cancer detection using computer-aided detection with diagnostic and screening mammography: prospective study of 104 cancers" *Am. J. of Roentgenol.*, vol. 187, pp. 20–28, 2006.
- [25] J.M. Ko, M.J. Nicholas, J.B. Mendel, P.J. Slanetz, "Prospective assessment of computer-aided detection in interpretation of screening mammography" *Am. J. of Roentgenol.*, vol. 187, pp. 1483–1491, 2006.
- [26] J. Tang, R.M. Ranjayyan, I. El-Naqa, Y. Yang, "Computer aided detection and diagnosis of breast cancer with mammogram: recent advances," *IEEE Transaction Information Technology in Biomedicine*, vol. 13, no. 2, pp. 236-251, 2009.
- [27] H.D. Cheng, X. Cai, X. Chen, L. Hu, X. Lou, "Computer aided detection and classification of microcalcification in mammograms: a survey," *Pattern Recognition*, vol. 36, no. 12, pp. 2967-2991, 2003.
- [28] J. Bozek, K. Delac, M. Grgic, "Computer aided detection and diagnosis of breast abnormalities in digital mammography, *proceeding of 50<sup>th</sup> international symposium ELMAR-2008*, Zadar, Croatia, pp. 45-52.
- [29] M. Rizzi, M. D'Aloia, B. Castagnolo, "Computer aided detection of microcalcifications in digital mammograms adopting a wavelet decomposition," *Integrated Computer-Aided Engineering*, vol. 16, Issue 2, pp. 91-103, 2009.
- [30] R.M. Nishikawa, "Current status and future directions of computer aided diagnosis in mammography," *Computerized Medical Imaging and Graphics*, vol. 31, pp. 224-235, 2007.

- [31] I. Christoyianni, A. Koutras, E. Dermatas, G. Kokkinakis, "Computer aided diagnosis of breast cancer in digitized mammograms," *Computerized Medical Imaging and Graphics* vol. 26, pp. 309–319, 2002.
- [32] R2: ImageChecker, <http://www.hologic.com/en/breast-screening/imagechecker/> (accessed October 2010).
- [33] S.M. Astley, F.J. Gilbert, "Review: Computer-aided detection in mammography," *Clinical Radiology*, vol. 59, pp. 390–399, 2004.
- [34] CADx Second Look, <http://www.cadxmed.com>, (accessed October 2010).
- [35] J.A. Baker, E.L. Rosen, J.Y. Lo, E.I. Gimenez, R. Walsh, M.S. Soo, "Computer aided detection (CAD) in screening mammography: sensitivity of commercial CAD systems for detecting architectural distortion" *Am. J. of Roentgenol.*, vol. 181, no. 4, pp. 1083–1088, 2003.
- [36] H. Soltanian-Zadeh, F. Rafiee-Rad, S. Pourabdollah-Nejad, "Comparison of multiwavelet, wavelet, Haralick, and shape features for microcalcification classification in mammograms," *Pattern Recognition*, vol. 37, Issue 10, pp. 1973–1986, 2004.
- [37] A. Hassanien, "Fuzzy rough sets hybrid scheme for breast cancer detection," *Image and Vision Computing*, vol. 25, no. 2, pp.172–183, 2007.
- [38] M.P. Sampat, M.K. Markey, A.C. Bovik, "Computer-aided detection and diagnosis in mammography," in *Handbook of Image and Video Processing*, Academic Press, 2005.
- [39] D. Raba, A. Oliver, J. Mart, M. Peracaula, J. Espunya, "Breast segmentation with pectoral muscle suppression on digital mammograms," *Lecture Notes in Computer Science*, Springer-Verlag Berlin Heidelberg, pp. 471-478, 2005.
- [40] H.D. Cheng, X.J. Shi, R. Min, L.M. Hu, X.P. Cai, H.N. Du, "Approaches for automated detection and classification of masses in mammograms," *Pattern Recognition*, vol. 39, Issue 4, , pp. 646-668, 2006.
- [41] R.M. Haralick, K. Shanmugam, I. Dinstein, "Texture features for image classification," *Transactions on Systems, Man, and Cybernetics*, vol. 3, No. 6, pp. 610-621, 1973.
- [42] T. Matsubara, H. Fujita, S. Kasai, M. Goto, Y. Tani, T. Hara, T. Endo, "Development of new schemes for detection and analysis of mammographic masses," *Proceeding Intel. Inform. Systems*, pp. 63–66, 1997.

- [43] L. Li, W. Qian, L.P. Clarke, R.A. Clark, J.A. Thomas, “Improving mass detection by adaptive and multiscale processing in digitized mammograms.” *Proc. of SPIE 3661-Medical Imaging: Image Processing*, pp. 490–498, 1999.
- [44] T. Matsubara, H. Fujita, T. Endo, K. Horita, M. Ikeda, C. Kido, et al, “Development of mass detection algorithm based on adaptive thresholding technique in digital mammograms,” In: *Third International Workshop on Digital Mammography*, K. Doi, M.L. Giger, R.M. Nishikawa, R.A. Schmitd (eds.) Elsevier, Amsterdam, pp. 391–396, 1996.
- [45] A.R. Dominguez, A.F. Nandi, “Enhanced multi-level thresholding segmentation and rank based region selection for detection of masses in mammograms,” In: *IEEE International Conference on Acoustics, Speech and Signal Processing 2007, ICASSP 2007*, Honolulu, HI, April 15-20, pp. 449–452, 2007.
- [46] C. Varela, P.G. Tahoces, A.J. Mendez, M. Souto, J.J. Vidal, “Computerized detection of breast masses in digitized mammograms,” *Computers in Biology and Medicine*. vol. 37, no. 2, pp. 214–226, 2007.
- [47] H.D. Li, M. Kallergi, L.P. Clarke, V.K. Jain, R.A. Clark, “Markov random field for tumor detection in digital mammography,” *IEEE Transactions on Medical Imaging*, vol. 14, no. 3, pp. 565–576, 1995.
- [48] A.R. Abdel-Dayem, M.R. El-Sakka, “Fuzzy entropy based detection of suspicious masses in digital mammogram images,” In: *IEEE Conference on Engineering in Medicine and Biology Society*, pp. 4017–4022, 2005.
- [49] G. Kom, A. Tiedeu, M. Kom, “Automated detection of masses in mammograms by local adaptive thresholding,” *Computers in Biology and Medicine*, vol. 37, no. 1, pp. 37–48, 2007.
- [50] Y.J. Lee, J.M. Park, H.W. Park, “Mammographic mass detection by adaptive thresholding and region growing,” *Int. J. Imaging Systems Technol.* vol. 11, no.5, pp. 340–346, 2000.
- [51] S.A. Hojjatoleslami, J. Kittler, “Region growing: a new approach,” *IEEE Trans. Image Process.* vol.7, no. 7, pp. 1079–1084, 1998.
- [52] Z. Huo, M.L. Giger, C.J. Vyborny, U. Bick, P. Lu, D.E. Wolverton, R.A. Schmidt, “Analysis of spiculation in the computerized classification of mammographic masses,” *Med. Phys.* vol. 22, no. 10, pp. 1569–1579, 1995.

- [53] M.A. Kupinski, M.L. Giger, "Automated seeded lesion segmentation on digital mammograms," *IEEE Trans. Med. Imag.* vol. 17, no. 4, pp. 510–517, 1998.
- [54] L. Kinnard, S.C.B. Lo, E. Makariou, T. Osicka, P. Wang, M.T. Freedman, M.F. Chouikha, "Likelihood function analysis for segmentation of mammographic masses for various margin groups," In: *IEEE International Symposium on Biomedical Imaging*, vol. 1, pp. 113–116, 2004.
- [55] H. Zhang, S.W. Foo, S.M. Krishnan, C.H. Thng, "Automated breast masses segmentation in digitized mammograms," In: *IEEE International Workshop in Biomedical Circuits and System*, pp. S2.2–1–S2.2–4, 2004.
- [56] M.R. Hejazi, Y.S. Ho, "Automated detection of tumors in mammograms using two segments for classification," In: *Lecturer Notes in Computer Science*, vol. 3767, pp. 910–921, 2005.
- [57] T.N. Pappas, "An adaptive clustering algorithm for image segmentation," *IEEE Transactions on Signal Processing*, vol. 40, no.4, pp. 901–914, 1992.
- [58] A.Z. Cao, Q. Song, X.L. Yang, S. Liu, "Breast mass segmentation on digital mammograms by a combined deterministic annealing method," In: *IEEE International Symposium on Biomedical Imaging*, vol. 2, pp. 1303–1306, 2004.
- [59] B. Sahiner, L.M. Hadjiiski, H.P. Chan, C. Paramagul, A. Nees, M. Helvie, J. Shi, "Concordance of computer-extracted image features with BI-RADS descriptors for mammographic mass margin," In: *M.L. Giger, N. Karssemeijer, (eds.) Proc. of SPIE Medical Imaging 2008: Computer-Aided Diagnosis*, vol. 6915, 2008.
- [60] N. Petrick, H.P. Chan, B. Sahiner, D. Wei, "An adaptive density weighted contrast enhancement filter for mammographic breast mass detection," *IEEE Transactions on Medical Imaging*, vol. 15, no. 1, pp. 59-67, 1996.
- [61] B.W. Hong, M. Brady, "A topographic representation for mammogram segmentation," In: *Lecturer Notes in Computer Science*, vol. 2879, pp. 730-737, 2003.
- [62] L. Yin, S. Deshpande, J.K. Chang, "Automatic lesion/tumor detection using intelligent mesh-based active contour," In: *IEEE International Conference on Tools with Artificial Intelligence*, pp. 390–397, 2003.



- [63] F. Fauci, S. Bagnasco, R. Bellotti, D. Cascio, S.C. Cheran, F. De Carlo, et al, “Mammogram segmentation by contour searching and massive lesion classification with neural network” In: *IEEE Nuclear Science Symposium Conference Record*, vol. 5, pp. 2695–2699, 2004.
- [64] Y. Yuan, M.L. Giger, H. Li, K. Suzuki, C. Sennett, “A dual-stage method for lesion segmentation on digital mammograms,” *Med. Phys.* vol. 34, no. 11, 4180-4193, 2007.
- [65] F. Zou, Y. Zheng, Z. Zhou, K. Agyepong, “Gradient vector flow field and mass region extraction in digital mammograms,” In: *21<sup>st</sup> IEEE International Symposium on Computer-Based Medical Systems, CMBS 2008*, Jyväskylä, June 17-19, pp. 41-43, 2008.
- [66] A.A. Ferreira, F. Nascimento, I.R. Tsang, G.D.C. Cavalcanti, T.B. Ludermir, R.R.B. de Aquino, “Analysis of mammogram using self-organizing neural networks based on spatial isomorphism,” In: *Proceedings of International Joint Conference on Neural Networks, IJCNN 2007*, Orlando, Florida, USA, August 12-17, pp. 1796-1801, 2007.
- [67] Y. Yuan, M.L. Giger, H. Li, C. Sennett, “Correlative feature analysis of FFDM images,” In: *Giger, M.L., Karssemeijer, N. (eds.) Proc. of SPIE Medical Imaging 2008: Computer-Aided Diagnosis*, vol. 6915, 2008.
- [68] G.D. Tourassi, R. Vargas-Voracek, D.M. Catarious, C.E. Floyd, “Computer-assisted detection of mammographic masses: a template matching scheme based on mutual information,” *Med. Phys.* vol. 30, no. 8, pp. 2123–2130, 2003.
- [69] S. Morrison, L.M. Linnett, “A model based approach to object detection in digital mammography,” In: *Proceedings of the IEEE International Conference on Image Processing*, vol. 2, Kobe, Japan, pp. 182–186, 1999.
- [70] S.L. Ng, W.F. Bischof, “Automated detection and classification of breast tumors,” *Comput. Biomed. Res.* vol. 25, pp. 218–237, 1992.
- [71] A. Oliver, J. Freixenet, M. Robert, E.R.E. Denton, R. Zwiggelaar, “Mammographic mass eigendetection,” In: *Medical Image Understanding and Analysis*, pp. 71–75. 2006.
- [72] J. Freixenet , A. Oliver , R. Marti , X. Llado, J. Pont , E. Perez , E.R. Denton, R. Zwiggelaar, “Eigendetection of masses considering false positive reduction

- and breast density information,” *Med. Phys.* vol. 35, no. 5, pp. 1840-1853, 2008.
- [73] Y. Hatanaka, T. Hara, H. Fujita, S. Kasai, T. Endo, T. Iwase, “Development of an automated method for detecting mammographic masses with a partial loss of region,” *IEEE Trans. Med. Imaging*, vol. 20, no. 12, pp. 1209-1214, 2001.
- [74] R. Zwiggelaar, T.C. Parr, I.W. Hutt, C.J. Taylor, S.M. Astley, C.R.M. Boggis, “Model-based detection of spiculated lesions in mammograms,” *Med. Image Anal.* vol. 3, no. 1, pp. 39-63, 1999.
- [75] N. Szekely, N. Toth, B. Pataki, “A hybrid system for detecting masses in mammographic images,” *IEEE Trans. on Instrum. Meas.* vol. 55, no. 3, pp. 944–952, 2006.
- [76] S. Liu, C.F. Babbs, E.J. Delp, “Multiresolution detection of spiculated lesions in digital mammograms,” *IEEE Trans. Image Process.* vol. 10, no. 6, pp. 874–884, 2001.
- [77] F. Sakellaropoulos, S. Skiadopoulou, A. Karahaliou, L. Costaridou, G. Panayiotakis, “Using wavelet-based features to identify masses in dense breast parenchyma,” In: *Lecturer Notes in Computer Science*, vol. 4046, pp. 557–564, 2006.
- [78] A. Oliver, J. Freixenet, J. Martí, E. Perez, J. Pont, E.R.E. Denton, R. Zwiggelaar, “A review of automatic mass detection and segmentation in mammographic images,” *Medical Image Analysis*, vol. 14, Issue 2, pp. 87-110, 2010.
- [79] A.E. Hassanien, J.M. Ali, H. Nobuhara, “Detection of spiculated masses in mammograms based on fuzzy image processing,” In: *Lecturer Notes in Computer Science*, vol. 3070, pp. 1002–1007, 2004.
- [80] J.M.H. Ali, A.E. Hassanien, “PCNN for detection of masses in digital mammogram,” *Neural Network World*, vol. 16, no. 2, pp. 129–141, 2006.
- [81] R. Mousa, Q. Munib, A. Moussa, “Breast cancer diagnosis system based on wavelet analysis and fuzzy-neural,” *Expert Systems with Applications*, vol. 28, pp. 713–723, 2005.
- [82] H.P. Chan, D.Wei, M.A. Helvie, B. Sahiner, D.D. Adler, M.M. Goodsitt, N. Petrick, “Computer-aided classification of mammographic masses and normal

- tissue: Linear discriminant analysis in texture feature space,” *Phys. Med. Biol.*, vol. 40, no. 5, pp. 857–876, 1995.
- [83] B. Sahiner, H.P. Chan, N. Petrick, D. Wei, M.A. Helvie, D.D. Adler, M.M. Goodsitt, “Classification of mass and normal breast tissue: A convolution neural network classifier with spatial domain and texture images,” *IEEE Trans. Med. Imag.*, vol. 15, no. 5, pp. 598–610, 1996.
- [84] N. Karssemeijer, G.M. te Brake, “Detection of stellate distortions in mammograms,” *IEEE Trans. Med. Imaging*, vol. 15, no. 5, pp. 611–619, 1996.
- [85] G.M. te Brake, N. Karssemeijer, “Single and multiscale detection of masses in digital mammograms,” *IEEE Trans. Med. Imaging*, vol. 18, no. 7, pp. 628–639, 1999.
- [86] R.M. Rangayyan, N.R. Mudigonda, J.E.L. Desautels, “Boundary modelling and shape analysis methods for classification of mammographic masses,” *Med. Biol. Eng. Comput.*, vol. 38, pp. 487–496, 2000.
- [87] B.S. Sahiner, H.P. Chan, N. Petrick, M.A. Helvie, L.M. Hadjiiski, “Improvement of mammographic mass characterization using spiculation measures and morphological features,” *Med. Phys.*, vol. 28, no. 7, pp. 1455–1465, 2001.
- [88] B.S. Sahiner, H.P. Chan, N. Petrick, M.A. Helvie, M.M. Goodsitt, “Computerized characterization of masses on mammograms: The rubber band straightening transform and texture analysis,” *Med. Phys.*, vol. 25, no. 4, pp. 516–526, 1998.
- [89] R.M. Haralick, “Statistical and structural approaches to texture,” *Proc. of IEEE*, vol. 67, pp. 786–804, 1979.
- [90] L. Shen, R.M. Rangayyan, J.E.L. Desautels, “Application of shape analysis to mammographic calcifications,” *IEEE Trans. Med. Imaging*, vol. 13, no. 2, pp. 263–274, 1994.
- [91] N.R. Mudigonda, R.M. Rangayyan, J.E.L. Desautels, “Gradient and texture analysis for the classification of mammographic masses,” *IEEE Trans. Med. Imaging*, vol. 19, no. 10, pp. 1032–1043, 2000.
- [92] N.R. Mudigonda, R.M. Rangayyan, J.E.L. Desautels, “Detection of breast masses in mammograms by density slicing and texture flow-field analysis,” *IEEE Trans. Med. Imaging*, vol. 20, no. 12, pp. 1215–1227, 2001.

- [93] L. Li, R.A. Clark, J.A. Thomas, "Computer-aided diagnosis of masses with full-field digital mammography," *Acad. Radiol.*, vol. 9, pp. 4–12, 2002.
- [94] L. Zheng, A.K. Chan, "An artificial intelligent algorithm for tumor detection in screening mammogram," *IEEE Trans. Med. Imaging*, vol. 20, no. 7, pp. 559-567, 2001.
- [95] R. Campanini, D. Dongiovanni, E. Iampieri, N. Lanconelli, M. Masotti, G. Palermo, et al, "A novel featureless approach to mass detection in digital mammograms based on support vector machines," *Phys. Med. Biol.*, vol. 49, no. 6, pp. 961–975, 2004.
- [96] C.B.R. Ferreira, D.L. Borges, "Analyses of mammogram classification using a wavelet transform decomposition," *Pattern Recognition Letters*, vol. 24, pp. 973-982, 2003.
- [97] E.A. Rashed, I.A. Ismail, S.I. Zaki, "Multiresolution mammogram analysis in multilevel decomposition," *Pattern Recognition Letters*, vol. 28, pp. 286–292, 2007.
- [98] J. Wei, B. Sahiner, L. Hadjiiski, H. Chan, N. Petrick, M. Helvie, M. Roubidoux, J. Ge, and C. Zhou, "Computer aided detection of breast masses on full field digital mammograms," *Med. Phys.*, vol. 32, no. 9, pp. 2827–2837, 2005.
- [99] R. Bellotti, F. D. Carlo, S. Tangaro, G. Gargano, G. Maggipinto, M. Castellano, et al, "A completely automated CAD system for mass detection in a large mammographic database," *Med. Phys.*, vol. 33, no. 8, pp. 3066–3075, 2006.
- [100] S. Timp, C. Varela, N. Karssemeijer, and B. Dacollian, "Temporal change analysis for characterization of mass lesions in mammography," *IEEE Trans. Med. Imag.*, vol. 26, no. 7, pp. 945–953, 2007.
- [101] A.R. Dominguez, A.K. Nandi, "Detection of masses in mammograms via statistically based enhancement, multilevel-thresholding segmentation, and region selection," *Computerized Medical Imaging and Graphics*, vol. 32, pp. 304-315, 2008.
- [102] F. Moayed, Z. Azimifar, R. Boostani, S. Katebi, "Contourlet-based mammography mass classification," *ICIAR 2007, Lecture Notes in Computer Science*, vol. 4633, pp. 923–934, 2007.

- [103] F. Moayedi, Z. Azimifar, R. Boostani, S. Katebi, "Contourlet-based mammography mass classification using the SVM family," *Computers in Biology and Medicine*, vol. 40, no. 4, pp. 373-383, 2010.
- [104] R.M. Rangayyan, L. Shen, Y. Shen, J.E.L. Desautels, H. Bryant, T.J. Terry, et al, "Improvement of sensitivity of breast cancer diagnosis with adaptive neighborhood contrast enhancement of mammograms," *IEEE Trans. Inf. Technol. Biomed.*, vol. 1, no. 3, pp. 161–170, Sep. 1997.
- [105] H. Cheng, Y. Lui, R. Freimanis, "A novel approach to microcalcification detection using fuzzy logic technique," *IEEE Trans. Med. Imag.*, vol. 17, no. 3, 1998.
- [106] H.D. Cheng H. Xu, "A novel fuzzy logic approach to mammogram contrast enhancement," *Information Science*, vol. 148, no. 1–4, pp. 167–184, 2002.
- [107] I. Daubechies, "*Ten Lectures on Wavelets*," SIAM, 1992.
- [108] A. Laine, J. Fan, W. Yang, "Wavelets for contrast enhancement of digital mammography," *IEEE Eng. Med. Biol. Mag.*, vol. 14, no. 5, pp. 536-550, 1995.
- [109] T. Balakumaran, Dr. I.L.A.Vennila, C.G. Shankar, "Detection of microcalcification in mammograms using wavelet transform and fuzzy shell clustering," *International Journal of Computer Science and Information Security (IJCSIS)*, vol. 7, no. 1, 2010.
- [110] A. Papadopoulos, D. I. Fotiadis, L. Costaridou, "Improvement of microcalcification cluster detection in mammography utilizing image enhancement techniques," *Computers in Biology and Medicine*, vol. 38, no. 10, pp. 1045-1055, 2008.
- [111] D.H. Davies, D.R. Dance, "Automatic computer detection of clustered calcifications in digital mammograms," *Phys. Med., Biol.*, vol. 35, no. 8, pp. 1111–1118, 1990.
- [112] D.H. Davies, D.R. Dance, C.H. Jones, "Automatic detection of clusters of calcifications," *SPIE Medical Imaging IV: Image Processing*, vol. 1233, pp. 185–191, 1990.
- [113] L.N. Mascio, J.M. Hernandez, C.M. Logan, "Automated analysis for microcalcifications in high-resolution digital mammograms," *SPIE Image Processing*, vol. 1898, pp. 472–479, 1993.

- [114] J. Dengler, S. Behrens, J.F. Desaga, "Segmentation of microcalcifications in mammograms," *IEEE Trans. Med. Imag.*, vol. 12, pp. 634–642, 1993.
- [115] S. Paquerault, L.M. Yarusso, J. Papaioannou, Y. Jiang, R.M. Nishikawa, "Radial gradient-based segmentation of mammographic microcalcifications: Observer evaluation and effect on cad performance," *Med. Phys.*, vol. 31, no. 9, pp. 2648–2657, 2004.
- [116] W. Qian, F. Mao, X. Sun, Y. Zhang, D. Song, R.A. Clarke, "An improved method of region grouping for microcalcification detection in digital mammograms," *Computerized Medical Imaging and Graphics*, vol. 26, no. 6, pp. 361–368, 2002.
- [117] D. Zhao, M. Shridhar, D.G. Daul, "Morphology on detection of calcifications in mammograms," *IEEE International Conference on Acoustics, Speech and Signal Processing*, pp. 129–132, March 23-26, 1992.
- [118] R.M. Nishikawa, M.L. Giger, K. Doi, C.J. Vyborny, R.A. Schmidt, "Computer-aided detection of clustered microcalcifications on digital mammograms," *Med. Biol. Eng. Comput.*, vol. 33, no. 2, pp. 174-178, 1995.
- [119] D. Betal, N. Roberts, G.H. Whitehouse, "Segmentation and numerical analysis of microcalcifications on mammograms using mathematical morphology," *British Journal of Radiology*, vol. 70, no. 837, pp. 903-917, 1997.
- [120] J.C. Fu, S.K. Lee, S.T.C. Wong, J.Y. Yeh, A.H. Wang, H.K. Wu, "Image segmentation feature selection and pattern classification for mammographic microcalcifications," *Computerized Medical Imaging and Graphics*, vol. 29, no. 6, pp. 419–429, 2005.
- [121] J. Salvado, B. Roque, "Detection of calcifications in digital mammograms using wavelet analysis and contrast enhancement," In: *IEEE International Workshop on Intelligent Signal Processing*, Faro, Portugal, pp. 200–205, September 2005.
- [122] S.N. Yu, K.Y. Li, Y.K. Huang, "Detection of microcalcifications in digital mammograms using wavelet filter and Markov random field model," *Computerized Medical Imaging and Graphics*, vol. 30, pp. 163–173, 2006.
- [123] W.J.H. Veldkamp, N. Karssemeijer, "Normalization of local contrast in mammograms," *IEEE Trans. Med. Imag.*, vol. 19, no. 7, pp. 731–738, 2000.

- [124] L. Zhang, W. Qian, R. Sankar, D. Song, R. Clark, "A new false positive reduction method for MCCs detection in digital mammography," *IEEE International Conference on Acoustics, Speech and Signal Processing*, pp. 1033–1036, May 7–11, 2001.
- [125] N.R. Pal, B. Bhowmick, S.K. Patel, S. Pal, J. Das, "A multi-stage neural network aided system for detection of microcalcifications in digitized mammograms," *Neurocomputing*, vol. 71, pp. 2625–2634, 2008.
- [126] R.N. Strickland, "Wavelet transforms for detecting microcalcifications in mammograms," *IEEE Trans. Med. Imaging*, vol. 15, no. 2, pp. 218–229, 1996.
- [127] S. Yu, L. Guan, S. Brown, "Automatic detection of clustered microcalcifications in digitized mammogram films," *J. Electron Imaging*, vol. 8, no. 1, pp. 76–82, 1999.
- [128] S. Yu, L. Guan, "A CAD system for the automatic detection of clustered microcalcifications in digitized mammogram films," *IEEE Trans. Med. Imaging*, vol. 19, no. 2, pp. 115–126, 2000.
- [129] I. El-Naqa, Y. Yang, M.N. Wernick, N.P. Galatsanos, R.M. Nishikawa, "A support vector machine approach for detection of microcalcifications," *IEEE Trans. Med. Imaging*, vol. 21, no. 12, pp. 1552–1563, 2002.
- [130] L. Wei, Y. Yang, R.M. Nishikawa, M.N. Vernick, A. Edwards, "Relevance vector machine for automatic detection of clustered microcalcifications," *IEEE Trans. Med. Imaging*, vol. 24, no. 10, pp. 1278–1285, 2005.
- [131] T. Matsubara, T. Ichikawa, T. Hara, H. Fujita, S. Kasai, T. Endo, T. Iwase, "Automated detection methods for architectural distortions around skinline and within mammary gland on mammograms," In: *Proc. 17th Int. Congr. Exhib. Comput. Assist. Radiol. Surg. (International Congress Series)*, pp. 950–955, June 2003.
- [132] T. Ichikawa, T. Matsubara, T. Hara, H. Fujita, T. Endo, T. Iwasem, "Automated detection method for architectural distortion areas on mammograms based on morphological processing and surface analysis," in *Proc. SPIE Med. Image 2004: Image Processing*, vol. 5374, J. M. Fitzpatrick and M. Sonka, Eds. San Diego, CA: SPIE, pp. 920–925, Feb. 2004.

- [133] Q. Guo, J. Shao, V. Ruiz, “Investigation of support vector machine for the detection of architectural distortion in mammographic images,” *J. Phys.: Conf. Series*, vol. 15, pp. 88–94, 2005.
- [134] G.D. Tourassi, D.M. DeLong, C.E. Floyd, “A study on the computerized fractal analysis of architectural distortion in screening mammograms,” *Phys. Med. Biol.*, vol. 51, no. 5, pp. 1299–1312, 2006.
- [135] N. Eltonsy, G. Tourassi, A. Elmaghraby, “Investigating performance of a morphology -based CAD scheme in detecting architectural distortion in screening mammograms,” In: *Proc. 20th Int. Congr. Exhib. Comput. Assist. Radiol. Surg. (CARS 2006)*, H.U. Lemke, K. Inamura, K. Doi, M.W. Vannier, A.G. Farman, Eds. Osaka, Japan: Springer-Verlag, Jun. 2006, pp. 336–338.
- [136] F.J. Ayres, R.M. Rangayyan, “Characterization of architectural distortion in mammograms,” *IEEE Eng. Med. Biol. Mag.*, vol. 24, no. 1, pp. 59–67, 2005.
- [137] F.J. Ayres, R.M. Rangayyan, “Reduction of false positives in the detection of architectural distortion in mammograms by using a geometrically constrained phase portrait model,” *Int. J. Comput. Assist. Radiol. Surg.*, vol. 1, no. 6, pp. 361–369, 2007.
- [138] S. Banik, R.M. Rangayyan, J.E.L. Desautels, “Detection of architectural distortion in prior mammograms of interval-cancer cases with neural networks,” *proc. 31<sup>st</sup> Annual International Conference of the IEEE EMBS*, Minneapolis, Minnesota, USA, September 2-6, 2009.
- [139] D. Scutt, G.A. Lancaster, J.T. Manning, “Breast asymmetry and predisposition to breast cancer,” *Breast Cancer Res.*, vol. 8, no. 2, R14, 2006.
- [140] T.K. Lau, W.F. Bischof, “Automated detection of breast tumors using the asymmetry approach,” *Computers and Biomedical Research*, vol. 24, pp. 273–295, 1991.
- [141] P. Miller, S. Astley, “Automated detection of mammographic asymmetry using anatomical features,” *Int. J. Pattern Recognit. Artif. Intell.*, vol. 7, no. 6, pp. 1461–1476, 1993.
- [142] P. Miller, S. Astley, “Automated detection of breast asymmetry using anatomical features,” in *State of the Art in Digital Mammographic Image Analysis, Series in Machine Perception and Artificial Intelligence*, vol. 9,



- K.W. Bowyer, S. Astley, Eds. River Edge, NJ:World Scientific, , pp. 247–261, 1994.
- [143] R.J. Ferrari, R.M. Rangayyan, J.E.L. Desautels, A.F. Frere, “Analysis of asymmetry in mammograms via directional filtering with Gabor wavelets,” *IEEE Trans. Med. Imag.*, vol. 20, no. 9, pp. 953–964, 2001.
- [144] R. J. Ferrari, R.M. Rangayyan, J.E.L. Desautels, R.A. Borges, A.F. Frere, “Identification of the breast boundary in mammograms using active contour models,” *Med. Biol. Eng. Comput.*, vol. 42, no. 2, pp. 201–208, 2004.
- [145] R.J. Ferrari, R.M. Rangayyan, J.E.L. Desautels, R.A. Borges, A.F. Frere, “Automatic identification of the pectoral muscle in mammograms,” *IEEE Trans. Med. Imag.*, vol. 23, no. 2, pp. 232–245, 2004.
- [146] R.J. Ferrari, R.M. Rangayyan, R.A. Borges, A.F. Frere, “Segmentation of the fibro-glandular disc in mammograms using Gaussian mixture modeling,” *Med. Biol. Eng. Comput.*, vol. 42, no. 3, pp. 378–387, 2004.
- [147] R.M. Rangayyan, R.J. Ferrari, A. F. Frere, “Analysis of bilateral asymmetry in mammograms using directional, morphological, and density features,” *J. Electron. Imag.*, vol. 16, no. 1, pp. 013003-1–013003-12, 2007.
- [148] S.G. Mallat, “*A Wavelet Tour of Signal Processing*,” Academic Press, 1999.
- [149] S.G. Mallat, “A theory for multiresolution signal decomposition: the wavelet representation,” *IEEE Transactions on Pattern Analysis and Machine Intelligence*, vol. 7, No. 11, pp. 674–93, 1989.
- [150] M. Al-Qdah, A. Ramli, R. Mahmud, “A system of microcalcifications detection and evaluation of the radiologist: comparative study of the three main races in Malaysia,” *Computers in Biology and Medicine*, vol. 35, pp. 905–914, 2005.
- [151] E. Candes, D. Donoho, “Curvelets, multiresolution representation, and scaling laws,” *Wavelet Applications in Signal and Image Processing VIII*, A. Aldroubi, A.F. Laine, M.A. Unser eds., Proc. SPIE , Vol. 4119, Sampling and Approximation, 2000.
- [152] E. Candes, L. Demanet, D. Donoho, L. Ying, “Fast discrete curvelet transforms,” *Multiscale Model. Simul.*, vol. 5, pp. 861-899, 2006.
- [153] W. Steeb, *The nonlinear workbook*, 4<sup>th</sup> edition, World Science, 2008.

- [154] D.L. Donoho, I.M. Johnstone, "Ideal spatial adaptation by wavelet shrinkage," *Biometrika*, vol 81, no.3, pp. 425-455, 1994.
- [155] S. Li, C. Liao, J.T. Kwok, "Gene feature extraction using  $t$ -test statistics and kernel partial least squares," *ICONIP 2006*, Part III, LNCS 4234, pp. 11–20, 2006.
- [156] N. Otsu, "A threshold selection method from gray-level histograms," *IEEE Transactions on Systems, Man, and Cybernetics*, vol. 9, no. 1, pp. 62-66, 1979.
- [157] R.C. Gonzalez, R.E. Woods, "*Digital Image Processing*," Second ed., Prentice Hall, 2001.
- [158] MIAS, <http://www.wiau.man.ac.uk/services/MIAS/MIASweb.html>, (Accessed, August 2008).
- [159] E. Candes, /<http://www.curvelet.org>, CurveLab-2.1.2 Toolbox, 2004.
- [160] T.G. Dietterich, "Approximate statistical tests for comparing supervised classification learning algorithms," *Neural Computation*, vol. 10 no. 7, pp. 1895-1923, 1998.

## PUBLICATIONS DERIVED FROM THIS STUDY

This study has been the basis for the following peer-reviewed journal papers and conference talks.

- Peer-Reviewed Journal Papers:
  - 1) **Mohamed Meselhy Eltoukhy**, Ibrahima Faye, Brahim Belhaouari Samir, “Breast cancer diagnosis in digital mammogram using multiscale curvelet transform,” *Computerized Medical Imaging and Graphics, Elsevier*, 34 (4), pp. 269-276, 2010.
  - 2) **Mohamed Meselhy Eltoukhy**, Ibrahima Faye, Brahim Belhaouari Samir “A comparison of wavelet and curvelet for breast cancer detection in digital mammogram,” *Computers in Biology and Medicine, Elsevier*, 40 (4), pp. 384–391, 2010.
  - 3) **Mohamed Meselhy Eltoukhy**, Ibrahima Faye, Brahim Belhaouari Samir, “Multiresolution based feature extraction method for breast cancer diagnosis in digital mammogram,” Submitted, 2010.
  - 4) **Mohamed Meselhy Eltoukhy**, Ibrahima Faye, Brahim Belhaouari Samir, “A statistical based feature extraction method for breast cancer diagnosis in digital mammogram using multiresolution representation,” Submitted, 2010.
  - 5) **Mohamed Meselhy Eltoukhy**, Ibrahima Faye, Brahim Belhaouari Samir, “Automatic detection of breast masses in digital mammograms”, submitted, 2010.
  - 6) **Mohamed Meselhy Eltoukhy**, Ibrahima Faye, Brahim Belhaouari Samir, “Automatic detection of Architectural distortion in digital mammograms”, under preparation, 2010.

- Refereed Conferences:

- 7) **Mohamed Meselhy Eltoukhy**, Ibrahima Faye, Brahim Belhaouari Samir, “Automatic detection of breast masses in digital mammograms using pattern matching” *Proceedings of 2010 IEEE-EMBS Conference on Biomedical Engineering and Sciences*, 30 November-2 December 2010, Kuala Lumpur, Malaysia.
- 8) **Mohamed Meselhy Eltoukhy**, Ibrahima Faye, Brahim Belhaouari Samir, “Curvelet based feature extraction method for breast cancer diagnosis in digital mammogram,” *Proceedings of the 3<sup>rd</sup> International Conference on Intelligent & Advanced Systems 2010 (ICIAS2010)*, 15-17 June 2010, Kuala Lumpur, Malaysia.
- 9) **Mohamed Meselhy Eltoukhy**, Ibrahima Faye, Brahim Belhaouari Samir, “Wavelet analysis: comparison of approximation and details for mammogram classification” *Proceedings of The 7th International Conference on Robotics, Vision, Signal Processing and Power Applications (RoViSP 2009)*, organized by School of Electrical and Electronic Engineering, Universiti Sains Malaysia (USM), December 2009, Langkawi, Malaysia.
- 10) Ibrahima Faye, **Mohamed Meselhy Eltoukhy**, Brahim Belhaouari Samir, “Digital mammograms classification using a wavelet based feature extraction method”, *IEEE, 2009 Second International Conference on Computer and Electrical Engineering*, December 2009, Dubai.
- 11) **Mohamed Meselhy Eltoukhy**, Ibrahima Faye, Brahim Belhaouari Samir, “Using curvelet transform to detect breast cancer in digital mammogram”, *Proceedings of The 5<sup>th</sup> International Colloquium on Signal Processing and its Application (CSPA) 2009*, 6-8 March 2009, Kuala Lumpur, Malaysia.
- 12) **Mohamed Meselhy Eltoukhy**, Ibrahima Faye, Brahim Belhaouari Samir, “Breast cancer diagnosis in mammograms using multilevel wavelet analysis”, *Proceedings of National Postgraduate Conference (NPC2009)*, at Universiti Teknologi PETRONAS, 25-26 March 2009, Perak, Malaysia.